

ASSESSMENT OF BURN SEVERITY OF LARGE WESTERN
WILDFIRES VIA MULTI-TEMPORAL LANDSAT IMAGERY
ANALYSIS AND CELLULAR AUTOMATA MODELING

THESIS

Presented to the Graduate Council
of Texas State University-San Marcos
in Partial Fulfillment
of the Requirements

for the Degree

Master of SCIENCE

by

Carl W. Schmiedeskamp, B.S.

San Marcos, Texas
May 2005

ACKNOWLEDGEMENTS

I would like to thank my mother, Marjorie Schmiedeskamp, for her unwavering belief in my abilities and my father, Carl Schmiedeskamp, Sr., for his expectation of excellence from me. My brothers and sister deserve many thanks for all of their support and encouragement. Without them, the decision to return to graduate school would just be something I would like to do someday.

I am extremely grateful to my thesis committee for all of their help and support. I owe a debt of gratitude to my thesis advisor, Dr. Deborah Bryan, for her support and advice on matters both pertaining to my thesis and beyond. Dr. Giordano deserves my thanks for his support and valuable recommendations during the writing of this paper. Finally, I would like to thank Dr. Fonstad for his advice and enthusiasm. I could not have done it without your help.

This manuscript was submitted on March 23, 2005.

TABLE OF CONTENTS

	Page
ACKNOWLEDGEMENTS.....	iii
LIST OF TABLES.....	vi
LIST OF FIGURES.....	vii
CHAPTER	
I. INTRODUCTION.....	1
Significance of Study	
II. LITERATURE REVIEW.....	6
Remote Sensing Analysis of the Impact of Wildfire on the Landscape Wildfire Behavior Modeling	
III. STUDY AREAS.....	23
IV. THEORETICAL FRAMEWORK.....	28
V. WORKING HYPOTHESES.....	32
VI. DATA: REMOTE SENSING ASSESSMENT OF WILDFIRE BURN SEVERITY.....	35
VII. DATA: WILDFIRE BEHAVIOR MODELING.....	43
VIII. METHODOLOGY: REMOTE SENSING ANALYSIS OF WILDFIRE BEHAVIOR.....	48
IX. RESULTS: REMOTE SENSING ANALYSIS OF WILDFIRE BURN SEVERITY.....	52
X. METHODOLOGY: WILDFIRE BEHAVIOR MODELING.....	65

XI.	TOPOGRAPHY, WEATHER, AND VEGETATION CHARACTERISTICS OF THE HAYMAN STUDY AREA.....	82
XII.	RESULTS: CELLULAR AUTOMATA WILDFIRE MODELING.....	92
XIII.	DISCUSSION.....	108
XIV.	CONCLUSIONS / FUTURE RESEARCH OPPORTUNITIES.....	121
	APPENDICES.....	124
	WORKS CITED.....	135

LIST OF TABLES

Table	Page
1. Percentage of total acreage assigned to each burn severity class: Hayman fire.....	55
2. Percentage of total acres assigned to each burn severity class: Missionary Ridge fire.....	58
3. Percentage of total acres assigned to each burn severity class: Rodeo-Chediski fire.....	61
4. Percentage of total acres assigned to each burn severity class: von Neumann version of fire behavior model with higher burn probability weights.....	98
5. Percentage of total acres assigned to each burn severity class: Moore neighborhood version of fire behavior model with low burn probability weights.....	101
6. Percentage of total acres assigned to each burn severity class: Moore neighborhood version of fire behavior model with higher burn probability weights.....	105

LIST OF FIGURES

Figure	Page
1. Location of Hayman fire study area.....	24
2. Location of Missionary Ridge fire study area.....	26
3. Location of Rodeo-Chediski fire study area.....	27
4. True-color pre-burn Landsat TM image of Hayman fire study area.....	37
5. False-color post-fire Landsat TM image of Hayman fire study area.....	37
6. False-color pre-fire Landsat TM image of Missionary Ridge study area.....	39
7. False-color post-burn Landsat TM image of Missionary Ridge study site.....	39
8. False-color pre-burn Landsat TM image of Rodeo-Chediski study area.....	41
9. False-color post-fire Landsat TM image of Rodeo-Chediski study area.....	41
10. Fuel model distribution across Hayman fire study site.....	44
11. Burn probability grid based on wind speed variation over the course of the Hayman fire event.....	45
12. Burn probability grid based on slope and aspect of Hayman fire study Site.....	47
13. Images used to digitize fire perimeters for each study site.....	50
14. “2.5” dimension representation of unsupervised classification image draped over true-color image of Hayman study site.....	51
15. Predicted versus actual fire boundary of Hayman fire event.....	54
16. Comparison of official Hayman fire severity map with unsupervised and supervised classification images.....	54
17. Predicted versus official boundary of Missionary Ridge fire.....	56

18. Unsupervised and supervised classification images of Missionary Ridge fire.....	57
19. Official burn severity map of Missionary Ridge fire.....	58
20. Predicted versus actual fire perimeter of the Rodeo-Chediski fire.....	60
21. Unsupervised and supervised classification images of Rodeo-Chediski fire.....	62
22. Official burn severity map of Rodeo-Chediski fire event.....	63
23. Vector wind speed data for Hayman fire.....	68
24. Unweighted burn probability grid for Hayman study area.....	70
25. Spread probability grid for Hayman study area.....	72
26. Estimated fire residence time grid for Hayman study site.....	74
27. Visual representation of burn probability assessment phase of fire model.....	77
28. Visualization of effects of wind direction weightings on burn probability.....	78
29. Accuracy assessment points.....	81
30. Elevation of Hayman study area.....	83
31. Typical vegetation zones characteristic of the Colorado Front Range.....	88
32. Fuel model distribution within Hayman study area prior to fire event.....	90
33. von Neumann and Moore neighborhoods.....	92
34. Output of von Neumann model with low wind weights.....	94
35. Output of von Neumann model with higher wind weights.....	96
36. Predicted burn severity from von Neumann model with higher wind weights.....	97
37. Graph of percentage of total acreage assigned to each burn severity class.....	98
38. Output image of grid cells identified as burned by Moore neighborhood model with lower wind weightings.....	100
39. Percentage of total acreage assigned to each burn severity class.....	102

40. Predicted burn severity output from Moore neighborhood version of fire behavior model with lower wind weightings.....	103
41. Cells identified as burned by Moore neighborhood model with higher burn probability weightings.....	105
42. Percentage of total acreage assigned to each burn severity class.....	106
43. Predicted burn severity output from Moore neighborhood version of fire behavior model with higher wind weightings.....	107
44. Comparison of accuracy of supervised versus unsupervised classification of dNBR images.....	109
45. Effects of clouds and cloud shadows on burn severity output from the dNBR algorithm.....	111
46. Images show progression of fire at 200 time step intervals as predicted by von Neumann version of fire behavior model with higher wind weights.....	115
47. Predicted burn severity output from all three primary versions of the fire behavior model.....	116

CHAPTER I

INTRODUCTION

On June 18, 2002, a small wildfire began in east central Arizona that rapidly expanded from 600 acres on the morning of June 19th to over 50,000 acres by late afternoon the same day (Wilmes 2002). The Rodeo-Chediski fire had begun. By July 7th, the fire had burned over 467,000 acres and destroyed over 470 human-built structures (Wilmes 2002; Zeiroth and Siderits 2003). The impact of this fire had wide-ranging effects on both the natural and human environment. Some burned areas within the Rodeo-Chediski fire boundary could require decades to recover.

The effects that wildfires have on the landscape can be substantial, and our ability to assess the impact of wildfires on the natural environment is currently limited. Although wildfire occurs naturally in many plant communities, human intervention has substantially altered the natural fire regime of many ecosystems. Since the early 1900's, fire suppression was the typical response to wildfires when equipment and manpower was available (Graham, McCaffrey, and Jain 2004). This policy of fire suppression allowed large quantities of fuel to accumulate in areas where regular wildfires would normally burn off excess material in the forest understory (Patterson and Yool 1998). Wildfires that now occur in areas where high accumulations of fuels exist burn much larger areas than in the past, and the severity of these wildfires are often much higher

than fires in the past as well. Scientists and forest managers have more recently realized the faults in this fire suppression policy and are now enacting new policies to allow some wildfires to burn out as would occur naturally.

Although fire suppression policies are changing due to a deeper understanding of the importance of wildfire in fire-dependent ecosystems, many forested areas are still prone to extremely severe fire events due to past fire suppression policies. Severe wildfires often consume most or all of the vegetation present, and forest recovery time from severe wildfires is often measured in decades or even centuries (Wright 2004). The removal of vegetation due to fire also makes soil highly prone to erosion (Miller and Yool 2002). Wildfires can potentially threaten property and lives after the fire due to potential landsliding resulting from the removal of vegetation on steep slopes (National Interagency Fire Center 2004). Legleiter et al. (2003) conducted research that showed that runoff increased as a result of wildfires in Yellowstone National Park, thus burned catchments may be more susceptible to flash flooding during storm events.

Due to the recent trend toward larger, more severe wildfires, it is critical to further our understanding regarding wildfire behavior, particularly in terms of wildfire burn severity. Improving our ability to assess the impact of fire on the landscape requires a multidisciplinary approach. Geographers are trained to utilize a variety of unique disciplines to analyze phenomena across space, thus they are uniquely suited to investigate this problem. Currently, Burned Area Emergency Response (BAER) teams assess the post-fire impact of wildfires on the landscape, particularly regarding the impact of soil erosion and the effects of vegetation removal on watersheds within the burned area (Graham et al. 2003). It is critical to assess burned areas as soon after a fire event as

possible to mitigate the adverse effects of fire. Remote sensing is a useful tool to assess burn severity patterns within the burned area. My study employed recently developed remote sensing techniques to validate their effectiveness in assessing burn severity of three large fire events that occurred in the western United States during the 2002 fire season.

Although remote sensing is a useful tool to analyze the impact of past fires on the landscape, the development of methods to model wildfire burn severity for past fires as well as potential fire events may improve our understanding of wildfire behavior. Researchers commonly develop models in order to simplify the real world to gain knowledge regarding a variety of Earth processes. “A model is an abstraction of an object, system, or process that permits knowledge to be gained about reality by conducting experiments on the model” (Clarke 2003, 1). Ecological processes, such as wildfire, are inherently spatial, thus spatial simulation models are a highly useful tool to model these processes (Moreno, Ablan, and Tonella 2002). My study incorporates topographic, weather, and fuel data to model wildfire behavior, particularly in terms of wildfire burn severity, using cellular automata. Comparison of remote sensing analysis with cellular automata modeling show the strengths and weaknesses of each approach in regard to fire severity assessment.

Significance of Study

Improving our ability to assess the impact of wildfire on the landscape is of great importance to researchers in a variety of fields because severe burns often have long-lasting adverse effects on the natural environment. As mentioned previously, Burned Area Emergency Response (BAER) teams are designed to arrive at fire location and

assess the burned area to identify sites that require treatments to mitigate the negative effects of severe wildfire (Graham et al. 2003). BAER teams are required to assess burn severity and submit their recommendations regarding post-fire rehabilitation to forest managers within eight days of fire containment. This creates intense time pressure for these teams, particularly when fire events are large. Due to the trend of large, increasingly severe wildfire, it is apparent that research into efficient fire severity assessment techniques is necessary. A number of remote sensing techniques have come about in the past few years that are improving our ability to assess wildfire burn severity. A portion of my study will utilize the differenced Normalized Burn Ratio (dNBR) at three large western US wildfires during the 2002 fire season to determine the effectiveness of the dNBR algorithm.

Although the dNBR algorithm has the potential to improve forest managers' ability to assess burn severity after a fire event has occurred, I developed a cellular automata (CA) based fire behavior modeling tool to assess potential burn severity as well. This tool could provide burn severity risk information to BAER teams both prior to and during fire events. The ability of the model to produce a burn severity risk map either prior to, during, or immediately after a fire allows BAER teams to identify areas of high burn severity risk. This would improve the efficiency of these fire effect mitigation teams. Additionally, forest managers could utilize this simulation model to identify areas possessing high fire severity risk prior to any fire event. This information would allow forest managers to apply appropriate fuel treatments to reduce excess fuels that tend to lead to severe wildfire (Graham, McCaffrey, and Jain 2004). I maintain that a

combination of remote sensing and fire behavior modeling techniques will improve our ability to assess wildfire burn severity patterns across the landscape.

CHAPTER II

LITERATURE REVIEW

Remote Sensing Analysis of the Impact of Wildfire on the Landscape

It is readily apparent that severe wildfire events have the potential to inflict extensive damage upon natural ecosystems, but the current body of knowledge regarding the application of remote sensing to burn severity analysis is still quite limited. My study will expand the body of knowledge concerning the application of space-based remote sensing platforms to the analysis of fire burn severity by applying an algorithm to pre-burn and post-burn Landsat images. The existing literature regarding wildfire burn severity analysis informs my proposed study. I will discuss a number of these past studies in the following section to underscore the importance of the existing body of knowledge on my proposed research.

Trends in Wildfire Burn Severity Analysis via Remote Sensing

Research into the application of satellite-based remote sensors to fire burn severity analysis began within the past twenty years, and the most thorough research into this field occurred primarily during the last decade. Prior to the advent of high spatial resolution satellite-based remote sensors, investigators used other methods to attempt to produce burn severity maps. Until about thirty years ago, the primary tools used to create

wildfire burn severity maps were aerial photographs, and they are still used for this purpose today (Miller and Yool 2002; Riano et al. 2003; Zhang, Wooster, et al. 2003). Landsat imagery has advantages over aerial photography in some instances. Miller and Yool (2002) found that their Landsat fire severity map had a minimum mapping unit of 30 meters, but similar burn severity analyses conducted using aerial photographs resulted in maps with a 20 hectare minimum mapping unit. In this instance, Landsat images produced a much more accurate burn severity map than analyses using aerial photographs.

The advent of satellite-based remote sensing platforms allowed researchers to address the issue of wildfire management from new perspectives. Researchers began to use thermal infrared (IR) detection systems to determine the temperature and approximate area of active fires (Fraser, Li, and Cihlar 2000; Giglio and Justice 2003; Giglio and Kendall 2001; Justice et al. 2002; Oertel et al. 2003; Wooster, Zhukov, and Oertel 2003; Zhang, Van Genderen, et al. 2003). Most of the space-based sensors used to conduct such studies have relatively low spatial resolutions of approximately 1 kilometer in the infrared bands used for fire detection. The Advanced Very High Resolution Radiometer (AVHRR) and Moderate Resolution Imaging Spectro-radiometer (MODIS) are two examples of relatively low resolution space-based remote sensors that are commonly used for active fire detection (Fraser, Li, and Cihlar 2000; Giglio and Justice 2003; Justice et al. 2002; Wooster, Zhukov, and Oertel 2003).

Although these sensors provide data that is of little value at large scales, Dozier developed a breakthrough technique in 1981 to extract sub-pixel fire temperature and area (Dozier 1981, Giglio and Kendall 2001; Giglio and Justice 2003). Although the

Dozier method of sub-pixel fire extraction permitted major improvements in the analysis of active fires, it did not allow researchers to determine the direct effects of fires on the landscape. Researchers could make general assumptions regarding the impact that an active fire would have on the vegetation present, but these assessment techniques did not allow for quantitative studies on the impact of fire on the landscape below because no direct assessment of the changes in electromagnetic reflectance of vegetation was conducted (Fraser, Li, and Cihlar 2000).

In order to study the impact of wildfire on the landscape, researchers devised multi-temporal algorithms to analyze pre-burn and post-burn changes in IR reflectance to analyze characteristics of fire burn scars. Researchers employed low-resolution satellite sensor platforms such as the AVHRR and SPOT vegetation (VGT) to accomplish these studies (Brivio et al. 2003; De Moura and Galvao 2003; Fraser, Fernandes, and Latifovic 2003; Fraser, Li, and Cihlar 2000; Maselli et al. 2003; Zhang, Wooster, et al. 2003). Because these research projects involved the use of low-resolution (1 kilometer cell size) sensor platforms, they were capable of detecting fire scars and estimating burned area resulting from wildfires, but they were incapable of classifying areas of burn severity.

The field of wildfire burn assessment changed dramatically with the launch of the Landsat family of remote sensing satellites. The Landsat Thematic Mapper (TM) and Landsat Enhanced Thematic Mapper (ETM) provided access to high spatial resolution remote sensing imagery that was previously unavailable. Many past studies used relatively high spatial resolution Landsat data to validate burn scar detection models that employed other moderate spatial resolution remote sensors, such as the AVHRR or SPOT

VGT (Brivio et al. 2003; Zhang, Wooster, et al. 2003). Most scientists accept Landsat images as a highly reliable data source for burn scar analysis.

The applications of Landsat imagery for wildfire burn severity analysis are numerous. The primary method used to extract fire burn scar information from remotely sensed data is based on multi-temporal analysis of pre-burn and post-burn images of the burned area. This trend in the field of burn severity analysis began well over a decade ago and continues today. “Change detection algorithms provide for quantification of the pattern and extent of fire effects” (Miller and Yool 2002, 483). Although the same general methods are in use today to conduct multi-temporal analyses of fire burn scars, the higher spatial resolution of Landsat data allows researchers to classify changes in IR reflectance into categories of burn severity (Miller and Yool 2002). Prior to the launch of the Landsat TM and ETM satellites, burn severity analysis using space-based remote sensor platforms was difficult due to the poor spatial resolution of existing sensors such as the AVHRR and SPOT VGT. As my study will employ Landsat imagery to classify IR surface reflectance values into areas of unburned, low, moderate, and high burn severity, I will focus on the relevant literature that has a bearing on my study in the following section.

Relevant Work in the Field of Study

Much of the existing literature that I will discuss in this section pertains to the methods used to extract classes of burn severity from Landsat images. Researchers have employed a number of algorithms to remotely sensed data to assess burn severity. One of the most commonly used algorithms to assess the impact of fire burn scars from Landsat imagery is the Normalized Difference Vegetation Index (NDVI) (Key and Benson 1999;

Miller and Yool 2002). The NDVI algorithm uses both the red and near IR portions of the electromagnetic spectrum to detect temporal changes in reflectance in vegetation to detect burn scars because healthy vegetation is highly reflective in the red and near IR bands (De Moura and Galvao 2003; Fraser, Li, and Cihlar 2000; Maselli et al. 2003; Zhang, Wooster, et al. 2003).

$$\text{NDVI} = (\text{Band 4} - \text{Band 3}) / (\text{Band 4} + \text{Band 3})$$

Although many researchers conducted studies using NDVI as the primary algorithm to analyze multi-temporal changes in IR reflectance, other researchers employed alternative methods to assess the impact of fire on the landscape. Patterson and Yool (1998) conducted a study comparing principal components analysis (PCA) and Kauth-Thomas (KT) transforms and concluded that the KT transform technique is superior to PCA in extracting wildfire burn severity data. In a more recent study, Miller and Yool (2002) discussed the strengths and weaknesses of KT, PCA, and NDVI algorithms and concluded that each of these algorithms falls short of a recently developed algorithm termed the Normalized Burn Ratio (NBR). The NBR is similar in design to NDVI in that it compares two wavelengths to analyze reflectance values of vegetation, but it replaces the red band of the spectrum with a mid-IR band (Key and Benson 1999; Miller and Yool 2002).

$$\text{NBR} = (\text{Band 4} - \text{Band 7}) / (\text{Band 4} + \text{Band 7})$$

“Mid-infrared bands are sensitive to moisture content of soil and vegetation ...and also penetrate thin clouds and smoke better than visible bands” (Miller and Yool 2002, 482). Although NDVI, KT transform, and PCA are all useful methods to extract burn severity data, Miller and Yool (2002) provide compelling evidence that the NBR is the

most effective algorithm that is currently available to extract burn severity data from Landsat images. For this reason, my study will employ burn severity analysis techniques used by Miller and Yool (2002).

Wildfire Behavior Modeling

Research into the field of wildfire behavior modeling over the past three decades produced a variety of general approaches to fire modeling. A number of software packages exist that operate based on a particular approach to fire behavior modeling. I will discuss each of the general fire prediction modeling approaches as well as some of the more popular fire modeling software packages that have been developed using the various approaches to model wildfire.

Approaches to Wildfire Behavior Modeling

In order to develop models capable of quantifying wildfire spread and fire intensity, it is necessary to develop an understanding of the physics of wildfire behavior. Two seminal works provided the necessary foundation for wildfire behavior modeling to become a useful tool for forest managers. Rothermel (1972) developed mathematical equations to predict fire behavior such as fire intensity and rate of spread. A number of input parameters are necessary to execute the Rothermel model, and many of these input variables are difficult to obtain without detailed field studies.

A second breakthrough study permitted wildfire behavior modeling with much fewer input fuel variables. Anderson (1982) devised a widely accepted method to simplify fuel descriptions for the Rothermel model of wildfire behavior prediction.

Anderson organizes forest fuels into 13 fire behavior fuel models and provides detailed descriptions of each of these fuel models (Anderson 1982). Researchers interested in wildfire modeling easily adapted the Rothermel (1972) fire behavior model to incorporate the fire behavior fuel models described in Anderson (1982).

BEHAVE, one of the more popular fire behavior modeling programs, came into use by fire management officials in 1984 and is still in use today (Andrews and Bevins 1999). This computer software package is based on fire behavior equations developed by Rothermel (1972) and incorporates the 13 fire behavior fuel models (Anderson 1982). The BEHAVE fire modeling program outputs predicted rate of spread as well as fire intensity at the flaming portion of the fire front, and recent revisions to the BEHAVE program now allow additional output variables to be measured, such as crown fire spread and tree mortality (Albright and Meisner 1999; Andrews and Bevins 1999). Although BEHAVE provides valuable data to decision makers, it is severely limited due to the fact that the output of the model is inherently non-spatial (Andrews and Bevins 1999; Weinstein et al. 2004). Most forests are characterized by heterogeneous fuel distributions (Koutsias and Karteris 2003; Miller et al. 2003; Miller and Yool 2002; Riano et al. 2003; Scott and Jones 1994). For this reason, the BEHAVE model is handicapped due to its inability to model fire behavior across space (Andrews and Bevins 1999; Weinstein et al. 2004).

FARSITE is another software package based on equations from the Rothermel (1972) model, but is superior to BEHAVE because it assesses wildfire behavior across space and time (Albright and Meisner 1999; Finney and Andrews 1999). FARSITE incorporates elliptical wave propagation techniques into the fire spread algorithm, which

is based on the Huygens' Principle (Albright and Meisner 1999; Weinstein et al. 2004).

The Huygens' Principle states that a number of small fires at the fire front burn in elliptical patterns based on the assumption that fuel type, slope, wind speed, and fuel moisture are all homogeneous within each ellipse (Albright and Meisner 1999).

FARSITE calculates fire spread and total burned area by drawing a boundary encompassing all burned ellipses at each time step (Albright and Meisner 1999). It is apparent that fuel type, slope, wind speed, and fuel moisture will not be uniform within each of the small ellipses created by the FARSITE program, but this program does provide valuable information to decision makers regarding potential wildfire behavior.

FlamMap, another software package that acts as an extension to FARSITE, also assesses wildfire behavior patterns over space, but it does not incorporate a temporal component, as does FARSITE. FlamMap is useful for visualization of fire behavior patterns in 2D as well as "2.5D," but is more limited than FARSITE due to the lack of a temporal component.

The use of artificial neural networks (ANNs) to assess wildfire behavior is a unique approach that allows the computer to learn the rules regarding the effect of various input variables such as fuel loading and slope on the output fire behavior patterns. "Artificial neural networks acquire knowledge by learning from examples and store that knowledge as synaptic weights in connections (networks) between processing nodes" (McCormick, Brandner, and Allen 1999, 2). Neural network models are often thought of as a "black box" because data is input into the model and output comes out of the model without knowing the rules used by the model to derive the output. Neural network algorithms have the ability to assess wildfire behavior at multiple spatial scales

(McCormick, Brandner, and Allen 1999). Although neural networks have the potential to improve wildfire behavior modeling, it appears that much work in this field remains to be completed. McCormick, Brandner, and Allen (1999) discuss the advantages of ANN in the field of wildfire behavior modeling in their paper, but do not attempt to operationalize the ANN model described.

The different approaches toward wildfire modeling discussed to this point have both strengths and weaknesses. Cellular automata (CA) modeling is another technique that presents a unique perspective on wildfire behavior modeling. Two-dimensional cellular automata models allow researchers to simulate the spatial pattern of fire over time (Moreno, Ablan, and Tonella 2002), thus they are ideal for wildfire behavior modeling. The remainder of this paper discusses the progress of cellular automata in the field of wildfire behavior modeling.

History of Cellular Automata Modeling

The concept of cellular automata was developed by von Neumann and Ulam in the 1940's and 1950's (Brown et al. 2004; Bryan 2000; Liang, Liu, and Eck 2001; Ungerer 2000). Although additional progress in the field of CA continued in the 1950's and 1960's, it existed in relative obscurity until 1970, when John Conway's "Game of Life" was introduced (Liang, Liu, and Eck 2001; Ungerer 2000). The release of "Life" reinvigorated the field of cellular automata modeling, and the value of cellular automata in the field of wildfire behavior modeling became apparent.

Complex ecological processes have often been investigated globally using differential equations, but cellular automata models allow researchers to model complex

spatial-temporal processes such as wildfire using a simple set of transition rules that relate the current state of the processing (i,j) cell and its neighbors to the future state of the (i,j) cell (Bandini and Pavesi 2004; Brown et al. 2004; Wu 2000). Cellular automata are discrete in that each grid cell is an entity unto itself, but the state of each cell is dependent on the state of its neighbors. Change in cell values occur simultaneously at discrete time steps. “Cellular automata are a locally-adaptive, globally evolving n dimensional array of cells which are capable of modeling self-organizing behavior in systems” (Bryan 2000, 1). Because CA simulation models often exhibit self-organizing behavior, researchers can represent complex spatial-temporal processes such as wildfire by considering local interactions of individual cells and their neighbors.

Recent Trends in Wildfire Modeling via Cellular Automata

Researchers have used a number of techniques to apply cellular automata to wildfire behavior modeling. Certainly, researchers can apply CA to the field of wildfire behavior modeling in a number of ways. While this paper focuses on applications of cellular automata modeling as a tool to predict behavior of individual fires, researchers apply CA to model broad-scale wildfire behavior over long time periods in order to assess trends of increasing fire severity as well as impacts of wildfire on global climate change (Lenihan et al. 1997). The MCFIRE fire severity model incorporates coarse-scale data (10 km pixel size) to predict overall potential for severe wildfire events over extended time periods, such as over 100 years (Lenihan et al. 1997). Although models such as this are useful for modeling small-scale events to assess overall impact on global climate, these models are of little or no use when assessing fire behavior at larger scales

for individual fire events. Scale is an important consideration during the model design portion of any wildfire modeling study.

Some researchers use percolation theory in their wildfire behavior models.

Percolation models are relatively simple cellular automata. Fire spread from one cell to another is based on the presence of unburned fuel in neighboring cells as well as the probability of spread to adjacent cells (Albright and Meisner 1999; Nahmias et al. 2000). Applications of percolation theory to fire behavior modeling have primarily focused on homogeneous fuel distributions (Nahmias et al. 2000). As discussed previously, the spatial distribution of fuels across the landscape is rarely homogeneous (Koutsias and Karteris 2003; Miller et al. 2003; Miller and Yool 2002; Riano et al. 2003; Scott and Jones 1994). Models employing percolation theory must be precisely calibrated in order to determine the probability of spread from one cell to another (Albright and Meisner 1999). This limits the ability of the model to predict fire behavior as the probability of spread must be determined based on the unique characteristics of each study site. Wildfire behavior models based on percolation theory must be recalibrated if applied in a physical setting other than which they were created (Albright and Meisner 1999; McCormick, Brandner, and Allen 1999; Nahmias et al. 2000).

Liu and Chou (1997) constructed a model to predict wildfire growth using cellular automata methodology. This model uses all cells in a 3x3 neighborhood to predict wildfire spread. The authors initially developed a “probability of fire spread” surface using linear regression methods. The following independent variables were considered in developing this probability surface: area of polygon, polygon perimeter, fire rotation weight defined by vegetation, distance of polygon from buildings, distance of polygon

from campgrounds, distance of polygon from roads, July maximum temperature, July maximum precipitation, spatial term of neighborhood effects (Liu and Chou 1997). A stepwise regression analysis of these independent variables resulted in the following regression equation:

$$UI = -8.89 - 2.445(\text{fire rotation weight}) - 0.2110(\text{July maximum temperature}) + 34.14(\text{spatial term of neighborhood effects}) \quad (1)$$

Determination of a fire occurrence probability value for each grid cell resulted from the above regression equation. The probability value for each cell was compared against random numbers generated for each of the cell's 8 neighbors to determine which cell would be ignited by the initially burning cell (Liu and Chou 1997). The authors employed the fire behavior equations developed by Rothermel (1972) to determine rate of fire spread and fireline intensity values. Although this model successfully identified more than 50% of the cells that burned in an actual fire that occurred in California, the model did not attempt to investigate additional fire characteristics beyond rate of spread and fireline intensity, which are included in most fire behavior models. Nevertheless, this model does show the power of grid automata methods in assessing wildfire growth.

The enormous fire events of the 1988 Yellowstone National Park Fire prompted the construction of EMBYR (Ecological Model for Burning the Yellowstone Region), a cellular automata-based computer simulation program. Similar to the CA model developed by Liu and Chou (1997), EMBYR is a probabilistic model in that fire spreads from one cell to its 8 neighboring cells based on the impact of fuel type, fuel moisture, wind speed, and wind direction on fire spread probability (Hargrove et al. 2000).

EMBYR incorporates the effects of firebrands, which are glowing embers carried downwind that can ignite unburned areas far from the fire front (Hargrove et al. 2000). Spot fires produced from firebrands often play a large role in fire behavior patterns, thus this is an important variable to consider (Rothermel 1972). Because EMBYR is a probabilistic model, it is useful to run the simulation model multiple times to generate an average pattern of fire spread.

Cellular automata models based on diffusion limited aggregation (DLA) model a variety of phenomena, such as urban growth. This process is based on the theory that growth of a phenomena occurs onto existing areas already possessing the phenomena in question. DLA processes were used as the basis of a cellular automaton to model wildfire as well (Clarke, Brass, and Riggan 1994). In this model, fire moves outward from a burning cell into the surrounding 8 cells. A random number is generated to determine which direction the fire will move, although weights are assigned to cells based on wind direction, wind magnitude, slope, aspect, and fuel loading (Clarke, Brass, and Riggan 1994). A burning cell will continue to propagate fire to its neighboring cells until no unburned fuel is available in the neighboring cells.

The authors of this article point out the critical importance of calibrating any cellular automata using an actual fire event for reference in the calibration process. Calibration of the CA model and analysis of the results of the simulation showed that pixels determined by the CA model to have greater than 50% odds of burning matched actual burned pixels 82.5% of the time (Clarke, Brass, and Riggan 1994). Although this model produced encouraging results, there are a number of limitations. Fuel loading values for each grid cell were obtained by assessment of red band reflectance of

vegetation, which is not an ideal method to assess fuel loading characteristics (Clarke, Brass, and Riggan 1994). The authors assigned wind speed and wind direction constant values. It is clear that these variables are not constant, but it is apparent that we must simplify the complexity of the vast number of variables in order to create a feasible model (Clarke 2003; Weinstein et al. 2004).

Formulating transition rules for the cellular automaton model is a primary consideration in the model design process. Because CA models are based on local interactions to model overall fire behavior, local rules must attempt to represent potential fire behavior as accurately as possible, while maintaining a sufficient degree of simplicity to permit the modeler to create a feasible model. Using a 3x3 cell neighborhood, Karafyllidis and Thanailakis (1997) developed the following formula to determine the state of cell (i, j) based on the current state of the (i, j) cell and its 8 neighbors:

$$S_{i,j}(t+1) = S_{i,j}(t) + (S_{i-1,j}(t) + S_{i,j-1}(t) + S_{i,j+1}(t) + S_{i+1,j}(t) + 0.83(S_{i-1,j-1}(t) + S_{i-1,j+1}(t) + S_{i+1,j-1}(t) + S_{i+1,j+1}(t))) \quad (2)$$

$S_{i,j}(t+1)$ represents the value of cell (i, j) at next time step $(t+1)$ equals the current state of cell (i, j) plus the current state of all neighboring cells. A value of “0” represents an unburned cell, and a value of “1” represents a completely burned cell. The value of $S_{i,j}(t+1)$ can range from 0 to 1, but cannot exceed 1. It is possible for the result of the above equation to exceed a value of 1, but the number is rounded down to 1 in these circumstances (Karafyllidis and Thanailakis 1997).

The authors modified the general local rule described above by assigning weights for all cells in the neighborhood for wind speed and direction as well as slope. The authors discussed the effects of fuel type on fire spread rate, but did not incorporate

this significant variable in their model. This article reinforces the importance of creating valid local transition rules for any CA-based wildfire modeling experiment, but limitations of the model in terms of the effects of the spatial distribution of heterogeneous fuels across the landscape limits the ability of this cellular automaton to model wildfire behavior with any degree of accuracy.

The limitations of the model proposed by Karafyllidis and Thanailakis (1997) generated further interest in the research community in regard to wildfire behavior modeling. Berjak and Hearne (2002) incorporated fire behavior equations developed by Rothermel (1972) into the cellular automaton developed by Karafyllidis and Thanailakis (1997) in an attempt to improve this CA model. Improvements in incorporating heterogeneous fuel distributions across the landscape were made possible by utilizing the 13 fire fuel models to include fuel loading, fuel moisture, and fuel bed depth into the CA model (Anderson 1982). This modification to the original cellular automaton enabled the model to determine if fuels from the burning (i, j) cell produced sufficient heat to ignite fuels in the neighboring cells (Berjak and Hearne 2002). This factor is a key consideration in landscapes characterized by spatially heterogeneous fuel distributions.

The incorporation of the Anderson (1982) fuel models into the cellular automaton did affect rate of fire spread when researchers conducted simulations using heterogeneous fuel distributions. Fuel moisture did not affect the shape of the fire fronts in the improved CA model, but fuel moisture did have an impact on the ability of fine fuels to burn more coarse fuels that possessed higher moisture contents (Berjak and Hearne 2002). Comparison of the results of actual fire events to the results of the wildfire behavior simulation confirm that the modifications to the original CA model developed

by Karafyllidis and Thanailakis (1997) clearly improved the predictive power of the model (Berjak and Hearne 2002).

Future Directions in Wildfire Behavior Modeling via Cellular Automata

It is apparent that recent research into wildfire behavior modeling via cellular automata simulations resulted in improvements in modeling techniques. Nevertheless, a number of future research opportunities exist in this field. The majority of attempts to predict wildfire behavior via cellular automata simulation have focused on predicting rate of fire spread, shape of fire patterns on the landscape, and calculating total area burned by wildfire. Each of the studies discussed are limited in their ability to predict wildfire behavior patterns. This is largely due to the extraordinarily complex nature of fire itself. Although it is necessary to simplify the complex process of wildfire in order to create a feasible spatial-temporal simulation model, additional considerations will undoubtedly improve the effectiveness of cellular automata simulations to model a wide range of fire characteristics.

One variable that wildfire behavior models overlook is the effect of burning cells behind the flaming front. Areas with high quantities of large diameter fuels (> 3 inches in diameter) such as logging slash continue to burn long after the fire front passes. Fuels such as this may continue to burn for days after the fire ignited them, and these extended fire residence times often lead to the liberation of organic compounds from the soil and increased soil hydrophobicity (Graham, McCaffrey, and Jain 2004). These changes in soil properties often result in severe soil erosion, which affects vegetation re-growth, watershed flash flood potential, and may result in landsliding (Legleiter et al. 2003; Miller and Yool 2002).

Incorporating residence time of burning fuels behind the fire front into the cellular automaton would be the first important step toward effectively modeling wildfire burn severity on an individual fire basis, which is a dimension of wildfire behavior modeling that has not been addressed in the literature to date. Mitigating the adverse effects of severe wildfire on the landscape is the primary concern of Burned Area Emergency Response (BAER) teams in the United States. Currently, BAER teams use pre-fire and post-fire remotely sensed imagery in concert with ground truth data to assess wildfire burn severity, but a CA based wildfire burn severity prediction model would allow BAER teams to identify areas that will likely require post-fire rehabilitation before the fire burns the areas in question (Graham, McCaffrey, and Jain 2004).

The incorporation of a burn severity component into CA based fire behavior models would be highly useful to fire managers as well. Clarke et al. (1994) point out that running simulations based on probabilistic cellular automata models multiple times allows for the calculation of fire risk. This same principle would allow forest managers to use a CA based wildfire burn severity model to estimate burn severity risk within forested areas. It is well known that fuel treatments, such as removal of excess fuels in the forest understory by means of prescribed fire or mechanical thinning, has an effect on fire propagation as well as fire severity (Graham, McCaffrey, and Jain 2004; Graham et al. 2003). Of the number of variables that affect wildfire burn severity, it is apparent that only fuels can be modified by humans to reduce risk of severe wildfire (Koutsias and Karteris 2003; Graham, McCaffrey, and Jain 2004). For this reason, it is critical to incorporate variables that assess the effect of fuels on wildfire burn severity in any fire burn severity model.

CHAPTER III

STUDY AREAS

Three large wildfire events in the western United States were included in this study. Each of these three wildfires took place during the 2002 fire season, in which a large number of particularly large, severe wildfires occurred. All three study sites possess vegetation characteristic of fire-dependent ecosystems that characterize the western United States. A combination of vegetation, weather, and topographic conditions interacted to produce the dramatic fire events observed at each of these sites.

Hayman Fire

The Hayman wildfire occurred on June 8, 2002 and rapidly grew to over 60,000 acres by the end of June 9, 2002 largely due to a combination of high wind conditions, prolonged drought, high fuel loadings, and topography. The fire died out on June 28, but burned approximately 138,000 acres of forest in the region before it was fully contained (Graham et al. 2003). This event was the single largest wildfire in recorded history in Colorado (Graham et al. 2003). The Hayman fire was located approximately 50 miles south-southwest of Denver, Colorado and approximately 30 miles northwest of Colorado Springs, Colorado (Figure 1).

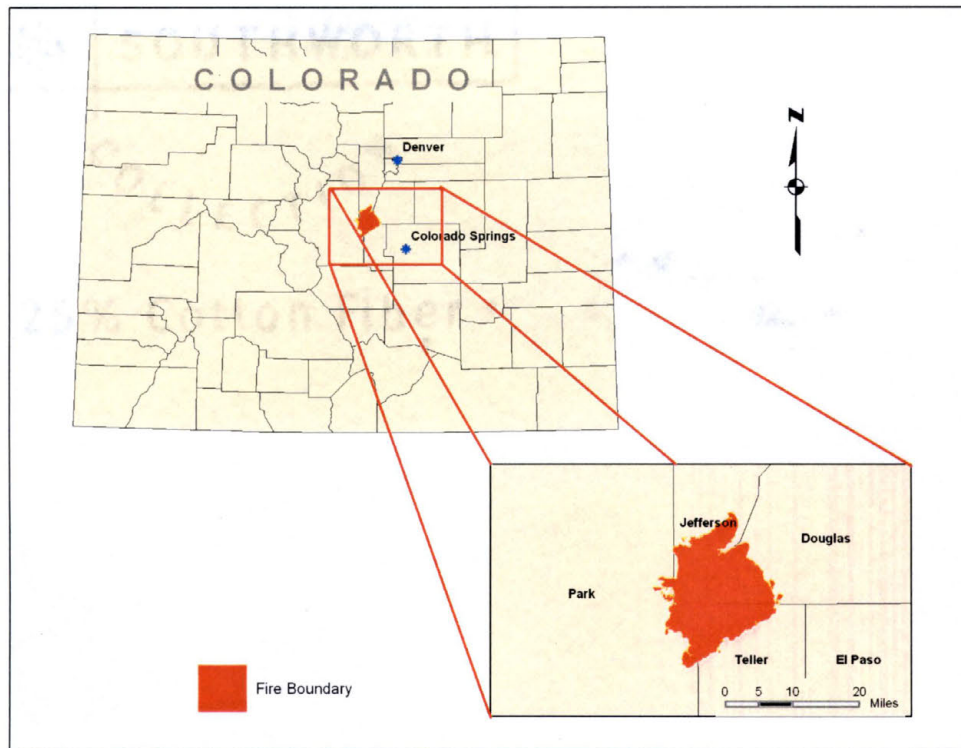


Figure 1: Location of Hayman fire study area

Ponderosa pine and Douglas-fir dominate the Hayman fire study area, although aspen and blue spruce are found throughout the area as well (Graham et al 2003). Slope aspect has a substantial impact on the amount of forest fuel available in the study area. Douglas fir was the predominant vegetation type on north-facing slopes while ponderosa pine was commonly found on south-facing slopes (Graham et al 2003). Terrain varies throughout the study area, ranging from more gentle slopes on the eastern side of the fire to rugged, steep terrain in the western and northern portions of the study area (Graham et al. 2003). Climate also played a major role in the Hayman fire. Forest fuel moisture was extremely low at the time of the fire due to drought conditions at the time of the fire (Graham et al. 2003). Fire weather varied from day-to-day, but large portions of the study area burned quickly on days with wind gusts as high as 51 miles per hour (Graham et al. 2003).

Missionary Ridge Fire

The Missionary Ridge fire ignited on June 9 2002 and rapidly burned through extremely dry forest fuels, eventually burning over of 70,000 acres in Southwestern Colorado (USDA Forest Service 2002). This Missionary Ridge fire was located approximately 10 miles northeast of Durango, Colorado (Figure 2). A mixture of deciduous trees (Gambel oak and aspen) and conifers (Douglas fir, lodgepole pine, ponderosa pine, Rocky Mountain juniper, Engleman spruce) characterizes the study area (USDA Forest Service 2002). Assessing burn severity in study sites possessing heterogeneous spatial distribution of forest fuels effectively demonstrates the effectiveness of the burn severity assessment algorithm.

As was the case in the Hayman fire, the vegetation present at the Missionary Ridge fire study area was extremely dry as a result of drought conditions. High fuel loads possessing little moisture allowed this fire to advance rapidly and burn certain portions of the study area severely (USDA Forest Service 2002). The terrain of the study area influenced the fuel loadings present at the study site, which in turn affected potential burn severity (Kushla and Ripple 1997; Patterson and Yool 1998).

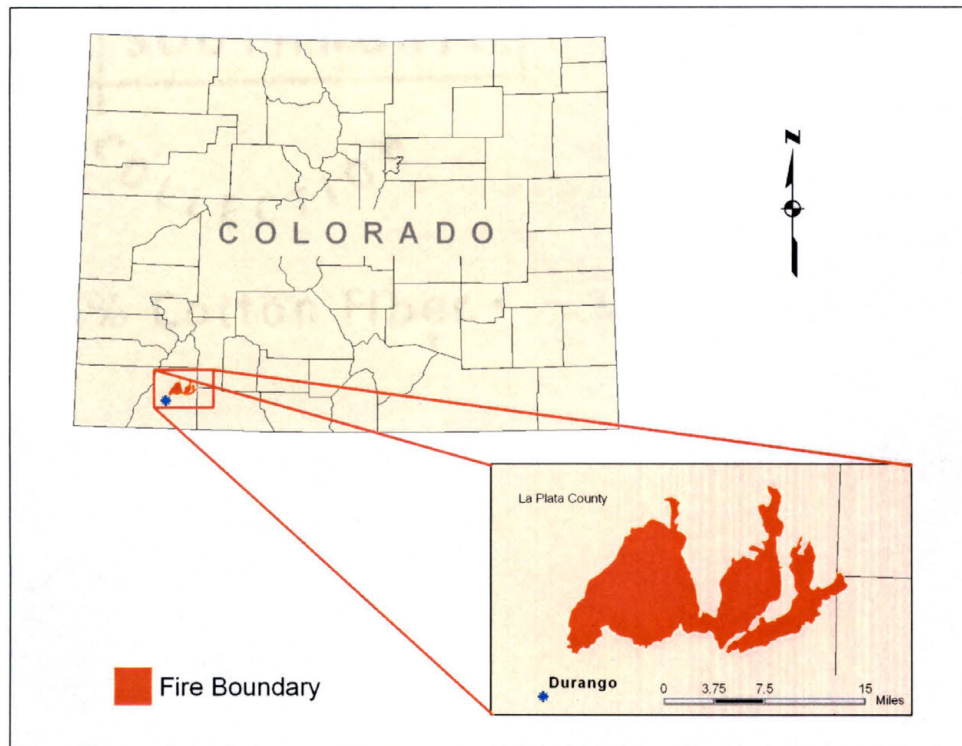


Figure 2: Location of Missionary Ridge fire study area

Rodeo-Chediski Fire

The Rodeo-Chediski fire was the largest wildfire in Arizona's recorded history (Wilmes et al. 2002). The fire was located approximately 100 miles northeast of Phoenix, Arizona (Figure 3). It began on June 18, 2002 and consumed approximately 467,000 acres of fuel by the time it was contained on July 7, 2002 (Wilmes et al. 2002). The fuels present prior to the fire event vary spatially, but the dominant plant species were conifers such as Ponderosa pine along with mixed Gambel oak, Manzanita, Ceanothus, and Mountain Mahogany (Wilmes et al. 2002). Drought conditions magnified the severity of the fire as well. Applying the differenced NBR algorithm to this study site will test the proposed burn severity assessment method in a vegetation regime unique to this study site.

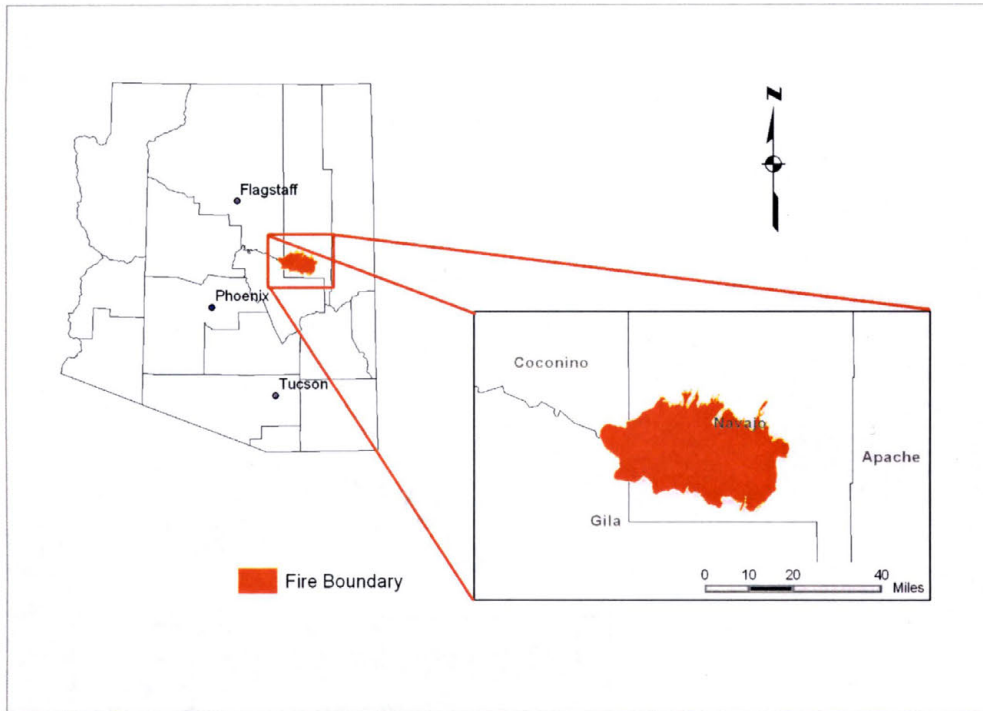


Figure 3: Location of Rodeo-Chediski fire study area

CHAPTER IV

THEORETICAL FRAMEWORK

My study employed remote sensing and geospatial modeling to analyze burn severity of large western US wildfires. As the spatial distribution of forest fuels is integral to developing a thorough understanding of wildfire behavior, particularly in terms of wildfire burn severity, it is necessary to understand how the existing forest structure developed into its state prior to the fire events studied. Plant succession theory, also known as vegetation dynamics theory, underpins my investigation. Plant succession theory describes forests as dynamic systems that seek equilibrium in a given environment.

Currently, the ability to predict wildfire behavior is limited. “When vegetation is distributed uniformly and continuously, fire will travel uninterrupted, but heterogeneity in forest canopy cover causes fires to spread along preferential paths” (Riano et al. 2003, 177). Plant succession theory explains why unique species coexist in ecosystems and provides insight into the pattern of vegetation recovery after a fire. Wildfires play an important role in plant succession. Fire affects plant growth and encourages competition of various plant species (Rieske 2002). I will discuss vegetation dynamics theory further as a framework for my study. Autogenic plant succession produced the vegetation regime that existed in the study areas prior to the fire event over an extended period of time. This form of plant succession is the result of the gradual rise of a plant community

from bare soil or from an abandoned field (Glen-Lewin, Peet, and Veblen 1992; Strahler and Strahler 2003). Damage caused by wildfires upsets the process of autogenic succession. An understanding of plant succession as it relates to both pre-fire and post-fire conditions is necessary to analyze wildfire burn severity as well as post-fire recovery.

Plant Succession: Pre-burn

Succession theory dictates the distribution of vegetation across space, and the spatial distribution of vegetation types has a substantial impact on fire behavior (Graham, McCaffrey, and Jain 2004; Miller et al. 2003; Riano et al. 2003). A number of factors influence vegetation dynamics in most ecosystems. Topography plays a major role in plant succession. “Different topographical patterns create different patterns of climatic conditions at multiple scales, which predetermine vegetation succession and dynamics” (Koutsias and Karteris 2003, 3096). Miller et al. (2003) concur that topography influences forest fuel distributions. Slope aspect often influences vegetation patterns. For example, forest fuels often vary from a north-facing slope to a south-facing slope because of differences in the amount of insolation received, precipitation levels, and wind effects (Koutsias and Karteris 2003; Miller et al. 2003). Slope also has an impact on the type of vegetation that will exist in a particular location. Certain vegetation types are well suited to steep slopes, but other plants have root systems that do not adapt well to these areas. It is apparent that topography may have a substantial impact on plant succession. Knowledge of the impact of topography on vegetation dynamics will allow for a more thorough understanding of wildfire behavior at the study site.

A number of additional factors that interact with topography also affect succession. Climate acts as a dominant factor in shaping the vegetative regime in all ecosystems (Scott and Jones 1994). Precipitation levels, wind direction and speed, humidity, and seasonality all affect the types of ground cover present. To a degree, topography causes variations in climate. Another variable that affects vegetation dynamics is availability of light. Plants must compete for light to survive and grow, and light is not uniformly available to all vegetation (Perry, Neuhauser, and Galatowitsch 2003). Topography influences light availability, particularly in terms of aspect. Plant succession theory provides valuable insight into the spatial distribution of vegetation and permits a more thorough analysis of the proposed burn severity model.

Plant Succession: Post-burn

An understanding of the autogenic successional regime is important to explain the existing plant community prior to a wildfire, but assessment of recovery after the fire event is also grounded in vegetation dynamics theory. The effects of a wildfire can be beneficial in some circumstances and devastating to a plant community in others. Wright (2004) compared a relatively low temperature fire in Shenandoah National Park to a devastating fire at Los Alamos, New Mexico. He noted that the low temperature fire in Shenandoah National Park allowed for the removal of large amounts of understory fuels. Plant succession quickly replaced damaged foliage to produce a healthy forest. The wildfire that burned Los Alamos, on the other hand, was a higher temperature fire due to climatic conditions and vegetation types present. The intense heat altered soil properties and impeded the progress of succession (Wright 2004). Past research in the field of

vegetation dynamics allows scientists to conclude that removal of undergrowth during the low temperature Shenandoah fire will allow fresh growth to compete for resources such as light and soil nutrients, whereas primary succession will need to occur in the bare soils resulting from the severe Los Alamos fire (Shugart 1984).

Investigations should also consider the effects of fire frequency on vegetation recovery. Ecosystems that are subject to frequent fires typically exhibit plant species that are well adapted to fire and can recover much more quickly than plant communities that are rarely affected by fire events. Franklin et al. (2001) performed computer simulations to evaluate vegetation dynamics in both frequent and infrequent fire regimes.

Simulations determined that infrequent fire regimes resulted in a landscape composed of long-lived species that were much more vulnerable to prolonged wildfire damage than plant communities that often experience wildfire events (Franklin et al. 2001).

Vegetation dynamics theory provides the necessary framework to analyze burn severity by providing a context for the pre-fire distribution of vegetation and supplies a model for assessment of post-fire vegetation recovery as well.

CHAPTER V

WORKING HYPOTHESES

The Relationship between Landscape Characteristics and Burn Severity

One of the primary goals of my research project is to determine the relationship between landscape characteristics and fire severity. A deeper understanding of these relationships could provide fire managers with a new tool to analyze the impact of wildfire on the natural environment. I believe that there is a relationship between landscape characteristics and wildfire burn severity. To test this hypothesis, I will divide this statement into two working hypotheses. One hypothesis addresses the possible relationship between forest fuel characteristics and burn severity, and the other addresses the influence of terrain characteristics on burn severity.

Hypothesis 1 Is there a relationship between forest fuel characteristics and wildfire burn severity? It is well known that wildfires spread and move due to the spatial distribution of fuels (Koutsias and Karteris 2003; Miller and Yool 2002; Riano et al. 2003; Scott and Jones 1994). “A spatial description of wildland fuels is essential to assessing fire hazard and risk across a landscape” (Miller et al. 2003, 239). While most existing literature addresses how fire movement is affected by vegetation, my study will attempt to establish if there is a relationship between fuel characteristics such as fuel loading and fuel particle size with burn severity at my study site in addition to simulating the propagation of fire across the landscape. A number of variables, such as fuel

distribution, wind direction, fuel moisture, and topography, affect fire spread and burn severity. Because many variables influence fire behavior, it is likely that a number of these variables work together to produce the observed effects of wildfire on the landscape. The ability of cellular automata to incorporate a number of unique variables into the spatial-temporal model will allow me to gain insight into the effects of forest fuel characteristics on overall burn severity patterns.

Hypothesis 2: My second working hypothesis that addresses the impact of the landscape on fire severity concerns the role of terrain in altering fire behavior. Is there a relationship between terrain and wildfire burn severity? A number of terrain characteristics potentially influence burn severity. Slope and aspect have the potential to impact fire behavior (Koutsias and Karteris 2003; Kushla and Ripple 1997; Miller et al. 2003; Patterson and Yool 1998). I analyzed these terrain characteristics to ascertain how they affected the burn severity model.

It is critical to note that the possibility of committing a Type I error in this section of the analysis is of great concern due to the relationship between certain terrain characteristics and other factors that could affect the results. For example, it is known that there is an established relationship between vegetation type and terrain characteristics such as aspect, slope, and elevation (Koutsias and Karteris 2003; Miller et al. 2003; Patterson and Yool 1998). Any existing relationship between vegetation type and fire severity could cause me to conclude that terrain influences burn severity because terrain and vegetation variables are interrelated, to a degree. Due to the complex nature of wildfire behavior, it is difficult in many circumstances to separate the impact of such

interrelated variables on fire behavior. Nevertheless, it is useful to investigate these relationships.

Impact of Fire Residence Time on Burn Severity

The second major goal of my proposed research was to address the impact of fires burning behind the fire front on wildfire burn severity. It appears that no existing wildfire behavior model accounts for the fact that large diameter fuels continue to burn for extended periods after the flaming fire front passes. As fires continue burning behind the fire front, additional heat is transferred into the soil, which often liberates organic compounds from the soil and tends to lead to soil hydrophobicity (Graham, McCaffrey, and Jain 2004). These changes in soil properties are characteristics associated with areas defined as high burn severity on BAER maps.

Hypothesis 3: Is there a relationship between fire residence time and fire burn severity? My CA based wildfire behavior model produced a general estimate of fire residence time based on fuel characteristics for each grid cell. Using the resulting estimate of fire residence time for each grid cell, a general estimate of total heat produced in each burning cell prior to fire extinction became possible. Classification of total energy release per burning cell permits a comparison of the resulting output surface from the model to existing BAER burn severity maps. Comparison of these maps assisted in the determination if any relationship exists between fire residence time and wildfire burn severity.

CHAPTER VI

DATA: REMOTE SENSING ASSESSMENT OF WILDFIRE BURN SEVERITY

The multi-temporal differencing algorithm that I employed to assess wildfire burn severity at each of my study sites requires both pre-fire and post fire Landsat images to assess changes in vegetation reflectance. Due to seasonal changes in vegetation reflectance, it is critical to obtain Landsat images acquired during the same season as the post-burn imagery (Fraser, Fernandes, and Latifovic 2003; Fraser, Li, and Cihlar 2000; Key and Benson 1999; Zhang, Wooster, et al. 2003). Multi-temporal analyses based on imagery acquired during different times of the year are subject to error due to these seasonal changes in vegetation reflectance. Pre-fire imagery acquired during prior years does not adversely affect the change detection algorithm as long as seasonality of the pre-fire and post-fire images is uniform (Key and Benson 1999; Miller and Yool 2002). I acquired all Landsat imagery from a USGS website devoted to disseminating data regarding their recent wildfire burn severity mapping projects (National Park Service and USGS 2004). The Landsat 5 Thematic Mapper (TM) satellite acquired all imagery used for this study.

Hayman Fire Data

Both the pre-fire and post-fire imagery for the Hayman fire were pre-processed TIFF format images. These images were orthorectified and projected to UTM Zone 13,

NAD 1927 datum. The two bands of interest in this layer, band 4 and band 7, were separated into separate layers using the “subset” function of ERDAS Imagine. This permitted me to plug each of the data layers into the differenced normalized burn ratio (dNBR) algorithm described previously. Landsat bands 4 and 7 both have spatial resolutions of 30 meters and 8-bit radiometric resolutions. I also used the pre-burn and post-burn Landsat images for general reference. The true-color pre-burn Landsat image was draped over elevation data for the study site for visualization purposes. I acquired 30-meter elevation data for the study site from the USGS Seamless Data Distribution system at <http://seamless.usgs.gov/>.

The date of acquisition for the pre-fire image was May 12, 2001, one year prior to the Hayman fire but less than one month prior to the fire event in terms of seasonality. This image reflects vegetation conditions that are relatively similar to the conditions present on the date of fire ignition. There is some cloud cover in the image, but the majority of the cloud cover lies to the northwest of the fire boundary. A few small clouds lie within the fire boundary. Variations in reflectance due to cloud cover and cloud shadows will have minimal impact on the dNBR algorithm.

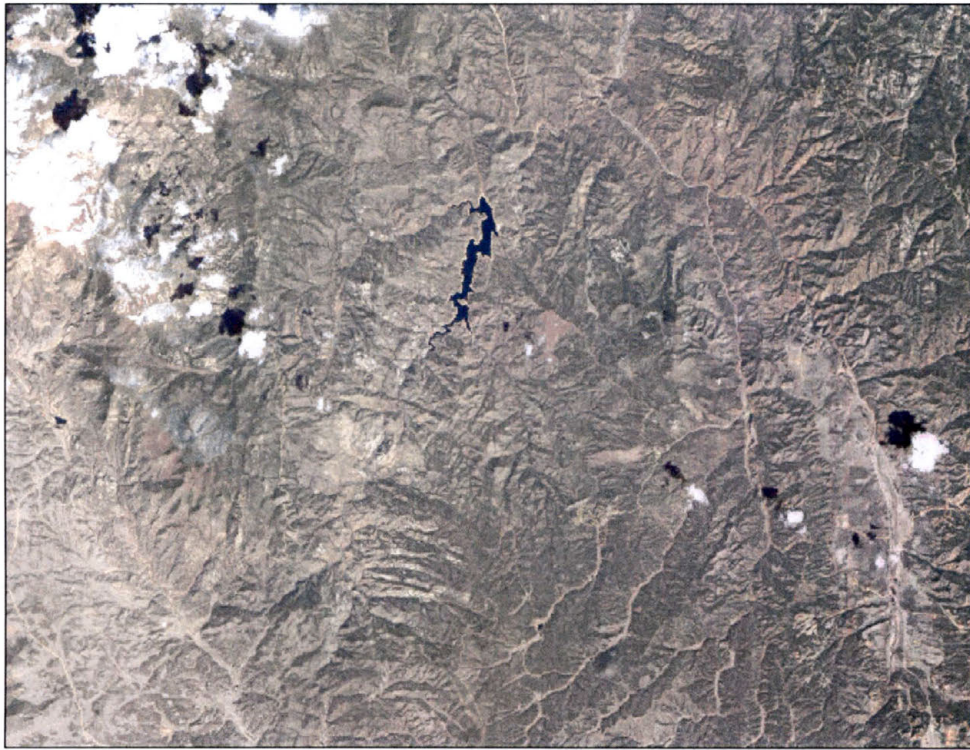


Figure 4: True-color pre-burn Landsat TM image of Hayman fire study area

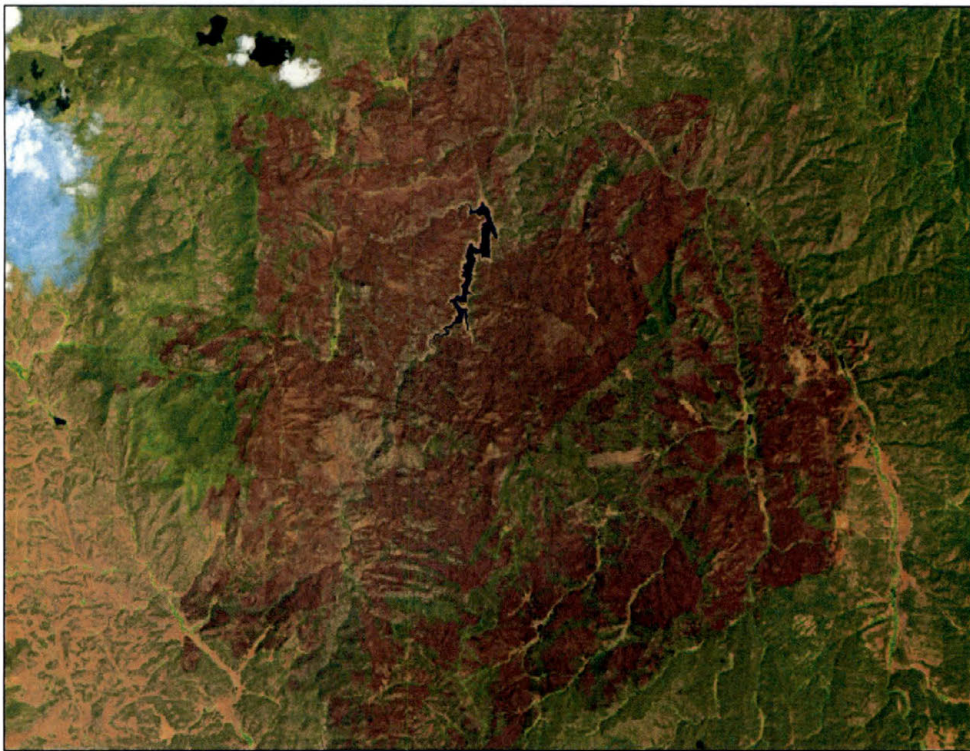


Figure 5: False-color post-fire Landsat TM image of Hayman fire study area

Metadata for the post-fire image shows that the date of acquisition was July 2, 2002, which is less than one week after the end of the Hayman fire event. It is apparent that smoke effects are minimal to nonexistent at the time of image acquisition. Again, there is some cloud cover in this image, but the few clouds in the image are outside the fire boundary. Cloud cover in the post-fire image is not an issue.

Missionary Ridge Data

Both the pre-fire and post-fire imagery for the Missionary Ridge fire were pre-processed TIFF format images. These images were orthorectified and projected to UTM Zone 13, NAD 1927 datum. I utilized the “subset” function of ERDAS Imagine to separate band 4 and band 7 into separate files for later use in the dNBR algorithm. All Landsat TM data used for this portion of the study has a spatial resolution of 30 meters and 8-bit radiometric resolution. False color pre-burn and post-burn Landsat images served as a general reference. A false color pre-burn Landsat image was draped over elevation data for the study site for visualization purposes. I acquired the elevation data mentioned above from the USGS Seamless Data Distribution system at <http://seamless.usgs.gov/>. The date of acquisition for the pre-fire Landsat image was June 11, 2001, which is one year prior to the fire event. As this image captured vegetation during the same season as the date of fire ignition, the impact of vegetation change from the pre-fire image to the time of the fire event is minimized. Cloud cover in the pre-fire image is nonexistent, thus there is no concern of cloud cover affecting results due to the pre-fire image.

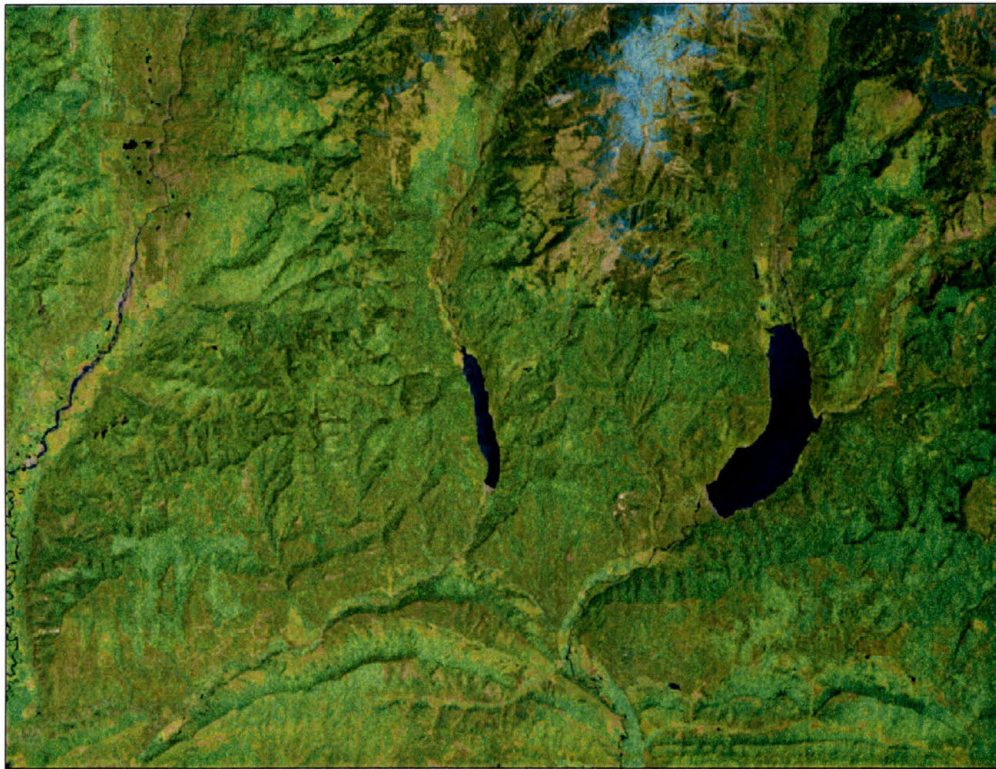


Figure 6: False-color pre-fire Landsat TM image of Missionary Ridge study area

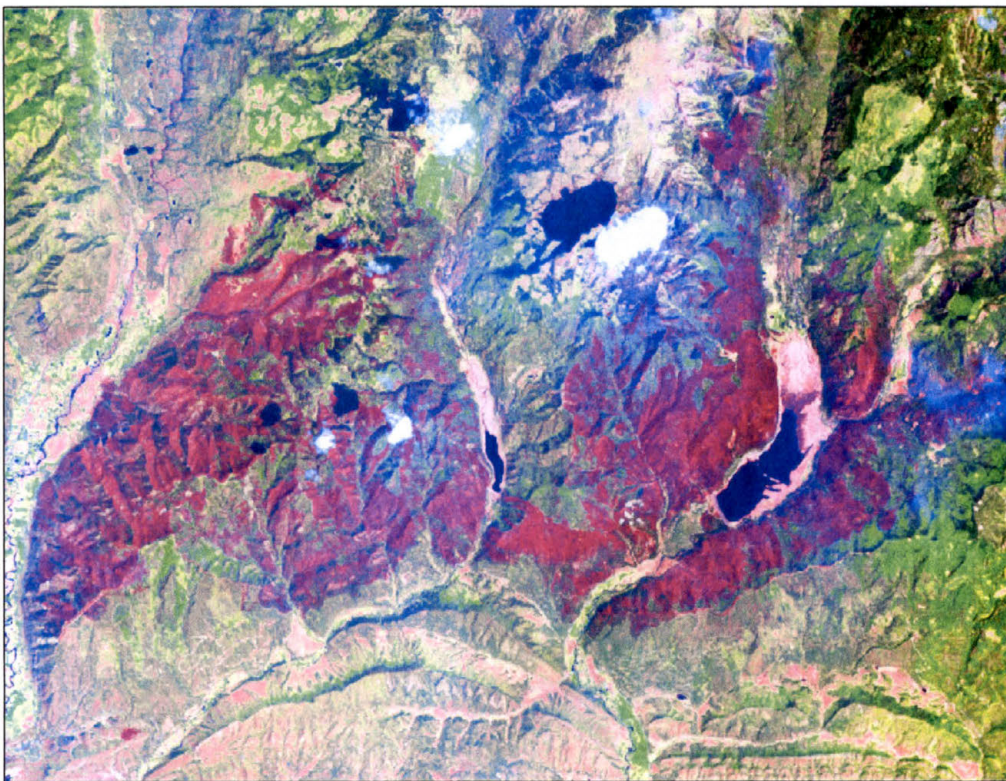


Figure 7: False-color post-burn Landsat TM image of Missionary Ridge study site

The post-fire Landsat TM image is dated June 30, 2002. The bulk of fire activity ended prior to this time, but thin smoke is still visible in this image due to small spot fires that were still burning at the time of image acquisition. Luckily, “mid-infrared bands penetrate thin clouds and smoke better than visible bands” (Miller and Yool 2002, 482). As the dNBR utilizes NIR and mid-IR bands, much of the smoke effects are minimized. Cloud cover in the post-burn image will have some impact on the results of the analysis due to a couple of small clouds and their shadows just left of center (Figure 7). Due to the limited availability of free Landsat data, this image is the best available for this study.

Rodeo-Chediski Data

Landsat imagery collected for the Rodeo-Chediski fire analysis are TIFF format images. Both images were acquired by the Landsat 5 TM satellite, were orthorectified, and then projected to UTM Zone 12, NAD 1927. I used the “subset” function of ERDAS Imagine to separate band 4 and band 7 into separate data layers for later incorporation in the dNBR model. Both of these bands have a spatial resolution of 30 meters and 8-bit radiometric resolution. I draped a false color infrared image of the study area during pre-fire conditions over a local elevation layer for visualization purposes. Elevation data originates from the USGS Seamless Data Distribution System via <http://seamless.usgs.gov/>.

The date of acquisition for the pre-fire image was June 5, 2002, which was two weeks prior to the fire event. Vegetation reflectance values in band 4 and band 7 would be relatively similar to reflectance values on the date of the fire event. The pre-fire image is cloud-free, thus cloud cover is not a concern in the pre-fire image (Figure 8).



Figure 8: False-color pre-burn Landsat TM image of Rodeo-Chediski study area

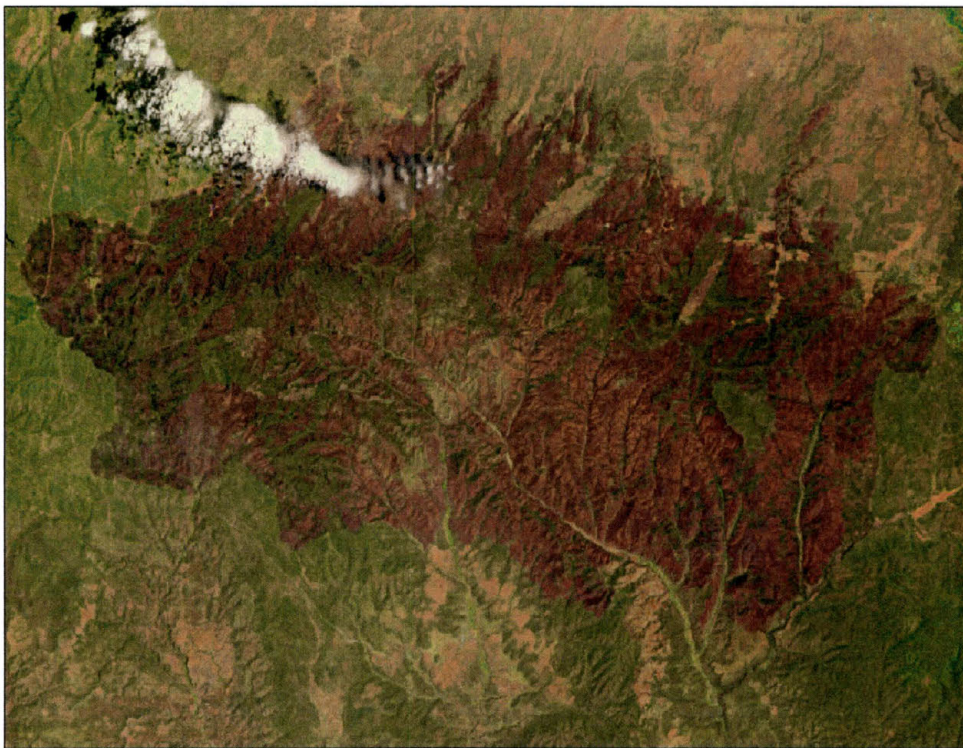


Figure 9: False-color post-fire Landsat TM image of Rodeo-Chediski study area

The date of acquisition of the post-fire image was July 7, 2002. This date is significant as it is same date that the Rodeo-Chediski was officially declared “contained.” It does not appear that smoke effects will have an impact on the results of the analysis, as a review of the images shows no active fires burning at the time of image acquisition. A band of clouds obscures a portion of the burned area in the post-fire image. This cloud cover will alter the reflectance values in both bands 4 and 7, thus the dNBR values for the obscured area will not be accurate. I will exclude the portion of the burned area obscured by cloud cover or covered in the cloud shadow to prevent inaccuracies in the dNBR results. Unfortunately, by excluding a portion of the study area from analysis, inaccuracies in area calculations will result.

CHAPTER VII

DATA: WILDFIRE BEHAVIOR MODELING

The modeling portion of my study requires more unique data types to produce a burn severity map than does the dNBR burn severity assessment algorithm. Forest fuel data are necessary to construct any fire behavior model. Classification of pre-fire Landsat TM images into Anderson (1982) fuel models yields a number of unique fuel variables such as fuel loading that I will include in the burn severity model. Ancillary GIS data from the US Forest Service in the form of georeferenced JPEG images will help inform the fuel model classification. The methods employed to classify Landsat imagery into Anderson (1982) fuel models will be discussed in the methodology section of the study. I will also discuss the various fuel types that characterize the study area in detail in Chapter 11. Figure 10 displays the heterogeneous distribution of fuels across the landscape of the Hayman fire study site. The heterogeneous distribution of forest fuels across the study area will affect fire propagation across the landscape (Koutsias and Karteris 2003; Miller and Yool 2002; Riano et al. 2003; Scott and Jones 1994). For this reason, it is necessary to incorporate the effects of changes in fuel type across space in the wildfire behavior model.

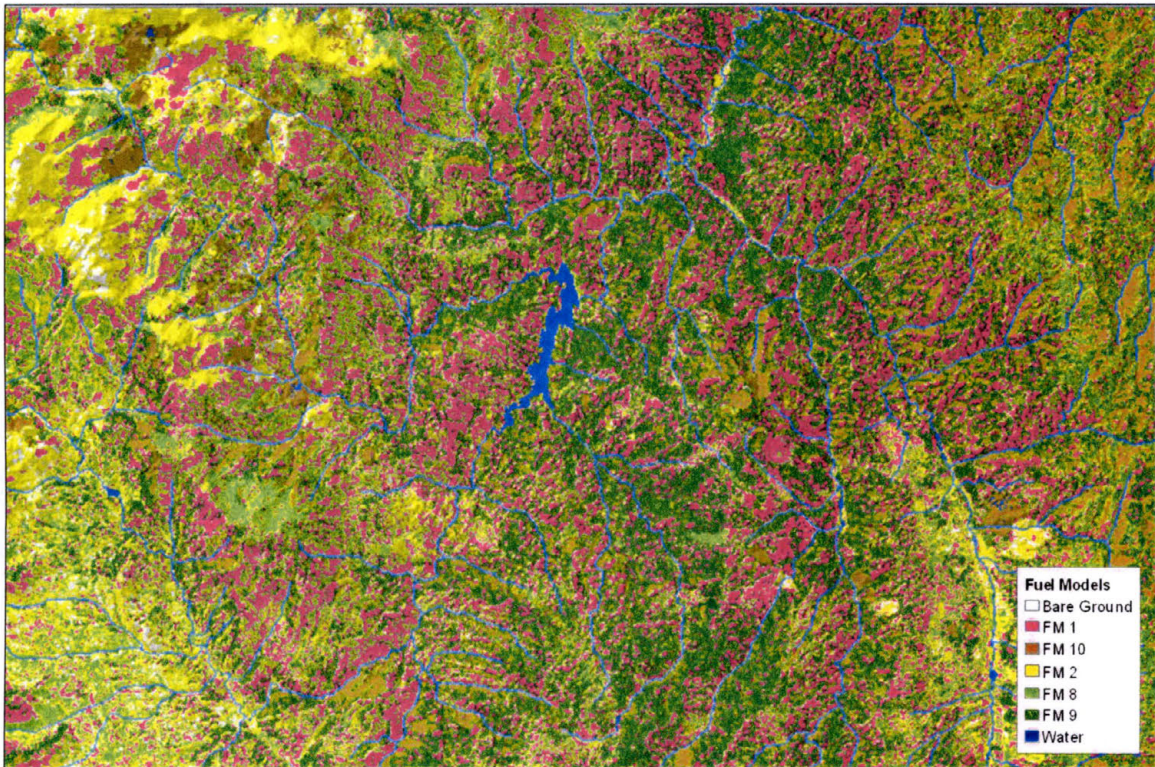


Figure 10: Fuel model distribution across Hayman fire study site

The cellular automata wildfire behavior model requires variables that incorporate weather conditions during the fire event. The primary weather variables for any fire behavior model are wind speed and wind direction (Berjak and Hearne 2002; Hargrove et al. 2000; Karafyllidis and Thanailakis 1997). Wind speed and wind direction was available online from the US Forest Service at http://www.fs.fed.us/rm/hayman_fire/text/02finney/02finney_appA.html. I produced a generalized wind speed grid using this data in concert with daily fire weather summaries provided by Graham et al. (2003). Figure 11 represents wind speed in terms of burn probability. Areas in blue represent periods of extremely high wind speeds, thus these areas were assigned a higher burn probability accordingly. Wind direction is

incorporated into the fire behavior model dynamically using weights to influence the probability of the (i,j) cell to burn based on the position of burning cells in reference to the (i,j) cell. For example, if burning cells upwind from the (i,j) cell exist, the likelihood of the fire burning the (i,j) cell at time $t + 1$ is higher than if the burning neighbor was downwind of the (i,j) cell.

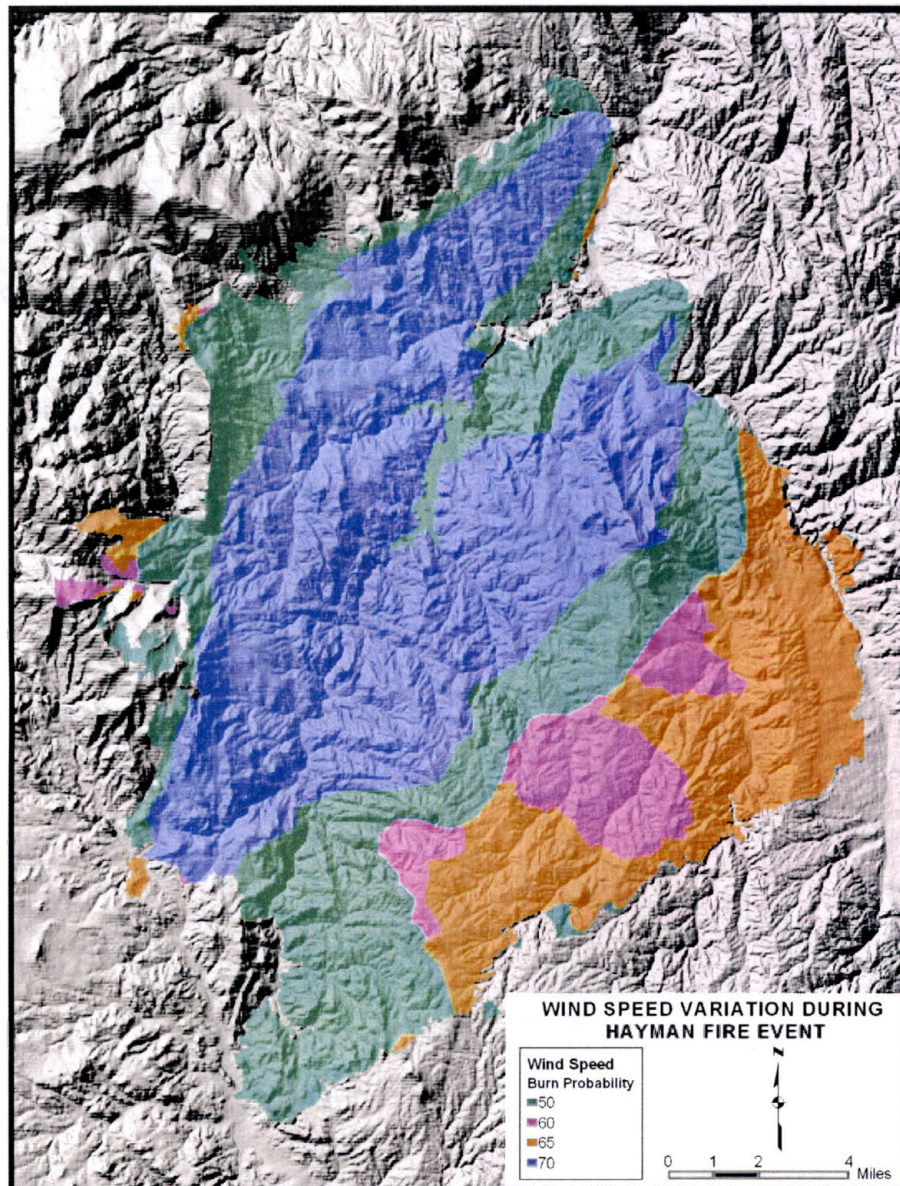


Figure 11: Burn probability grid based on wind speed variation over the course of the Hayman fire event

As topography has a substantial impact upon wildfire behavior, I will utilize topographic data to create additional grid layers for my cellular automaton model. I acquired Digital Elevation Models (DEMs) from the USGS Seamless Data Distribution System at <http://seamless.usgs.gov/website/seamless/viewer.php>. The DEMs used for my study possess 30 meter resolution. This cell size is appropriate as all other data layers incorporated into the model, including the Landsat TM imagery, possess 30 meter spatial resolution. Slope and slope aspect have an impact on wildfire behavior (Berjak and Hearne 2002; Clarke, Brass, and Riggan 1994; Karafyllidis and Thanailakis 1997). I will derive slope and aspect layers to include in the wildfire burn severity model using the USGS 30 meter DEM to incorporate these two topographic variables into the fire burn severity model. Figure 12 shows the resulting burn probability grid constructed to incorporate topography into the wildfire behavior model. As winds generally blew from the southwest over the course of the two-week period of fire activity, steep slopes that faced the wind were assigned a higher burn probability than lee slopes. Berjak and Hearne (2002) confirm that slopes facing the wind, particularly steep slopes, burn more quickly and more readily.

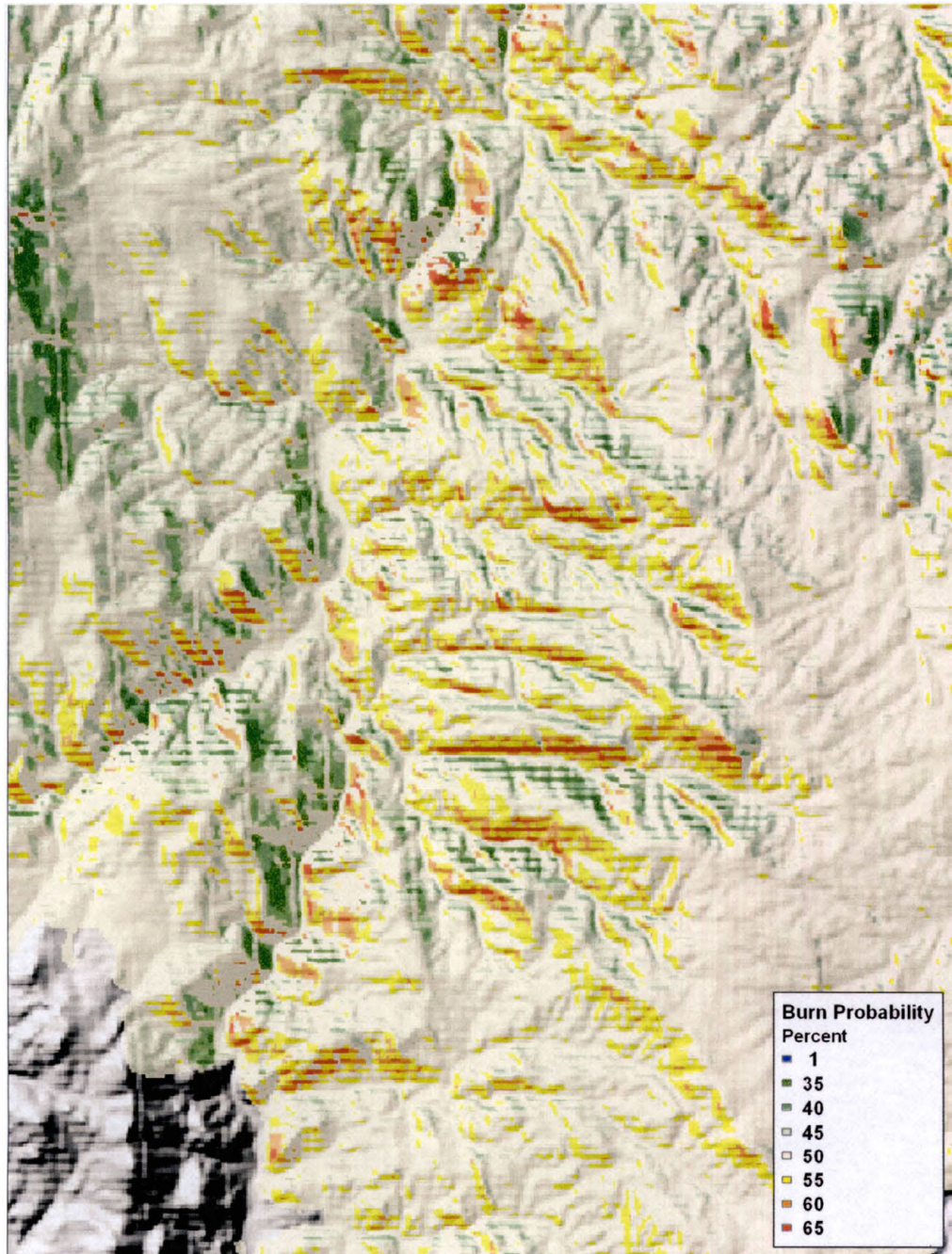


Figure 12: Burn probability grid based on slope and aspect of Hayman fire study site

CHAPTER VIII

METHODOLOGY: REMOTE SENSING ANALYSIS OF WILDFIRE BEHAVIOR

The differenced Normalized Burn Ratio (dNBR) is the critical analysis method required to operationalize my study. I utilized the functionality of ERDAS Imagine to construct the dNBR model. The NBR is calculated the same way as NDVI, but different bands of the electromagnetic spectrum substitute for the bands that are plugged into the NDVI formula. The dNBR takes the pre-fire NBR reflectance values and subtracts the post-fire NBR reflectance values to show changes in reflectance from the pre-burn to post-burn image (Key and Benson 1999; Miller and Yool 2002). As ERDAS Imagine does not have a predefined function available to calculate the dNBR values for each of my study sites, I utilized the Modeler function of ERDAS Imagine to construct a model to calculate dNBR values for each study area (See Appendix for dNBR model diagram). After construction of the dNBR model, I plugged band 4 and band 7 from both the pre-fire and post-fire images into the model and ran the dNBR algorithm for each of my three study sites.

After running the dNBR algorithm for each of my study sites, I ran an unsupervised classification process that employs the ISODATA clustering algorithm on each of the resulting dNBR layers using ERDAS Imagine. After a review of existing burn severity assessment maps produced by BAER teams, I chose to use four classes in the unsupervised classification method: unburned, low, moderate, and high burn severity.

A four-category classification matches the burn severity assessment maps produced by BAER teams (Graham et al. 2002; Robichaud et al. 2003; USDA Forest Service 2002; Wilmes et al. 2002). I left the convergence threshold at .950, and a maximum of 20 iterations was sufficient for unsupervised classifications for each of the three dNBR layers as only 4 iterations maximum were necessary to reach the convergence threshold. I used the raster attributes function to create a pseudo-color scheme for each of the four classes. I assigned a dark green color to unburned pixels, yellow to low burn severity pixels, orange to moderate severity pixels, and red to high burn severity pixels. This improved visualization of the spatial variation of burn severity over grayscale images.

I conducted supervised classifications for each of the three dNBR layers to determine if supervised classification methods classified burn severity more effectively than unsupervised classification (Miller and Yool 2002). I utilized the “inquire cursor” to view dNBR values for various pixels and compared them to dNBR signature values that typically correlate with each of the four burn severity classes (Key and Benson 2004). Areas of interest (AOI) were digitized into polygons and used in the signature data file for the supervised classification.

Upon completion of the unsupervised and supervised classifications, I utilized ESRI ArcGIS 8.3 to digitize the estimated fire perimeter using the dNBR image, post-burn band 4 image, the original false color (5, 4, 2) post-burn image, and the result of the supervised classification as references for digitizing the fire boundary for each study site. Each of these images, when viewed in concert with one another, provided highly useful data to discriminate the fire boundary. Figure 13 displays the four images used for reference during the digitizing process.

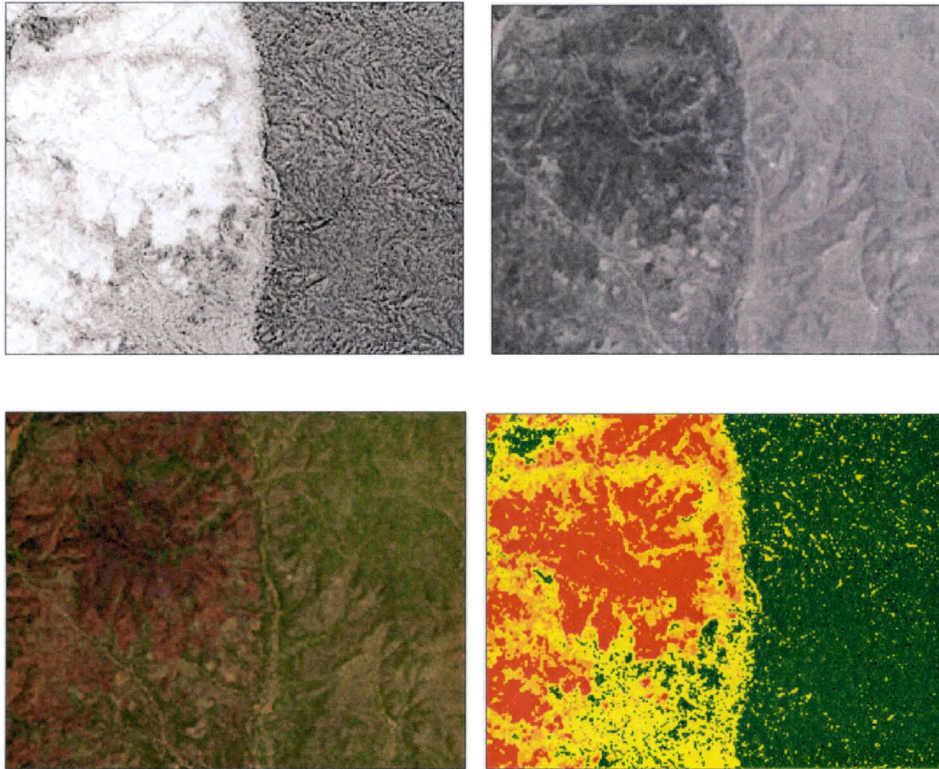


Figure 13: Images used to digitize fire perimeters of each fire event. Upper left: dNBR image; Upper right: band 4 image; Lower left: false color image; Lower right: image resulting from supervised classification of dNBR values

I saved boundary coordinates in ESRI shapefiles in ArcGIS. ArcGIS easily calculated the area of the estimated fire boundary using the coordinates from the digitized fire boundary. This fire perimeter layer is highly useful for additional reasons. Once the fire perimeter was established for each of the study areas, I utilized the power of the Spatial Analyst tool within ArcGIS to convert the vector format shapefile to raster.

Reclassification of this raster data layer permitted me to assign all pixels within the fire boundary a value of “1” and all pixels outside the fire boundary a value of “0.” This produced a raster fire perimeter layer. I then used the Raster Calculator function within the Spatial Analyst toolbar to multiply both the unsupervised and supervised classifications by the fire perimeter layer, which assigned a value of “0” to all areas

outside the fire boundary. This effectively eliminated all data outside of the fire boundary. The remaining pixels of the supervised and unsupervised classification layers still possessed their original pixel values, as they were multiplied by “1.” The clipped supervised and unsupervised layers contained the desired end product: classified areas of unburned, low, moderate, and high burn severity.

As a visualization tool, I acquired elevation data, clipped it to the study areas via the application of an analysis mask, and converted it to “2.5D” in ArcScene. I then assigned the original pre-burn Landsat images elevation values to drape them over the elevation data. The clipped unsupervised and clipped supervised classification layers were then draped on top of the pre-fire Landsat image to display the burn severity patterns across the landscape. Figure 14 presents a 2.5D example of the unsupervised classification of dNBR values draped over a Landsat image of the Hayman study site.

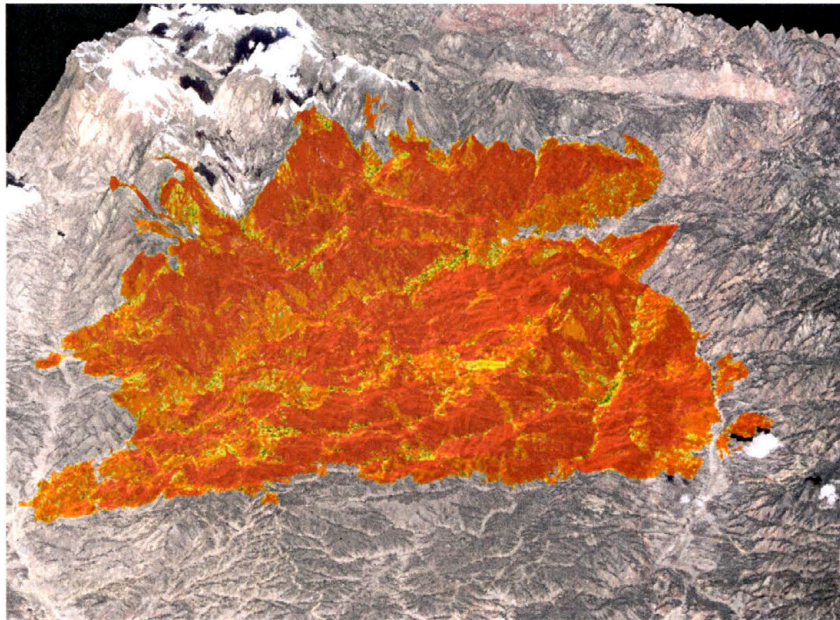


Figure 14: “2.5” dimension representation of unsupervised classification image draped over true-color image of Hayman study site

CHAPTER IX

RESULTS: REMOTE SENSING ANALYSIS OF WILDFIRE BURN SEVERITY

I compare the results from the multi-temporal analysis of Landsat TM imagery to Burned Area Emergency Response (BAER) maps, which are created via a variety of different remote sensing platforms and then adjusted with ground truth field data (Bobbe et al. 2001). Because BAER maps incorporate ground truth data, they lend more credibility to the study than remotely sensed data alone. BAER burn severity maps are generally accepted as fairly accurate representations of the spatial variation of wildfire burn severity across a landscape (Bobbe et al. 2001; Miller and Yool 2002). For this reason, I use BAER maps as an accuracy assessment tool for my remote sensing analysis. I will discuss the accuracy of the estimated fire perimeter, accuracy of the unsupervised classification method, accuracy of the supervised classification method, and issues that potentially introduce error into the results of the analysis for each study site. I assessed overall accuracy of my results using the Accuracy Assessment tool in ERDAS Imagine as well as BAER burn severity acreage data to determine how well the unsupervised and supervised classifications estimated total acreages of unburned, low, moderate, and high burn severity within the fire boundary in terms of percentage of the total burned area.

Hayman Burn Severity Analysis

The primary goal of this study was to validate the effectiveness of the dNBR algorithm as a method to assess wildfire burn severity. Analysis of the results of the Hayman fire portion of this study provides useful data toward this end. Digitizing the Hayman fire boundary yielded an estimated area for the Hayman fire of 141,999 acres. Review of the BAER team burned area data shows that approximately 138,096 acres burned as a result of the Hayman wildfire (Graham et al. 2003). The estimated fire area determined in my study was 3,903 acres larger than the actual area burned, which represents a difference of 2.8% of the total burned area (Figure 15).

Unsupervised classification of the dNBR result for the Hayman fire appeared to assign many more pixels a high burn severity value than actually occurred. General comparison of the BAER burn severity map with the results of the unsupervised classification shows that the unsupervised classification method overestimated areas of moderate and high burn severity and underestimated unburned and low burn severity classes (Figure 16). Table 1 provides a tabular view of the percentage of the burned area assigned to each burn severity class compared to results from the BAER team. It is readily apparent that the unsupervised classification heavily underestimated unburned area and areas of low burn severity while overestimating areas of moderate and high burn severity. Comparison of the results of the unsupervised classification against the BAER map using ERDAS Imagine Accuracy Assessment tool resulted in an overall classification accuracy of 50%.

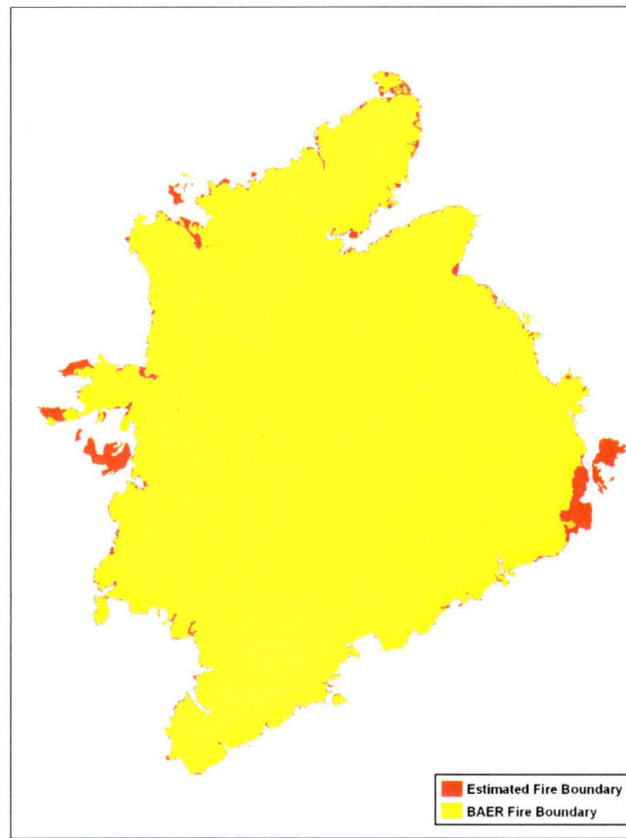


Figure 15: Predicted versus actual fire boundary of Hayman fire event

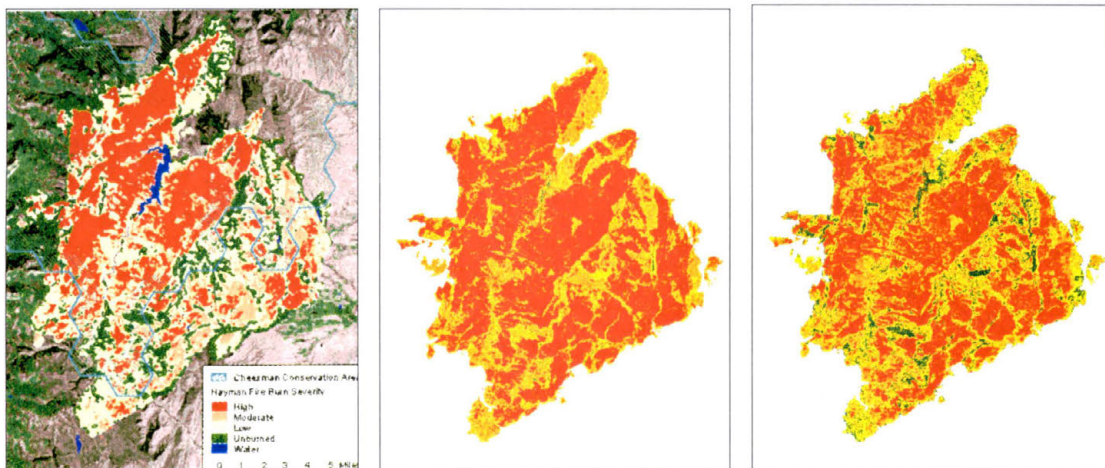


Figure 16: Left: official fire severity map of Hayman fire; Center: unsupervised classification result; Right: supervised classification result

Supervised classification appeared to pick out classes of burn severity more accurately. Review of figure 16 shows that the supervised classification picked out areas

of unburned or low burn severity more effectively than unsupervised classification. Table 1 confirms the improvement in classification accuracy of the supervised classification. Supervised classification underestimated unburned areas by a large margin. Results show that supervised classification predicted total acreage of low burn severity with superior accuracy when compared to the unsupervised classification. Areas of moderate burn severity were substantially overestimated by the supervised classification, but total acres classified as high burn severity matched BAER estimated with a high degree of accuracy (Table 1). Accuracy assessment via ERDAS yielded an overall classification accuracy of 60% for the supervised classification results.

	Unburned	Low	Moderate	High
BAER results	15.2%	34.1%	15.9%	34.8%
Unsupervised	0.6%	4.2%	38.3%	56.8%
Supervised	6%	19%	42.1%	32.9%

Table 1: Percentage of total acreage assigned to each burn severity class: Hayman fire

Missionary Ridge Burn Severity Analysis

Digitizing the estimated fire perimeter for the Missionary Ridge fire based on the dNBR, post-burn band 4, false color (5, 4, 2) post-burn Landsat image, and supervised classification image resulted in an estimated burn area of 64,941 acres. The official estimated burn area by the Missionary Ridge BAER team was 72,964 acres. Total burned area was estimated with 89% accuracy. The general shape of my estimated fire perimeter appears to agree with the shape of the BAER fire perimeter (Figure 17).

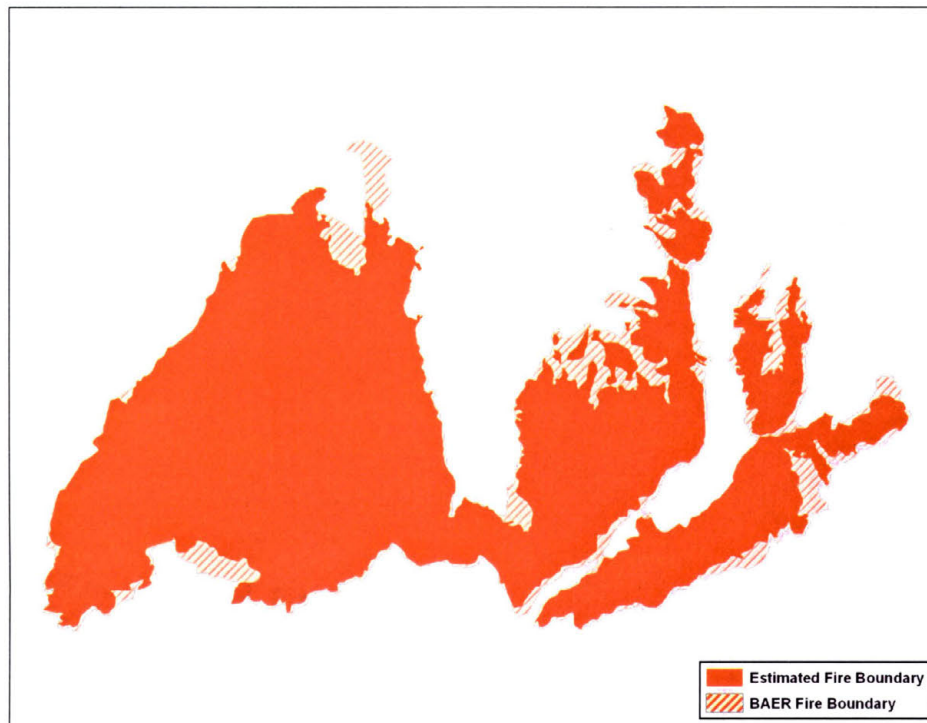


Figure 17: Predicted versus official boundary of Missionary Ridge fire

As was the case with the Hayman fire analysis results, the unsupervised classification method underestimated unburned areas or spots characterized as low burn severity and overestimated areas of moderate and high burn severity (Table 2). Unsupervised classification underestimated percentage of unburned areas by a large margin, but performed relatively well on areas of low, moderate and high burn severity (Table 2). Comparison of the unsupervised classification results to the BAER burn severity map in ERDAS Imagine Accuracy Assessment tool yielded an overall classification accuracy of 45%. Comparison of the spatial pattern of burn severity of the unsupervised classification result and the BAER severity map shows that overall burn severity patterns match up at small scales (Figures 18 and 19). Portions of the BAER fire perimeter that were not included in my estimated fire boundary are characterized as unburned or low burn severity per the BAER map. This may explain a portion of the

difference in estimated versus actual areas of unburned to low burn severity in the Missionary Ridge fire perimeter.

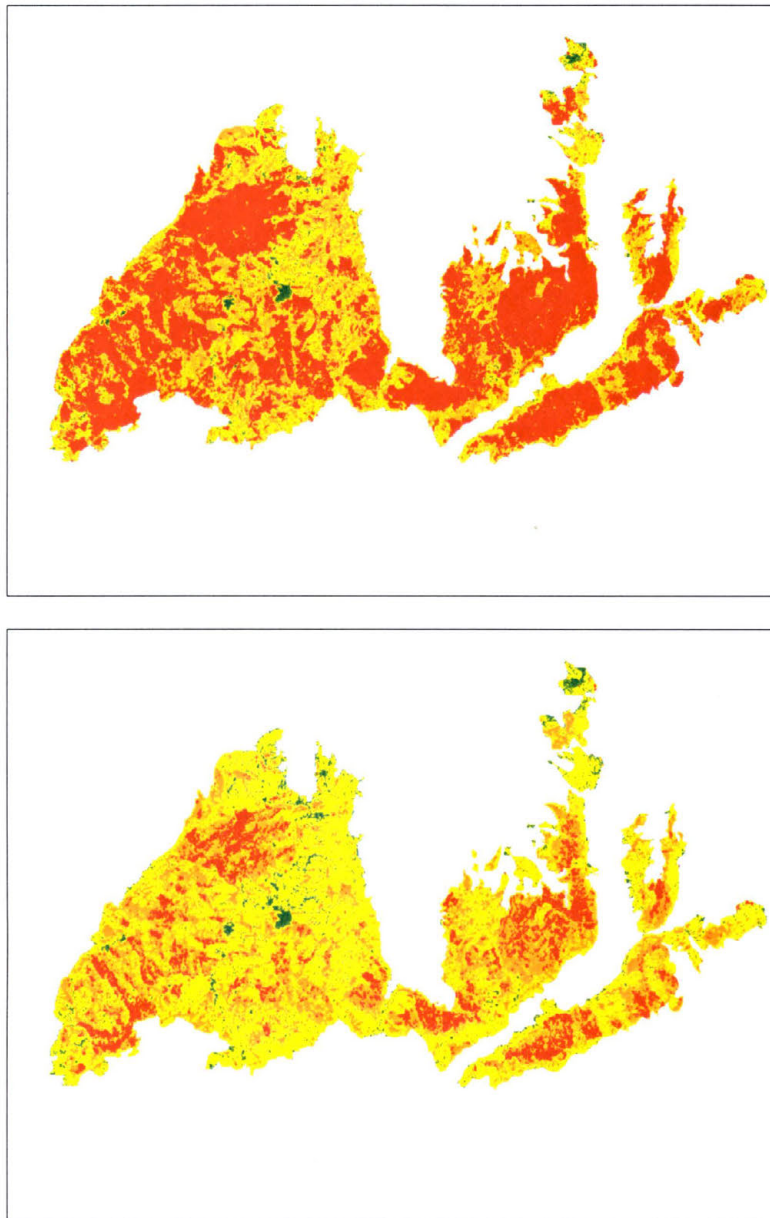


Figure 18: Top: unsupervised classification result of dNBR analysis of Missionary Ridge fire; Bottom: supervised classification image

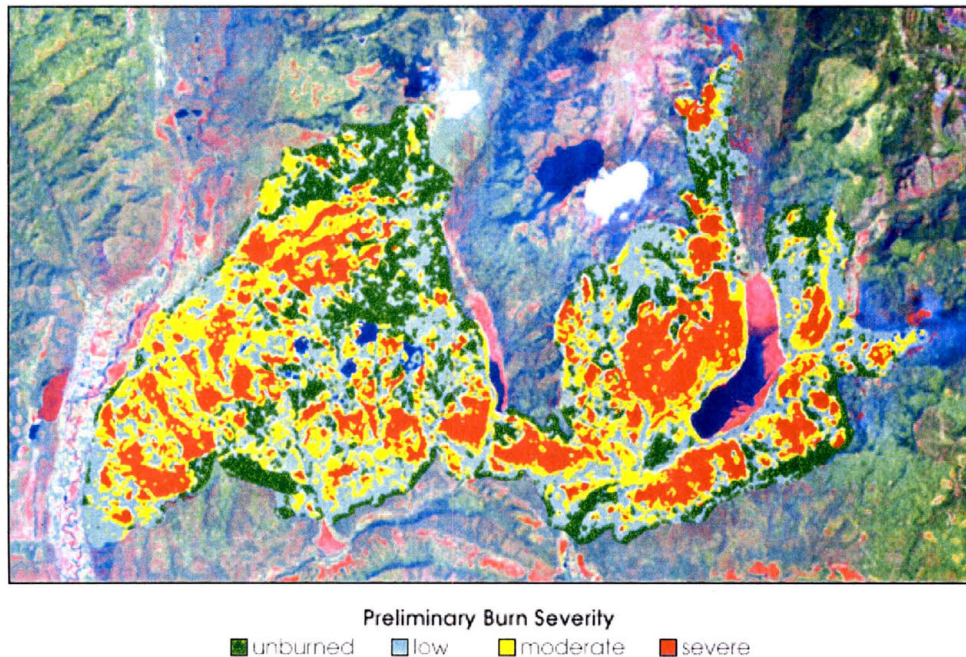


Figure 19: Official burn severity map of Missionary Ridge fire

	Unburned	Low	Moderate	High
BAER	20.2%	19%	29.9%	30.9%
Unsupervised	1.6%	14.5%	36.6%	47.3%
Supervised	3.5%	42.9%	43.3%	10.2%

Table 2: Percentage of total acres assigned to each burn severity class: Missionary Ridge fire

Review of figures 18 and 19 shows that the supervised classification of the dNBR values agrees fairly well with the BAER burn severity map in terms of smaller-scale burn severity patterns. Table 2 shows that the supervised classification procedure underestimated total acreage of unburned areas by a substantial amount but overestimated total area of the low and moderate burn severity classes by a large margin. It is possible that subtle differences in dNBR values in many areas caused unburned pixels to be included in the low burn severity category. The supervised classification results in Table

2 also show that areas of high burn severity were underestimated by a large percentage. It is likely that some areas assigned to the moderate burn severity class were assigned to the high burn severity class in the BAER findings. Determining breakpoints in dNBR values to create each of the four burn severity classes is clearly a concern when analyzing results from dNBR analyses. Comparison of the supervised classification results to the BAER burn severity map via ERDAS Accuracy Assessment tool show that the overall classification accuracy was 75%.

Two small clouds and their shadows in the post fire image have a small impact on results from the dNBR analysis. As the dNBR algorithm assesses changes in reflectance in pre-burn to post-burn NBR images, bright clouds and their dark shadows impact the values in the resulting dNBR image. A review of figure 18 shows that two green (unburned) spots to the left of center in both the unsupervised and supervised classification maps are the result of the shadow of the two small clouds in the post-burn images. I confirmed this via overlay of the post-burn Landsat image in ArcGIS. Although this error does not affect a large portion of the study area, it is important to note the impact of error such as this causes inaccuracies in classification of burn severity.

Rodeo-Chediski Burn Severity Analysis

The estimated burned area for the Rodeo-Chediski fire as determined by digitizing the fire boundary as identified by the dNBR image was 437,293 acres. BAER team estimates the burned area as 467,066 acres (Wilmes et al. 2002). The estimated fire boundary accurately predicted the total burned acreage of the Rodeo-Chediski fire with 93.6% accuracy. My estimated fire boundary agrees well with the BAER fire boundary

with the exception of a large cloud that obscures a part of the northwest portion of the burn scar (Figure 20). I chose to exclude this area from the fire perimeter to prevent classification error in the dNBR image analysis. Had I included this portion in the fire perimeter, accuracy would improve slightly. Nevertheless, the dNBR algorithm allowed me to define the Rodeo-Chediski fire boundary with a high degree of accuracy.

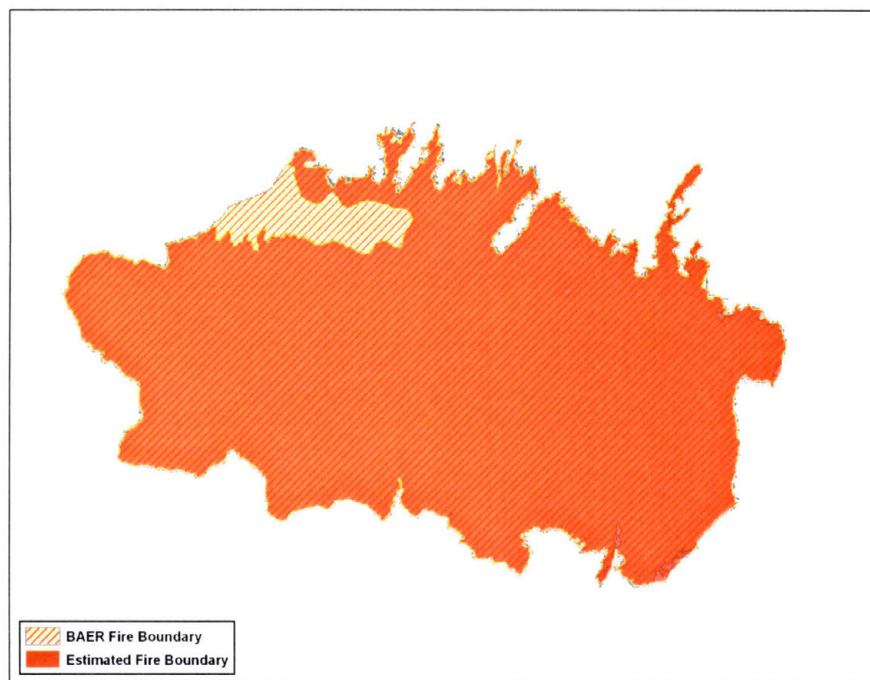


Figure 20: Predicted versus actual fire perimeter of the Rodeo-Chediski fire

Assessment in the accuracy of the unsupervised and supervised classification of the dNBR data is based in part on the predicted number of acres of each burn severity classification as compared to actual acreage of each burn severity class as determined by BAER teams. The Rodeo-Chediski BAER report does not list the actual number of acres associated with each burn severity type, but an accompanying environmental impact statement (EIS) includes percentage of the total burned acreage for each burn severity class (Zieroth and Siderits 2003). The EIS combines the unburned and low burn severity

classes together. Table 3 reflects the combined unburned/low burn severity class as it is impossible to separate the two classes without further information.

As was the case with both the Hayman and Missionary Ridge fires, the unsupervised classification procedure underestimated the percentage of burned area assigned to the unburned/low class and overestimated the percentage of the total burned area assigned to the moderate and high burn severity classes (Figures 21 and 22). BAER team findings determined that 47% of the total area within the fire perimeter was unburned or suffered low burn severity while the remaining burned areas were almost evenly divided among the moderate and high burn severity classes (Table 3). The unsupervised classification procedure identified only 7% of the area within the fire perimeter as unburned or low burn severity. The unsupervised classification assigned approximately twice as many pixels to the high burn severity class as the BAER team results. Accuracy assessment of the unsupervised classification results estimated a classification accuracy of 55%.

	Unburned / Low	Moderate	High
BAER	47%	26%	27%
Unsupervised	7%	37.7%	55.3%
Supervised	28.4%	30.2%	41.5%

Table 3: Percentage of total acres assigned to each burn severity class: Rodeo-Chediski fire

A review of the results from the supervised classification procedure (Table 3) for the Rodeo-Chediski study area shows that supervised classification assigned pixels to the appropriate burn severity class with more success than unsupervised classification.

Analysis of the results of the supervised classification procedure shows that areas of

unburned to low burn severity were underestimated, but percent burned area classified as moderate burn severity by the BAER teams closely matches the results of the supervised classification procedure. This classification method did overestimate total percent area assigned to the high burn severity class. The ERDAS Imagine Accuracy Assessment tool generated an overall classification accuracy of 70%. A review of figures 21 and 22 shows that the burn severity map resulting from the supervised classification procedure agrees well with the BEAR team map.

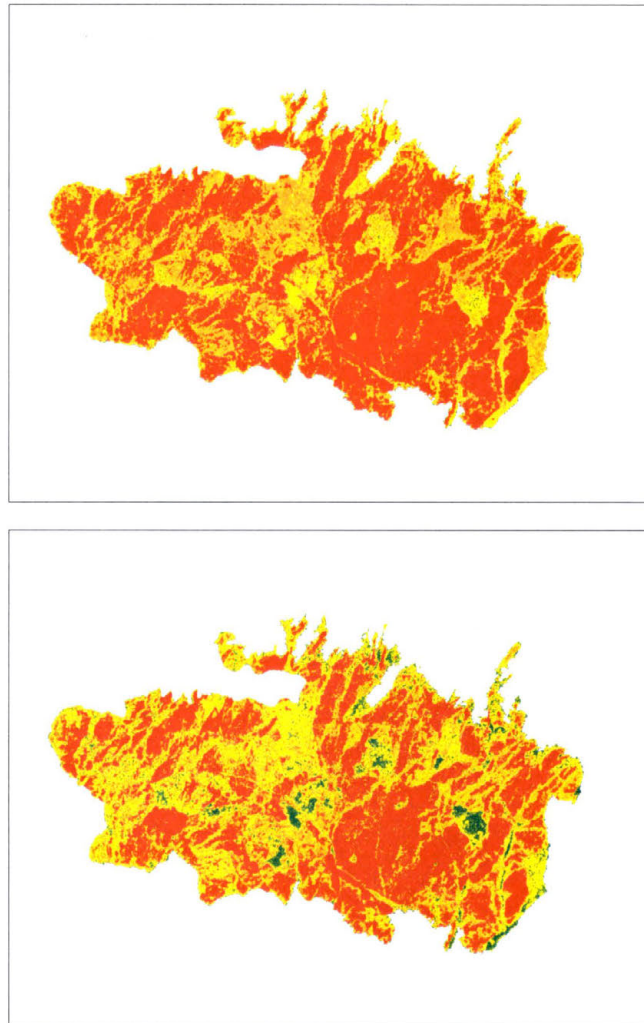


Figure 21: Top: Unsupervised classification image of Rodeo-Chediski fire; Bottom: Supervised classification image

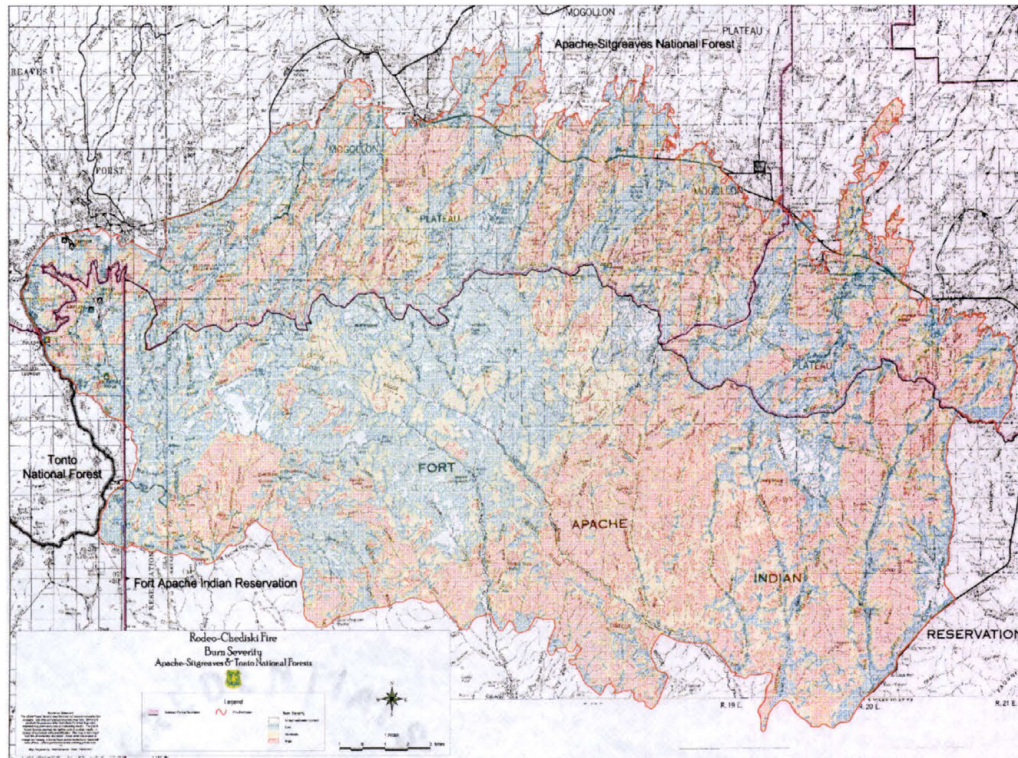


Figure 22: Official burn severity map of Rodeo-Chediski fire event

Two potential sources of error are of primary concern for results stemming from the Rodeo-Chediski fire portion of the study. Classification error is one of these two sources of error, and it is one present in the results for each of my study sites. Due to the relative nature of burn severity assessment, it is sometimes difficult to determine the appropriate dNBR value to assign as the breakpoint between class values. For example, a minor change in the breakpoint value between the moderate and high burn severity classes can potentially result in the misclassification of thousands of acres of forest in large wildfires. The second major source of error in the results for the Rodeo-Chediski fire is the fact that a large cloud obscured a substantial portion of the northwest section of the fire boundary in the post-fire image. I chose to exclude areas obscured by the cloud or the cloud shadow to prevent misclassification of burned pixels. This prevented

accurate assessment of total burned area, which eliminated the possibility of assessing burn severity in this portion of the fire boundary. Due to the large size of the Rodeo-Chediski wildfire, the percentage of the burned area excluded from the analysis due to cloud cover is relatively small, as my findings resulted in a total burned area for the Rodeo-Chediski fire within 6.4% of the BAER team estimated. The impact of cloud cover in my study, though important to consider in the results of the analysis, was not large enough to affect the results of the dNBR analysis significantly.

CHAPTER X

METHODOLOGY: WILDFIRE BEHAVIOR MODELING

In general, the existing attempts to employ cellular automata modeling to wildfire behavior have been targeted to relatively small wildfires encompassing several hundred acres that usually burn out on the same day as fire ignition (Clarke 1994; Berjak and Hearne 2002). The fire event that my cellular automaton was designed for encompassed over 140,000 acres and burned actively for over two weeks over a landscape with heterogeneous fuels, rugged terrain, and dynamic weather conditions. For this reason, my goal was to produce a model that provided a general estimate of wildfire behavior in terms of fire propagation and burn severity. The CA based model can be broken into three phases: burn probability assessment, fire spread phase, and energy output / fire residence time calculation phase. I will discuss each of these phases of the model in this chapter, beginning with the methods used to process the primary data layers needed for each of these phases.

Burn Probability Grid Construction

The first stage of the cellular automata model is the “burn probability assessment” phase. Construction of a “burn probability” grid is necessary for the model to determine which grid cells are likely to burn, and which cells are less likely to burn. Fuel type,

wind speed, slope, and terrain are all variables that have an impact on burn probability that are included in the burn probability grid. I included each of these variables in the overall burn probability grid.

As mentioned previously, fuel characteristics have an impact on fire behavior (Berjak and Hearne 2002; Karafyllidis and Thanailakis 1997; Koutsias and Karteris 2003; Miller and Yool 2002; Riano et al. 2003; Scott and Jones 1994). No detailed fuel map existed prior to this study, thus the construction of a raster grid representing the Anderson (1982) fuel models was necessary. Using the pre-fire Landsat TM image and a relatively low resolution JPEG image of Anderson (1982) fuel models constructed by the USDA Forest Service for the study area as a reference, I employed ERDAS Imagine to conduct a supervised classification of the pre-fire Landsat image to produce a raster representing the spatial distribution of fire behavior fuel models across the study area. The resulting fuel map appears to agree well with known characteristics of the study site in that grassland-type fuels (FM 1) are commonly found on southerly slopes while more dense stands of forest (FM 9) are common on northerly slopes (Graham et al. 2003). Other attempts to produce fuel grids as inputs for cellular automata models used more arbitrary methods, such as unsupervised classification of red-band reflectance (Clarke 1994).

The resulting fuel type grid was then reclassified using ArcGIS 8.3 into a burn probability grid based on the fuel characteristics of each Anderson (1982) fire behavior fuel model. Determination of burn likelihood based on fuels was accomplished by visual comparison of fuel type to burn likelihood using the supervised dNBR image of the Hayman study area. Review of the fire behavior characteristics described in Anderson (1982) further informed my assessment of burn probability for each fuel type.

Topographic variables of slope and aspect were also incorporated into the burn probability grid. Existing literature shows that both slope and aspect have an impact on fire behavior. Fire burns more quickly and more readily up increasingly steep slopes, but fire burns more slowly and less readily on the lee side of slopes (Karafyllidis and Thanailakis 1997; Berjak and Hearne 2002). As fire spreads most readily in the direction of wind, slope aspect must be taken into consideration as well. For this reason, I chose to produce one burn probability grid using a weighted combination of both slope and aspect variables. I constructed separate burn probability grids for slope and aspect and then added the two raster grids together using the raster calculator function of ArcGIS 8.3. The resulting layer had little value on its own, but careful evaluation of the unique values of each class allowed for reclassification of this layer into an overall probability grid. For example, an area of extreme slope (35 – 70%) was assigned a 70% burn probability value based solely on slope. If that area also possessed a southwesterly slope, which was the general trend of wind during the course of the fire event, the burn probability grid value would be 65%. The addition of these two integer grids would produce a value of 135. As I know that a value of 135 represented areas of steepest slope and aspect most directly facing the wind, these areas were assigned an overall burn probability value of 65%, which is the highest burn probability value possible based on topography in this model.

Wind speed was also taken into consideration during the construction of the overall burn probability grid. I manually digitized a fire progression map produced during the Hayman fire case study that displays the fire boundary during each day of the fire event (Graham et al. 2003). Using wind speed data from the weather stations located in the study area along with data provided by Graham et al. 2003, I was able to associate

wind speed data for each vector polygon in the digitized fire progression map. Figure 23 shows a classified vector layer displaying wind speed within the Hayman fire boundary. Using ArcGIS 8.3, I converted the vector layer into a raster grid and reclassified the grid into burn probability values.

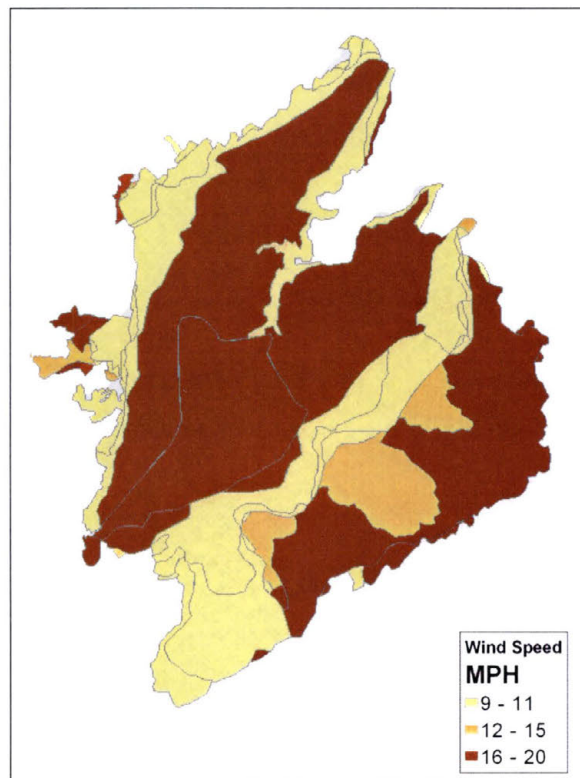


Figure 23: Vector wind speed data for Hayman fire

Creation of the overall burn probability grid required combining the burn likelihood grids created for fuels, aspect and slope, and wind speed. ArcGIS 8.3 raster calculator easily allowed for this operation. A weighted overlay addition operation allowed for a combination of fuel, topographic, and wind variables into the final burn probability grid. The following equation was used to produce the weighted burn probability grid:

$$\text{Burn_prob} = ((0.4[\text{fuel_prob}]) + (0.3[\text{terrain_prob}]) + (0.3[\text{wind_speed}])) \quad (3)$$

The fuel layer was assigned a slightly higher weight than the other two variables due to the fact that the literature provides more information on the effects of fuel on fire propagation than the other variables, and fuel is the only variable that humans have the ability to control (Graham, McCaffrey, and Jain 2004). Figure 24 displays the final burn probability grid input into the “burn probability assessment” stage of the wildfire behavior model. Note that the Cheesman reservoir, the large water body displayed in bright green, does show a 15% burn probability. Naturally, water will not burn! The model avoids burning these areas thanks to the “fire spread probability” grid discussed next.

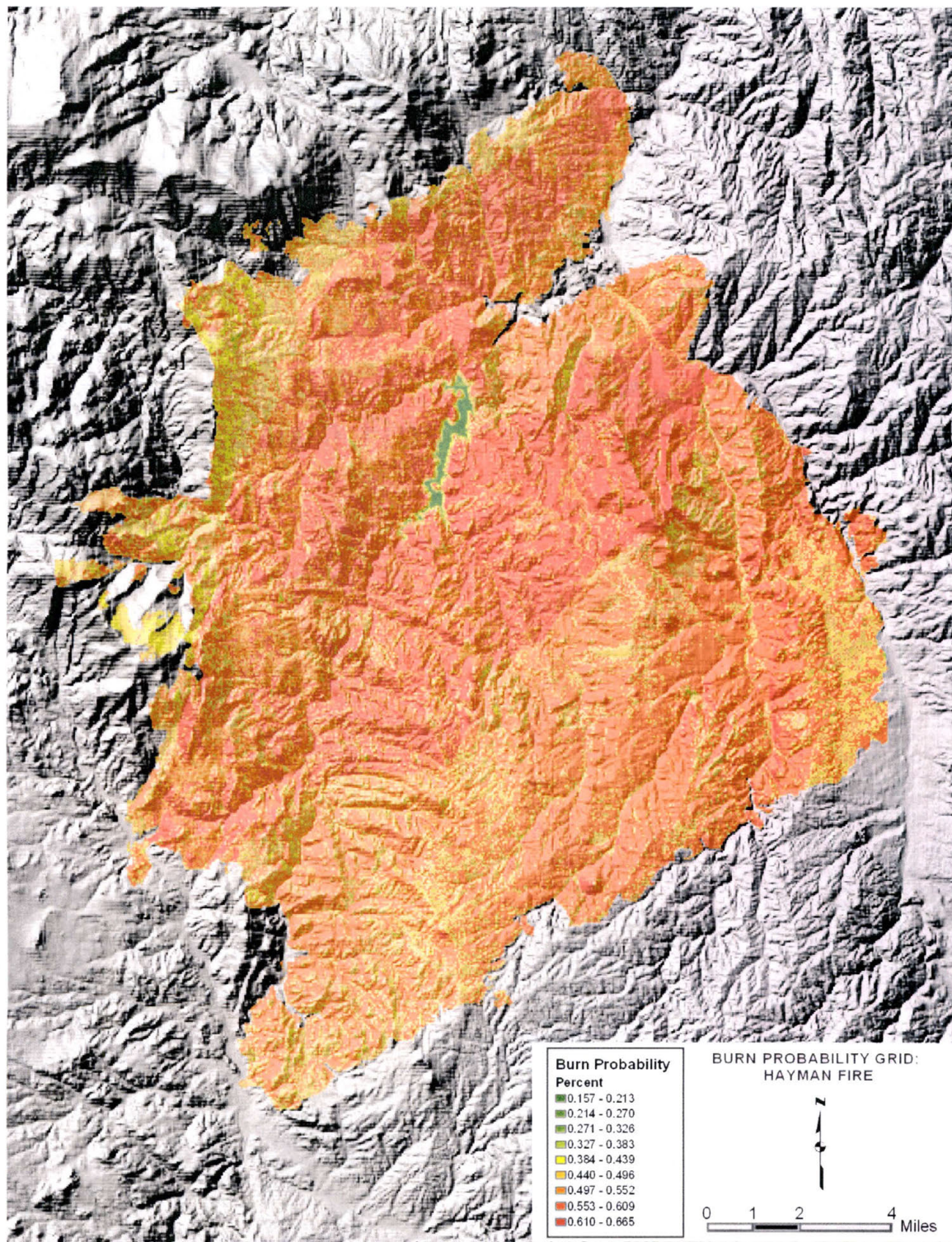


Figure 24: Unweighted burn probability grid for Hayman study area

Spread Probability Grid Construction

The primary purpose of the spread probability grid is to attempt to model the spread of fire over time as accurately as possible. While the “burn probability” grid determines if a cell is likely to burn at all, the spread probability grid is designed to determine the likelihood that a cell will burn at any particular time step. For example, grassland and shrubland fuels (fuel models 1 and 2) burn very rapidly, thus they are able to burn over each 30 meter grid cell very easily in one ten-minute time step. For this reason, it is highly likely that a fire burning these fuel types will spread to neighboring cells at time step $t + 1$. Grid cells assigned to fuel model 8 burn very slowly, thus it is unlikely that they will burn across an entire grid cell and propagate fire to its neighbors during the first burning time step. Essentially, the purpose of the spread probability grid is to “slow down” the progress of the fire for fuels that burn more slowly than faster burning fuels.

The BEHAVE fire modeling software package is commonly used by fire ecologists and forest service personnel to determine fire behavior characteristics such as fire spread rates. This software package is based on the fire behavior equations developed by Richard Rothermel (1972) which are widely accepted in the fire behavior modeling community. Given the overall conditions of the Hayman fire site, I determined fire spread rates for each of the five primary fuel types that characterize the study area. Fire spread probabilities were assigned to each fuel type based on likelihood of fire to burn entirely across a burning cell and propagate fire to its neighbors at time step $t + 1$. Figure 25 displays the spread probability grid input into the cellular automata wildfire behavior model. Note that locations denoted in red are areas designated as having a zero

probability of spread. These are the only locations where fire spread is not allowed to occur. Bodies of water or areas classified as bare ground in the fuels layer have a spread probability of zero.

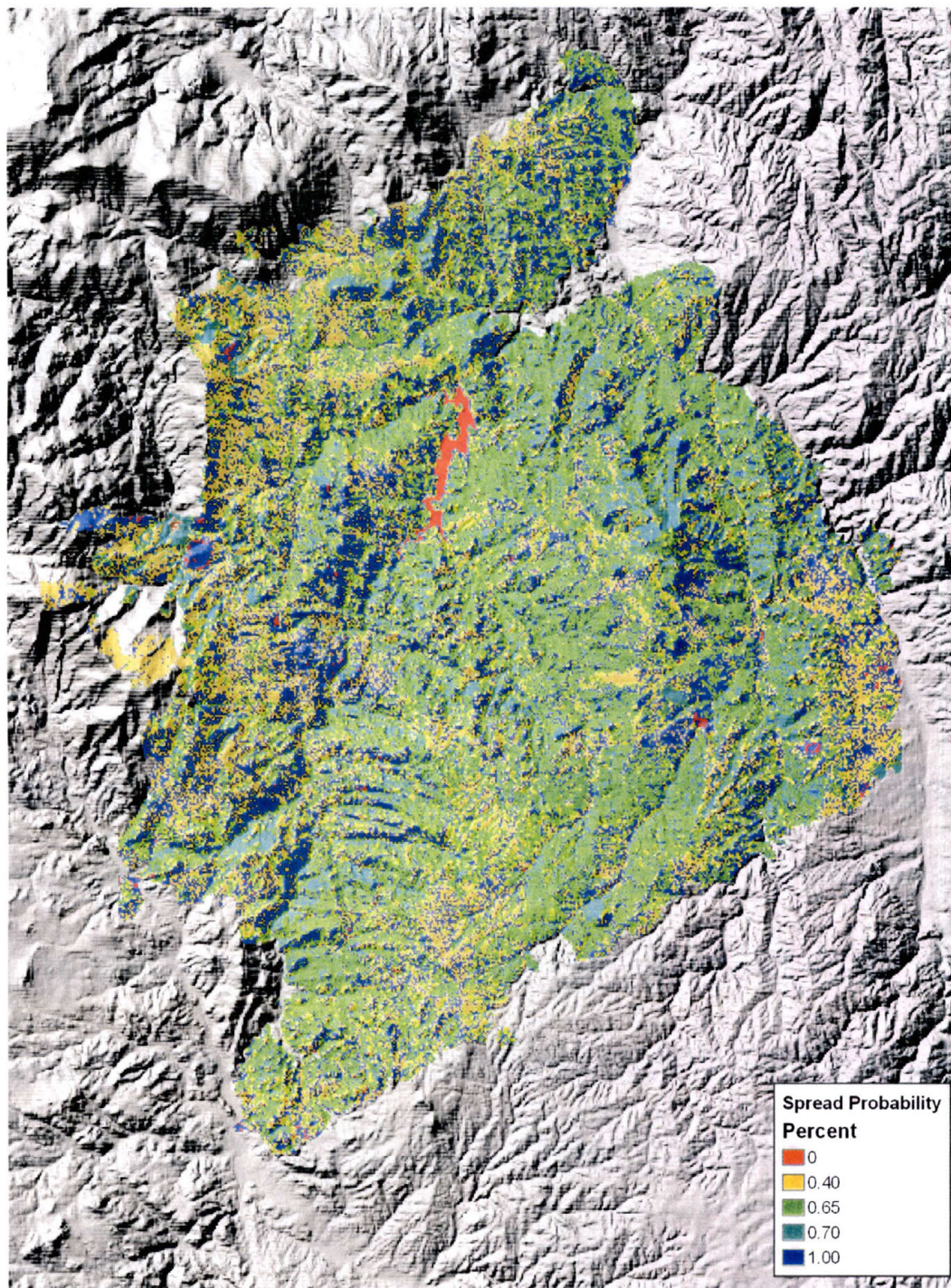


Figure 25: Spread probability grid for Hayman study area

Figure 25 shows the spread probability values initially assigned to each grid cell, but the model dynamically adjusts the burn probability at each time step to account for the fact that as a cell burns over the course of multiple time steps, it is more and more likely to propagate fire to its neighboring cells. For example, while a burning (i,j) cell possessing fuel model 8 fuel type is assigned only a 40% chance of propagating fire to its neighboring cells at time $t + 1$, as the cell continues to burn at time $t + 2$ and $t + 3$, it becomes increasingly likely that fire will spread to its neighboring cells. The model ties the fuel residence time layer, which will be discussed in the next section, to the spread probability layer. By the time only one time step remains before the burning (i,j) cell runs out of fuel, the fire spread probability is multiplied by a factor of two. It is likely that the fire will spread before the (i,j) cell is extinguished.

Fire Residence Time Grid Construction

One of the goals of this cellular automata based wildfire behavior model is to assess wildfire burn severity. To attempt to achieve this goal based on my hypothesis that there is a relationship between total energy release per grid cell and burn severity, it is necessary to generate a rough estimate of the number of time steps a cell will burn prior to fire extinction. Fire residence time is the term used to describe the amount of time a fire burns behind the actively burning fire line. Once the flaming fire front passes through a vegetated area, the fire often continues to burn behind the flaming front. The fire residence time grid allows the cellular automaton to incorporate this variable into the equation. Figure 26 shows the residence time grid created for the Hayman fire site.

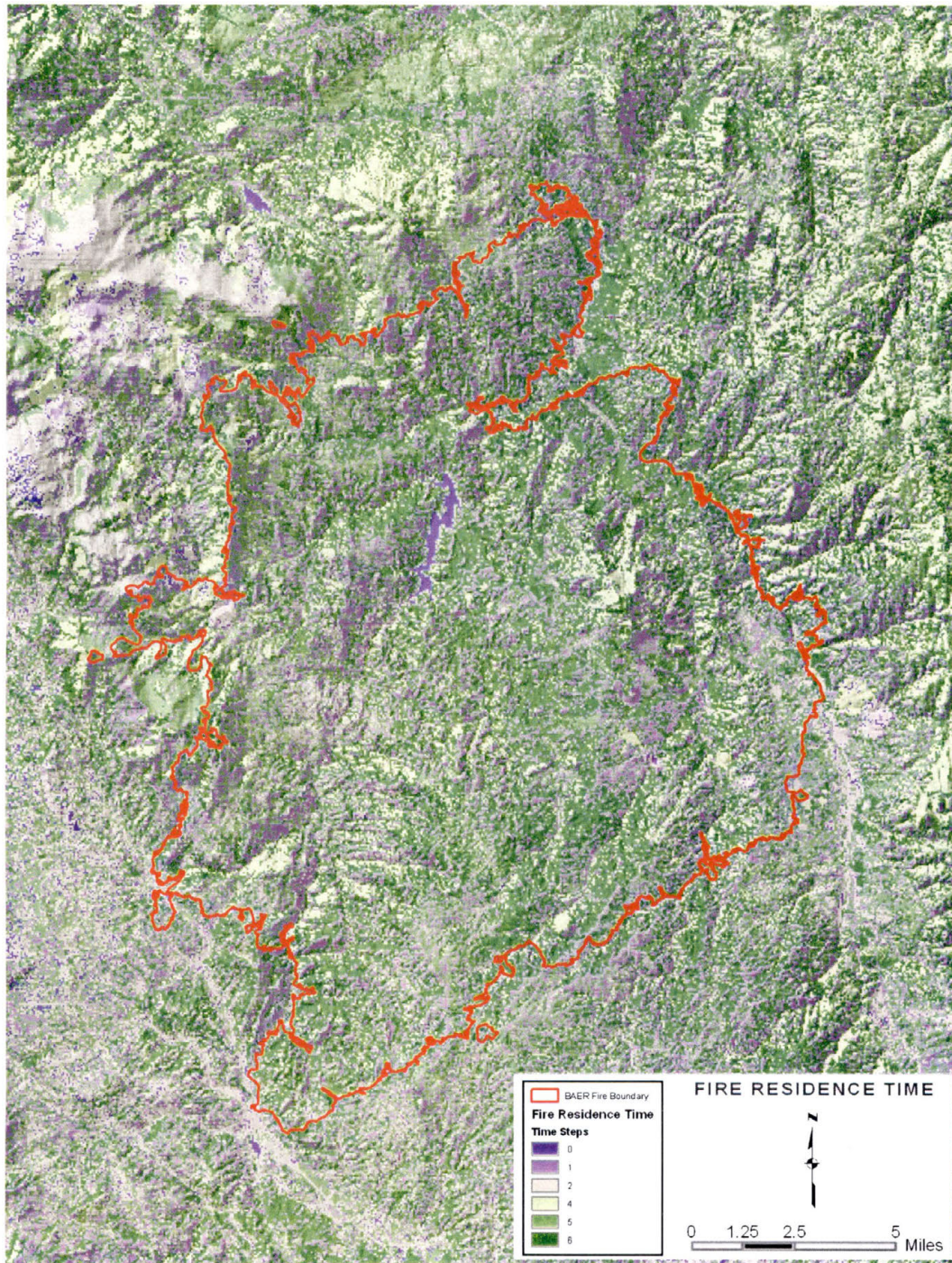


Figure 26: Estimated fire residence time grid for Hayman study site

Using BEHAVE fire modeling software, a general estimate of the amount of heat released per unit area is possible given weather, fuel, and topographic conditions of the Hayman study area. Carlton (2003) indicates that all fuels within the Anderson (1982)

fire behavior fuel models are estimated to contain 8,000 BTU's of energy per pound of fuel. Using this value as a constant and the heat per unit area estimate for each fuel type, the amount of fuel consumed per square foot per time step is estimated and converted to tons of fuel per grid cell consumed per time step. Anderson (1982) provides the total fuel loading per grid cell, which includes live and dead fuels. As wildfire generally does not completely consume all live and larger diameter fuels, only 60% of the live and coarse fuels were considered available for combustion along with 100% of fine fuels such as pine needles and grasses. Subtraction of the number of tons of fuel consumed per time step from the total number of tons of fuel available per pixel provides us with an estimate of the number of time steps that any particular grid cell will burn. It must be noted that the heat per unit area value obtained from the BEHAVE software was reduced by 50% after the first time step to represent the fact that once the flaming front passes by, smoldering combustion takes place. Smoldering combustion is less intense than flaming combustion, thus the need for reducing the initial heat per unit area value is apparent. The following formula yields the fire residence time for each grid cell:

$$\text{Fuel consumption } (F) = ((b * h) * 9682.56 \text{ ft}^2) / 2000 \text{ lbs/ton} = \# \text{ tons consumed during each time step}$$

b = heat per unit area obtained from BEHAVE software (BTU / ft²)
(b is reduced by 50% after first time step)

h = heat content of 1 lb of fuel (Value is constant: $h = 1 \text{ lb} / 8000 \text{ BTU}$)

9682.56 ft² = area of each grid cell

R = fire residence time (# of time steps fire burns)

$$\text{Fire Residence Time } (R) = \text{Total Fuel Loading Per Grid Cell} - \text{Fuel Consumption } (F) \text{ at each time step} \quad (4)$$

Model Description

The cellular automata model incorporates the burn probability grid, spread probability grid, and fire residence time grid in three stages, although the outcome of the model at each time step is dependent on the values of these derived from each stage of the model. The model is probabilistic in nature, which means that the output of the model will vary from one simulation run to the next. In contrast, physical models have fixed rules that result in the same outcome after each model iteration. A strength of stochastic models is that averaging the results of numerous model iterations allows for the generation of “risk maps” (Clarke 1994). As one of the primary objectives of my model is to attempt to produce a model to predict areas at risk to severe wildfire damage, a probabilistic model is the appropriate choice for my study.

I chose to employ ERDAS Imagine software to produce the wildfire behavior model due to its built-in ability to analyze, process, and visualize spatial data in 2D and 3D. The ERDAS Imagine Modeler tool allowed for the construction of each of the three stages needed to execute my cellular automata model in spatial terms, but the Modeler tool lacks the ability to represent change over time due to its inability to conduct iterative loops (Messina et al. 1999). Although the Modeler tool does not allow for looping procedures, it is possible to export the model into ERDAS Spatial Modeler Language (SML) and edit the SML script to accommodate looping procedures. This modification procedure allowed me to construct a cellular automata model that simulates the spread of wildfire at discrete time steps.

As discussed previously, the CA based wildfire behavior model assesses the pattern of the burn across space and attempts to identify areas of unburned, low,

moderate, and high burn severity in three stages. The initial stage assesses the likelihood that any particular cell will burn. The second phase determines the likelihood that fire will spread from a burning neighbor to the (i,j) cell at time $t + 1$. The third stage determines how many time steps a burning cell will continue to burn before all available fuel is consumed. I will discuss how each of the three phases of the wildfire behavior model execute to produce the final outputs of the model. All three of these phases, taken together, make up the transition rules to determine if fire will propagate to neighboring cells.

Burn Probability Assessment

This initial step in the wildfire behavior model inputs the overall burn probability grid discussed previously and compares the values of each grid cell to a randomly generated number in ERDAS. If the burn probability value of the (i,j) cell is greater than or equal to the randomly generated number, then the (i,j) cell will burn. This assumes that a burning neighbor exists and the probability of spread rule discussed shortly is met as well. Figure 27 displays a visualization of this phase of the CA model.

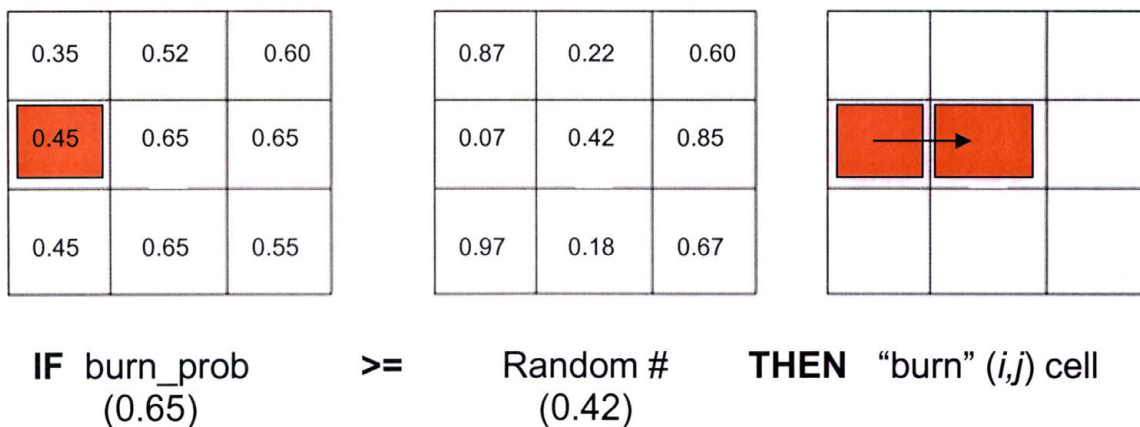


Figure 27: Visual representation of burn probability assessment phase of fire model

Up to this point, wind direction has no bearing on fire spread. I incorporated wind direction into the burn probability assessment phase of the model dynamically by modifying the burn probability value for each grid cell based on the position and number of burning neighbors at each time step. As we know, fire tends to spread in the direction of wind (Berjak and Hearne 2002; Clarke 1994; Karafyllidis and Thanailakis 1997). A set of rules were created to assign weights to the burn probability value to increase burn probability if one or more burning neighbors were upwind from the unburned (i,j) cell. On the other hand, if only one burning neighbor was downwind from the unburned (i,j) cell, the burn probability value was actually decreased to represent the fact that fire is less likely to burn against the direction of wind. Adjustment of these weights over the course of a number of model runs was necessary to produce a simulated “fire” that propagated over the landscape effectively. Figure 28 shows a snapshot of how the location of the burning cells affect the burn probability weights of unburned cells as the fire progresses.

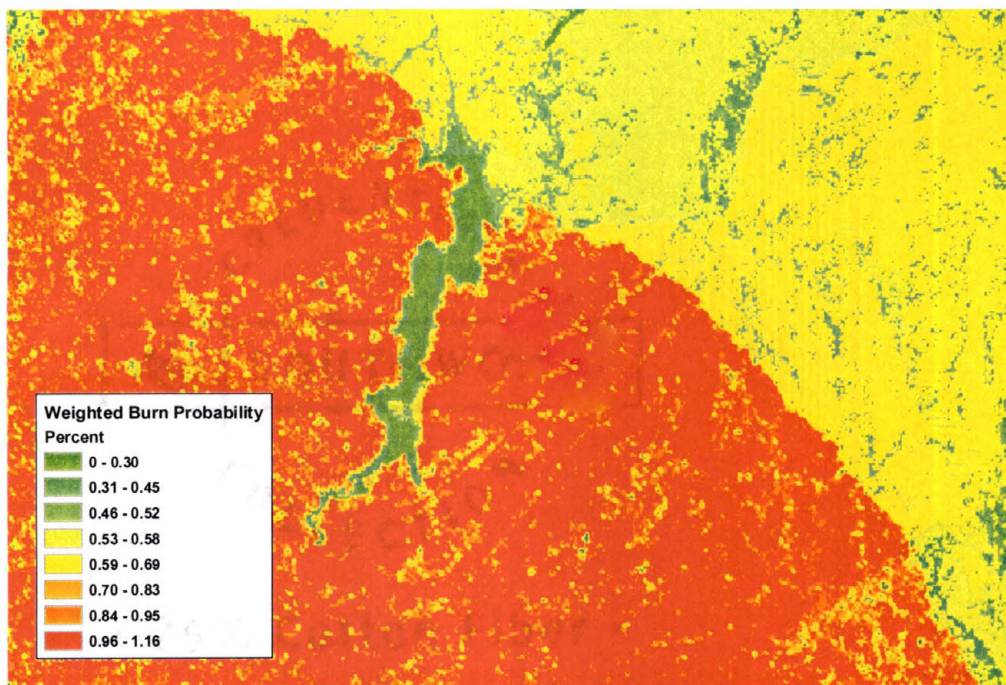


Figure 28: Visualization of effects of wind direction weightings on burn probability

Spread Probability Assessment

The spread probability phase of the model operates in much the same way as the burn probability assessment phase, except its purpose is to “slow down” the progress of fire through fuels with a lower rate of spread. The spread probability grid discussed previously is compared to a randomly generated number produced in ERDAS. If the spread probability value is greater than or equal to the random number, then the fire will spread to the processing cell, assuming that the conditions of the burn probability assessment stage are met as well. To incorporate time into the spread probability phase of the model, I used a set of weights that modified the spread probability value to increase the likelihood of fire spread as the fire residence time value for that burning cell neared the value of zero, which indicates that all fuel in the cell has been consumed. Essentially, this rule states that the more time steps a cell has been burning, the more likely it is to be able to propagate fire to its neighboring cells.

Fire Residence Time Phase

The third phase of my model determines the number of time steps each burning cell will continue to actively burn prior to fire extinction. While a cell is actively burning, it can propagate fire to its neighboring cells. The fire residence time grid discussed previously is input into the model to determine how many time steps a fire will burn at any particular grid cell prior to fire extinction. Once a grid cell begins to burn, the model subtracts one unit of fuel from the residence time grid at each time step. A cell will continue to burn and potentially propagate fire to its neighbors until the residence time grid reaches zero, at which time the fire is extinguished.

Burn Severity Estimation

After running the wildfire behavior model a number of times and averaging the results, I was able to general estimate of which cells were more than 50% likely to burn. Using the equation created for the fire residence time estimation for each fuel type, I determined the total energy output per grid cell based on the fuel type present prior to fire ignition. A final line was added to the fire residence time calculation to derive the total amount of energy released per grid cell. Reclassification of the original fuel model layer based on energy release for each fuel type produced an overall energy release grid. Multiplication of this energy release grid with the averaged output grid produced from the CA model produced the final burn severity risk map for the study site.

Fuel consumption (F) = $((b * h) * 9682.56 \text{ ft}^2) / 2000 \text{ lbs/ton} = \# \text{ tons consumed during each time step}$

b = heat per unit area obtained from BEHAVE software (BTU / ft²)
(b is reduced by 50% after first time step)

h = heat content of 1 lb of fuel (Value is constant: $h = 1 \text{ lb} / 8000 \text{ BTU}$)

9682.56 ft² = area of each grid cell

R = fire residence time (# of time steps fire burns)

Fire Residence Time (R) = Total Fuel Loading Per Grid Cell – Fuel Consumption (F) at each time step

$$\text{Overall energy output per cell } (e) = (R * b) * 9682.56 \text{ ft}^2 \quad (5)$$

Model Validation

In order to assess the overall accuracy of the output of the cellular automata model, I selected 100 random grid cells within the Hayman fire study area as accuracy

assessment points. The Accuracy Assessment tool within ERDAS Imagine generated the random point locations, and I converted these X-Y values into a point shapefile in ArcGIS 8.3. Figure 29 displays the randomly selected points within the Hayman fire boundary. Running the cellular automata model a number of times and averaging the results produced the final output surface. Comparison of the burn severity classes predicted by the cellular automata model to the supervised dNBR burn severity classes provides valuable insight into the ability of the wildfire behavior model to accurately predict wildfire burn severity at the Hayman study area.

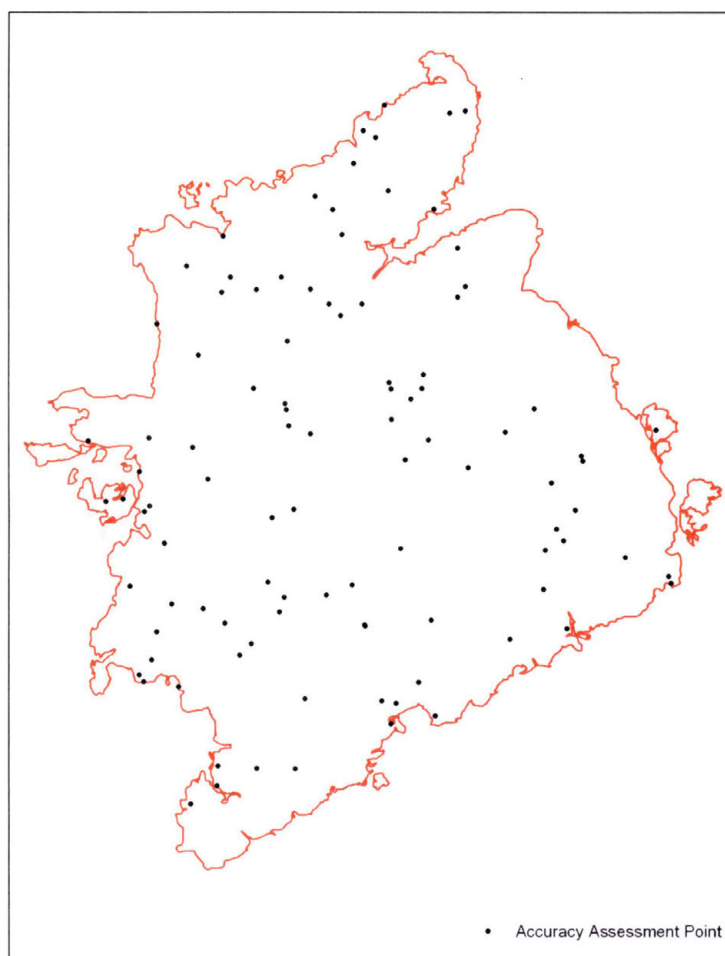


Figure 29: Accuracy assessment points

CHAPTER XI

TOPOGRAPHY, WEATHER, AND VEGETATION CHARACTERISTICS OF THE HAYMAN STUDY AREA

Due to data availability, I limited the wildfire behavior modeling portion of my study to the Hayman fire event discussed previously. The 2002 Hayman fire, being the largest wildfire event in recorded history in Colorado, generated sufficient attention to warrant Congressman Mark Udall of Colorado to request the US Forest Service to create a Hayman Fire Review Panel to conduct a thorough investigation into the causes and effects of the fire (Graham et al. 2003). The resulting investigation produced various spatial datasets that I was able to incorporate into my model of the Hayman fire. A number of characteristics present at the study site prior to and during the fire interacted to produce the resulting fire spread patterns and fire effects observed. I examine the topographic, vegetation, and weather conditions present at the study site in this section.

Topography of the Hayman Fire Study Site

As topography has a significant impact on wildfire behavior, it is necessary to incorporate topographic characteristics into any fire behavior model. The topography of the Hayman fire varies across the study area. This variation in topography may reveal changes in fire behavior across space. Figure 30 shows changes in elevation across the study site. The Kenosha and Tarryall Mountains form a portion of the western boundary

of the Hayman fire (Graham et al. 2003). The highest elevations found in the study area are in this location, with elevations commonly exceeding 10,000 feet. The lowest elevations are found in the north and northeastern portion of the fire perimeter following the direction of flow of the South Platte River, which is the primary drainage system in the study area.

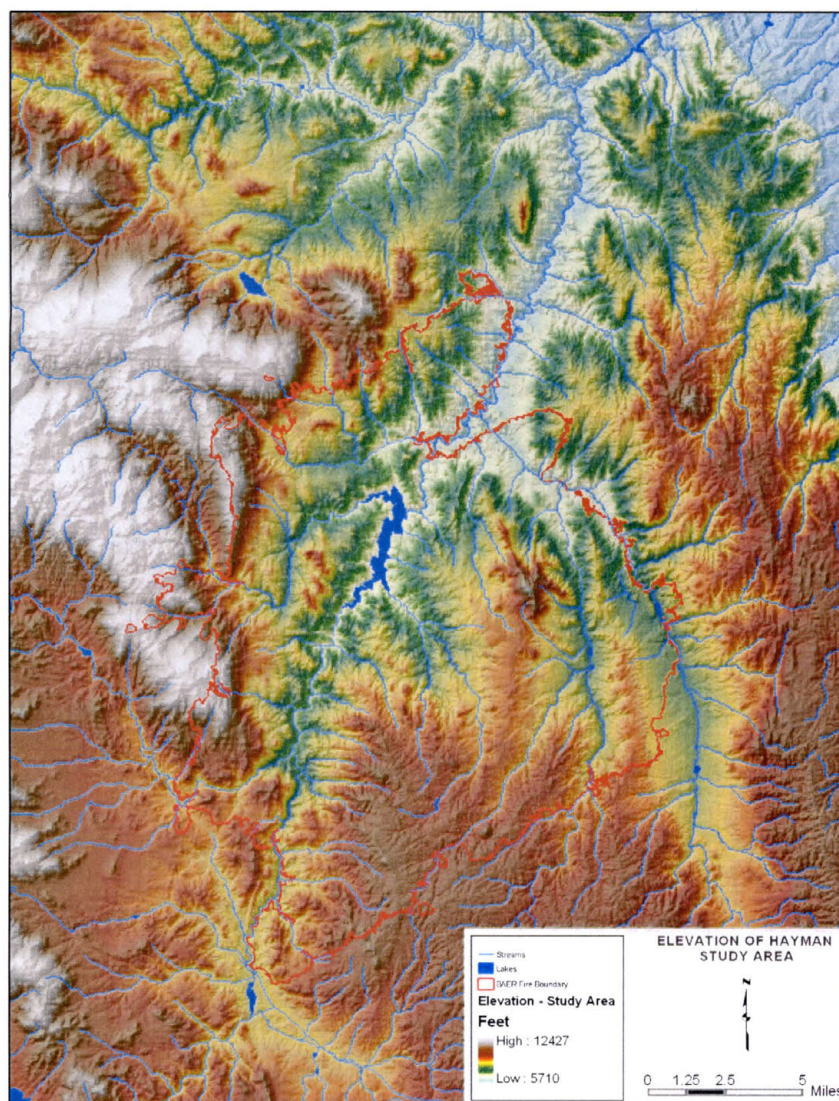


Figure 30: Elevation of Hayman study area

Elevations found downstream of the Cheesman Reservoir, the largest body of water within the fire perimeter, typically range from 6500 – 7500 feet. The southeast

portion of the burned area exhibits the most gentle terrain found within the study area, with slope values commonly below 5% in most areas not directly adjacent to streams or creeks. Terrain in the South Platte River drainage basin, which dominates the central portion of the study area, is relatively rugged. Slope commonly exceeds 25% in this portion of the study area. The heterogeneous terrain in the study area will likely have an impact on the fire behavior observed at the study site (Koutsias and Karteris 2003; Kushla and Ripple 1997; Miller et al. 2003; Patterson and Yool 1998). Graham et al. (2003) point out that there are no major topographic barriers within the fire perimeter that would impede the spread of fire across the landscape.

Weather Conditions Prior/During Hayman Fire

Drought conditions existed in Colorado throughout 2002 and the winter months of late 2001 (Graham et al. 2003). Due to the lack of spring precipitation and reduced amounts of snowmelt due to winter drought conditions, vegetation and soil was extremely dry at the time of fire ignition on June 8, 2002. Fuel moisture was extremely low in both May and June. A common measure of vegetation conditions for fire risk modeling is 1000-hour fuel moisture, which represents moisture levels in dead fuels 3-8 inches in diameter. 1000-hour fuel moisture levels prior to the fire event were near 10% in the days prior to fire ignition, which is substantially below average 1000-hour fuel moisture conditions (Graham et al. 2003). Drought conditions in the months prior to the Hayman fire resulted in extraordinarily dry forest fuels that turned into the largest fire event in recorded history in Colorado.

Daily Weather Conditions of Hayman Fire

The study area has a number of automated weather data collection systems that provide hourly weather information across the study area. Although wind direction varied to some degree over the course of each day, I will look at overall trends in weather patterns for my model. On June 8, 2002, temperature reached 85° F with relative humidity ranging from 6% to 92% over the course of the day (Graham et al. 2003). Winds were from the southwest with sustained winds of approximately 16 mph with gusts exceeding 30 mph at times. Ignition of the fire occurred at approximately 3:00pm on June 8, and the fire burned approximately 1,000 acres by the morning of June 9 (Graham et al. 2003).

June 9th saw the most dramatic fire spread of the Hayman fire. About 60,000 acres burned due in large part to the extreme weather conditions present on this day. High temperature was 86° F and relative humidity remained below 30% for the day (Graham et al. 2003). Sustained southwest winds averaging 15 mph with gusts exceeding 40 mph drove flames over large areas in short periods. This combination of low relative humidity and high winds aligned with the topography of the South Platte River drainage resulted in the remarkable progress of the wildfire across the landscape (Graham et al. 2003). Weather conditions on June 10 were similar to June 9, although relative humidity was substantially higher with slightly lower average wind speed.

June 11th through June 16 did not see the large increases in total burned area. Winds on each of these days generally blew from the north, and wind speeds averaged around 10 mph (Graham et al. 2003). Relative humidity for each of these days was much

higher than the extremely low humidity values noted on June 9. Weather patterns began to shift again on June 17. Southwest to westerly winds with an average wind speed of 8 mph with gusts exceeding 40 mph at times characterized the study site (Graham et al. 2003). Relative humidity on June 17 ranged from 5% to 91%. June 18th exhibited similar weather conditions, although relative humidity was slightly lower than the 17th. Wind speeds were higher than June 17 as well.

June 19th saw another change in weather conditions. Winds began blowing from the north at approximately 10 mph with gusts exceeding 25 mph (Graham et al. 2003). Relative humidity increased during daytime hours; exceeding 50% at most weather stations near the study area. One nearby weather station recorded one-third of one inch of rain just before midnight on June 19 (Graham et al. 2003). Winds once again blew from the southwest on June 20, with sustained winds averaging 12 mph with gusts over 25 mph. Relative humidity was substantially higher than June 19, and minor amounts of rainfall were recorded at some weather stations within the study area (Graham et al. 2003). Similar weather conditions and small amounts of precipitation occurred on June 21. Although the Hayman fire was not officially deemed to be “contained” until July 2, the fire progressed very little after June 21-22. The weather conditions present on each day of the Hayman fire contributed to fire propagation across the study area. It is important to consider these weather conditions when constructing a fire behavior model as they have such a strong impact on model output (Berjak and Hearne 2002; Hargrove et al. 2000; Karafyllidis and Thanailakis 1997).

Vegetation in the Study Area

As is typical of forested landscapes occurring across the Colorado Front Range, the Hayman study site possessed a spatial distribution of fuel types that are dependent on topographic characteristics that vary across the burned area. Typically, south-facing slopes are more xeric in nature than north-facing slopes. For this reason, south-facing slopes tend to possess more open stands of ponderosa pine as well as grasslands and shrublands (Graham et al. 2003). North-facing slopes, on the other hand, are often characterized by more dense stands dominated by Douglas-fir with some blue spruce and aspen mixed in with these other tree species (Graham et al. 2003). Elevation also affects the type of fuels present in the study area. Fuels in the lowest elevations (5,000 – 6,000ft) are generally grasslands and shrublands, while more dense stands of mixed conifer and subalpine coniferous forests are typical of elevations between 7,000 – 10,000 feet. Figure 31 shows elevation values across the study area classified into zones of elevation to represent areas where vegetation type may change due to elevation.

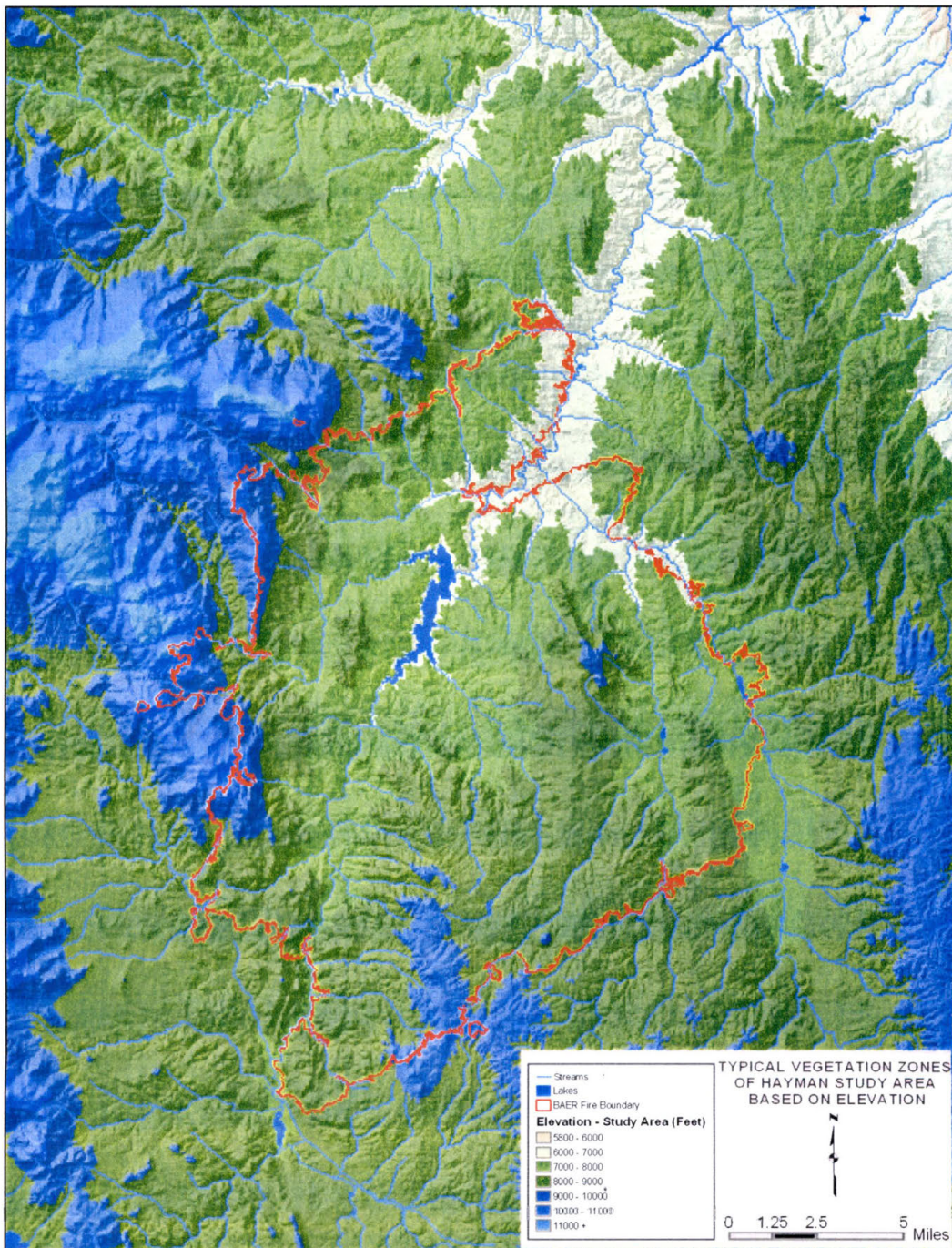


Figure 31: Typical vegetation zones characteristic of the Colorado Front Range

To simplify fire behavior calculations, vegetation across the study area was classified into Anderson (1982) fuel models discussed previously. Figure 32 exhibits the heterogeneous distribution of the Anderson (1982) fuel models within the Hayman fire

boundary. The primary fuel models that exist in the Hayman fire area are Fuel Model (FM) 1, FM 2, FM 8, FM 9, and FM 10. The FM 1 fuels are grassland fuels that typically burn very quickly given the high wind speeds during the Hayman fire event. Fuel loading is typically less than 1 ton per acre, which is relatively low compared to other fuel models present. Shrubland fuels are assigned to FM 2. Fire also propagates across FM 2 fuels very quickly, and fuel loadings of 4 tons per acre are common (Anderson 1982). Open stands of ponderosa pine with grass and sporadic shrubs are generally classified as FM 2 fuels. Fuel model 8 is characterized by fires that move rather slowly due to the lack of abundant surface fuels. Fuel loadings of approximately 5 tons per acre are normal for FM 8, but the surface fuel layer is very thin, which prevents rapid surface fire spread (Anderson 1982). Fuel model 9 is commonly found on north-facing slopes dominated by more dense stands of vegetation such as Douglas-fir. Fuel loadings of 3.5 tons per acre are common. Fires tend to spread faster in fire fuel behavior model 9 than fuel model 8 as larger quantities of surface fuels are present (Anderson 1982). Fuel model 10 is characterized by larger quantities of large diameter (> 3 inches) dead woody fuels that have collected over the years, and fire spread rates are similar to fire spread rates found in fuels designated as fuel model 9 (Anderson 1982).

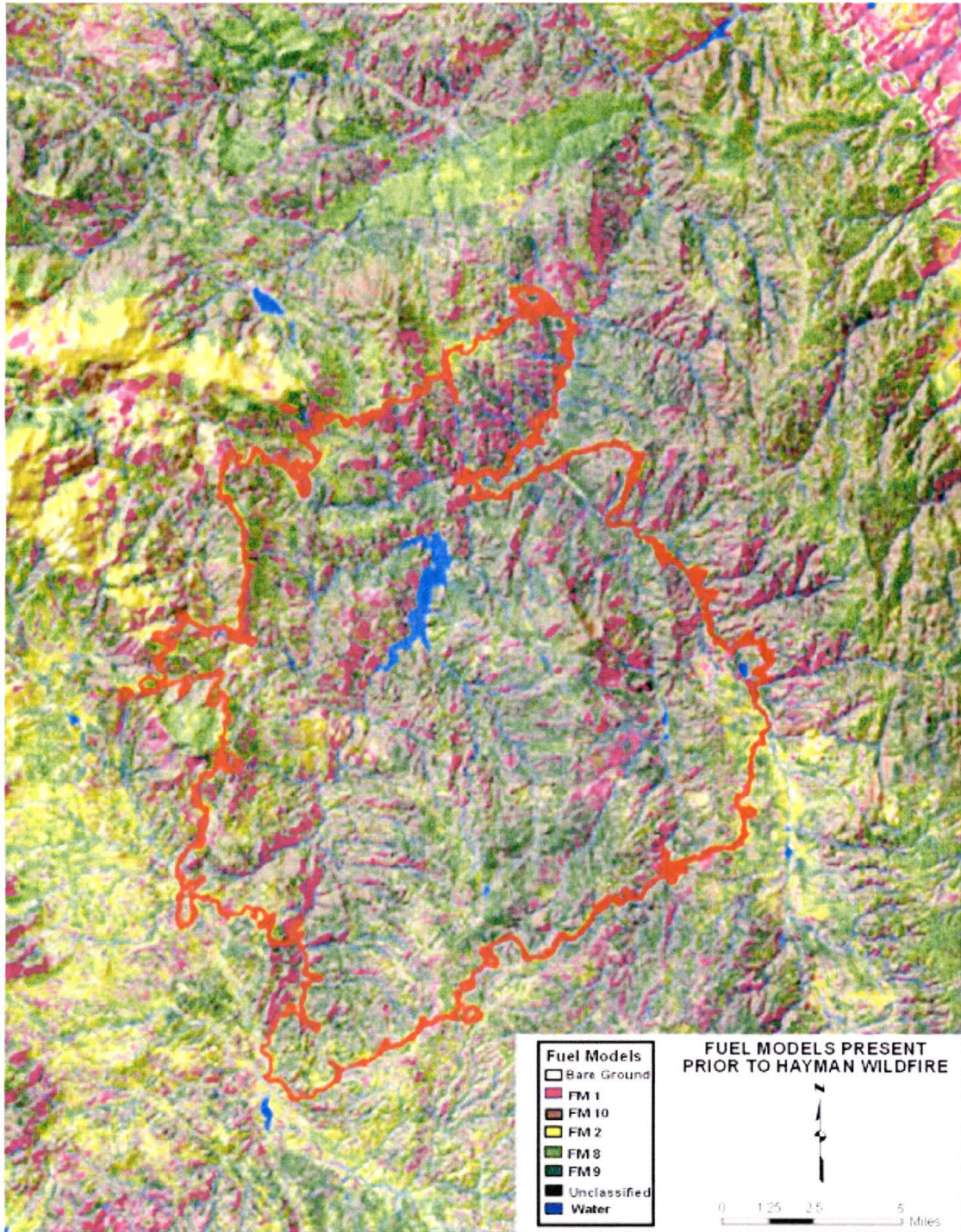


Figure 32: Fuel model distribution within Hayman study area prior to fire event

A number of vegetation characteristics affected wildfire behavior across the study site. As mentioned in the weather characteristics section of this chapter, fuels across the

Hayman fire area were extremely dry due to drought conditions during the months prior to the fire event. Fuel moisture levels have a definite impact on fire spread (Berjak and Hearne 2002). Surface fuel bed depth affects the rate of fire spread from one fuel type to another (Anderson 1982). Fuel bed depths of FM 1, FM 2, and FM 10 all exceed one foot in depth. Each of these fuel types propagate fire across the landscape faster than FM 8 and FM 9, although fire spread rates in FM 9 are close to the spread rate of FM 10. The presence of “ladder fuels” affects the likelihood of fire reaching the forest canopy, which causes torching of entire stands of trees in some circumstances. Fuel model 9 and fuel model 10 possess vegetation that often act as ladder fuels, thus torching of the forest overstory is most common in these fuel types (Anderson 1982).

Fuel treatments, such as prescribed fires and mechanical thinning of trees, affect fire behavior by reducing the amount of fuel available to wildfires (Graham, McCaffrey, and Jain 2004). Few large fuel treatments existed prior to the Hayman fire, although a number of small fuel treatment sites existed that had little impact on fire severity (Graham et al. 2003). Previous wildfires in the vicinity of the Hayman fire did affect fire spread in some locations by reducing available fuels. A review of figure 32 above shows a long oval-shaped fire scar north of the fire boundary in light green. This area was burned during the 1996 Buffalo Creek fire and otherwise would probably have been assigned to FM 9 or FM 10 had the Buffalo Creek fire not occurred. Although this burn scar does not intersect with any portion of the Hayman fire perimeter, smaller fires inside the Hayman fire boundary did reduce fuel loadings, but their impact was minimal when considering the scale of the entire fire event.

CHAPTER XII

RESULTS: CELLULAR AUTOMATA WILDFIRE MODELING

In order to model the propagation of fire across the study area as accurately as possible, a number of trial runs were performed using various weightings for the burn probability grid. As my model is stochastic in nature, a number of iterations of the model given the same weights for the burn probability layer are necessary to produce the overall burn severity risk map. Due to the number of time steps required to represent over two weeks of fire activity during the Hayman fire event, the model is quite computationally intensive. I ran two different versions of the fire behavior model, one based on the four neighbor von Neumann neighborhood and the same model based on the eight neighbor Moore neighborhood. Figure 33 displays the two neighborhoods used for each model. I will discuss the results of the wildfire model output using both von Neumann and Moore neighborhoods. I ran both versions of the model using light wind direction weights to modify the initial burn probability grid and again using heavier weights in an attempt to improve the pattern of fire spread across the study area.

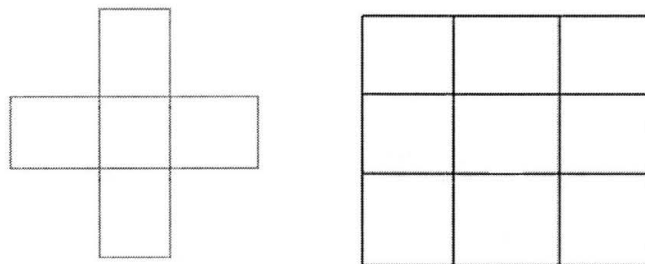


Figure 33: von Neumann and Moore neighborhoods

Von Neumann Neighborhood: Light Burn Probability Weightings

The first attempt to execute the cellular automata model used the following weights to incorporate wind direction with the burn probability (P) grid:

```
IF 1 burning upwind neighbor THEN P * 1.25
IF 2 burning upwind neighbors THEN P * 1.50
IF 1 burning downwind neighbor THEN P * 0.9
IF 2 burning downwind neighbors THEN P * 1.15
IF 3 burning neighbors THEN P * 1.50
IF 4 burning neighbors THEN P * 1.75
```

Although these weightings did increase burn probability values for grid cells downwind from burning neighbors, the resulting output from the model only burns a portion of the area burned during the actual fire event. Additionally, the predicted total burned area was 83,010 acres. The official Burned Area Emergency Response (BAER) team report concluded that the Hayman fire burned approximately 117,000 acres, a difference of almost 34,000 acres (Graham et al. 2003). No further analysis was conducted on this result as burn probability weightings appeared to be too low to accurately represent fire spread. Figure 34 displays the output from this version of the model.

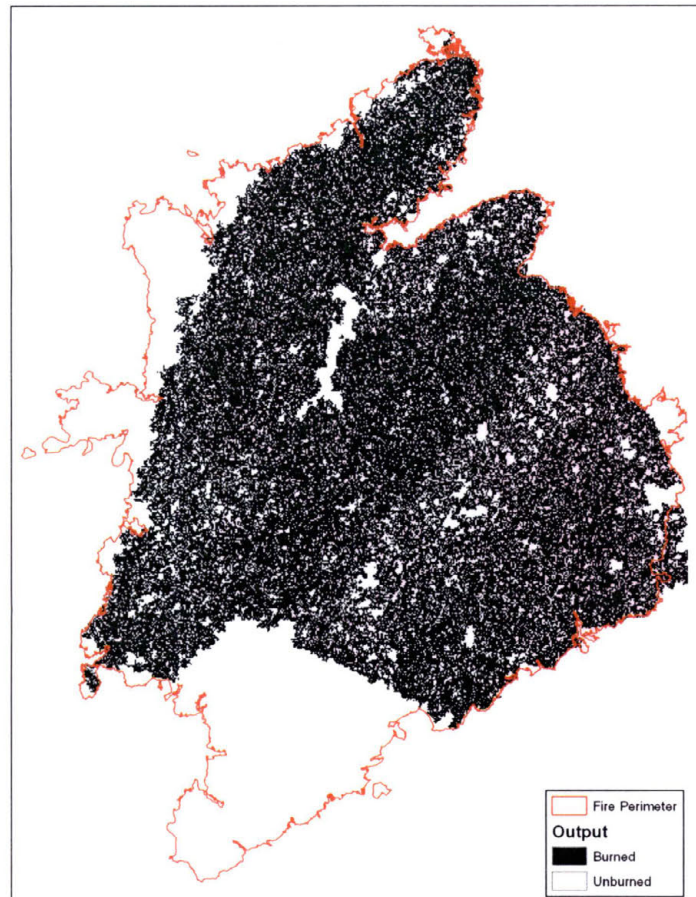


Figure 34: Output of von Neumann model with low wind weights

Von Neumann Neighborhood: Higher Wind Weightings

After reviewing the result of the output of the fire behavior model described previously, I increased the weights to increase the impact of wind direction on the burn probability grid. The following weights modified the burn probability values in this variation of the model:

IF 1 burning upwind neighbor THEN P * 1.35
 IF 2 burning upwind neighbors THEN P * 1.75
 IF 1 burning downwind neighbor THEN P * 0.95
 IF 2 burning downwind neighbors THEN P * 1.25
 IF 3 burning neighbors THEN P * 1.75
 IF 4 burning neighbors THEN P * 1.85

After reviewing the output from the initial run of this version of the model, it appeared that the revised burn probability grid weighting rules dramatically improved the propagation of fire across the landscape. An average of ten separate model runs produced a grid identifying the cells that are more than 50% likely to burn by the cellular automaton. The final output grid predicts a total burned area of 129,530 acres, which is 10.7% larger than the 117,000 acres actually burned within the 138,000 acre Hayman fire perimeter (Graham et al. 2003). Figure 35 displays the cells identified as more than 50% likely to burn per this version of the model. It appears that the bulk of the burned area missed by the model is located near the western and southwestern edge of the BAER fire boundary.

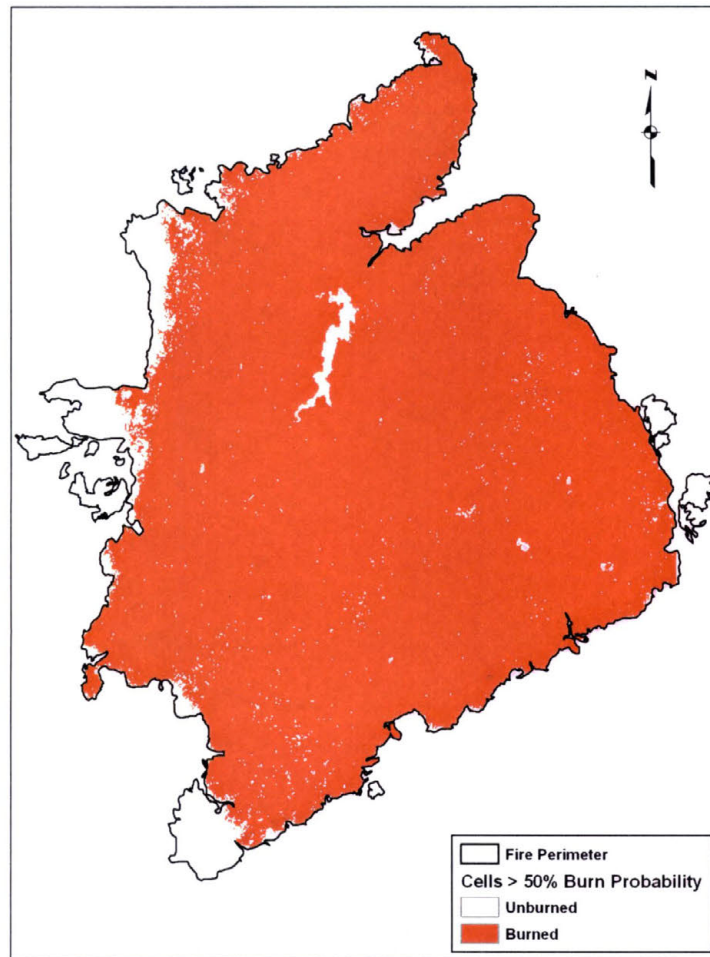


Figure 35: Output of von Neumann model with higher wind weights

Assessment of the randomly selected accuracy assessment points reveals that of the cells identified as burned by the model, 95.5% of them were also classified as burned by the supervised classification of the dNBR image of the Hayman study site. Overall, of the cells classified as burned in the dNBR image, the CA model identified grid cells as burned with 94.7 % accuracy.

Accuracy assessment of the burn severity output was broken down into individual burn severity classes to compare how well the fire severity model predicted burn severity patterns across the landscape. Figure 36 displays the predicted burn severity output, which was based on classification of energy output per grid cell.

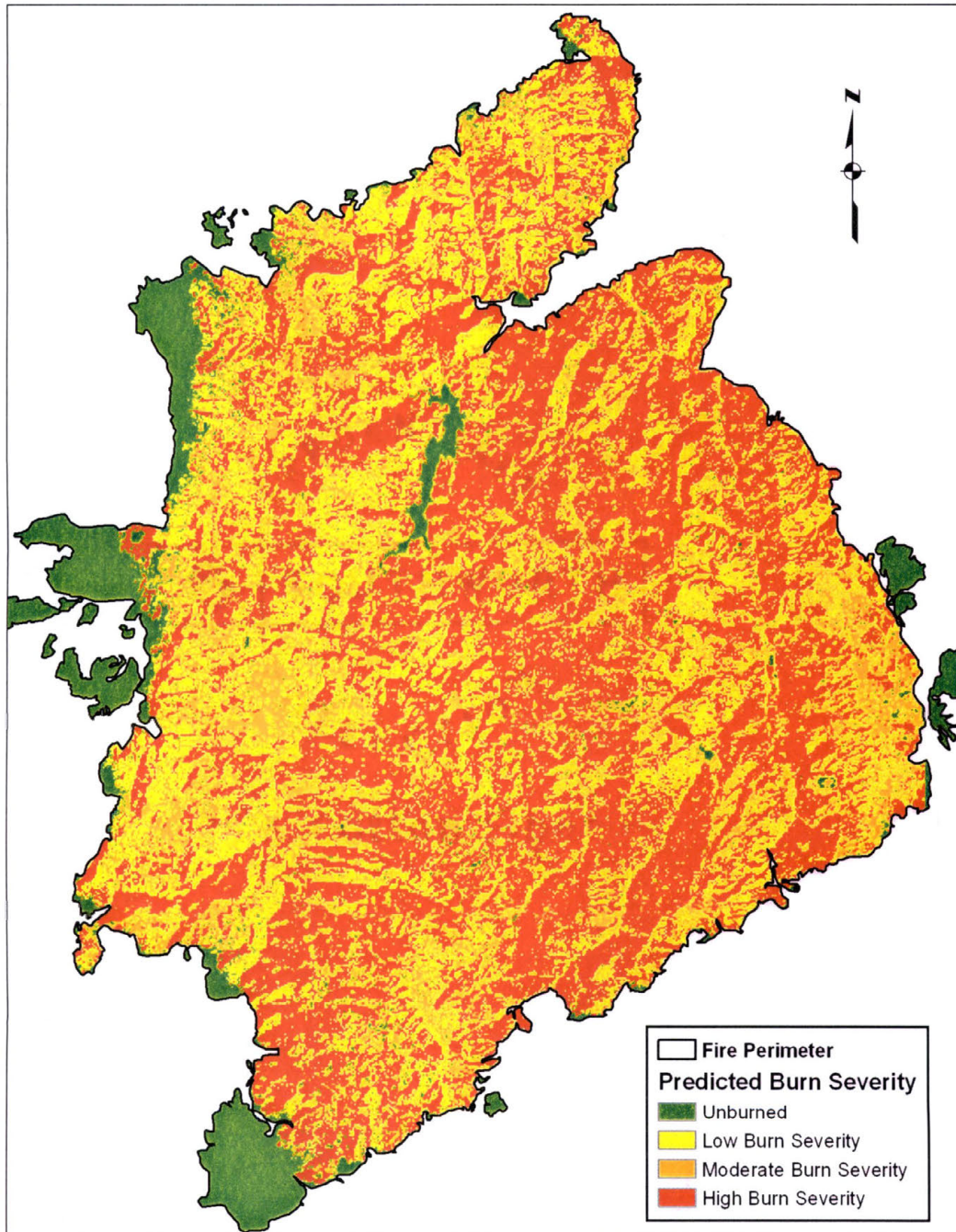


Figure 36: Predicted burn severity from von Neumann model with higher wind weights

A review of table 4 and figure 37 show that the model output predicted the percentage of total acreage assigned to each burn severity class quite well. It appears that the model underestimated total acreage assigned to unburned and low burn severity

classes but overestimated the moderate and high burn severity classes. Although this data is useful in assessing the effectiveness of the model output, it is critical to view this data from a spatial point of view. I will discuss the accuracy of the model in predicting burn severity at the randomly selected accuracy assessment points in the next section.

	Unburned	Low	Moderate	High
Model Results	8.7%	24.2%	21.1%	45.9%
BAER	15.2%	34.1%	15.9%	34.8%

Table 4: Percentage of total acres assigned to each burn severity class

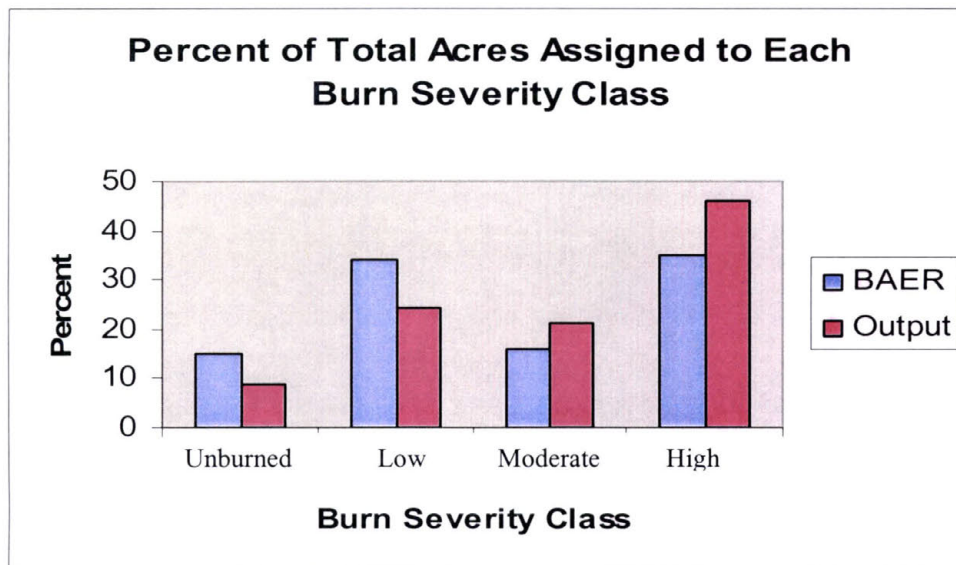


Figure 37: Graph of percentage of total acreage assigned to each burn severity class

An analysis of the accuracy assessment points generated allows us to determine how well the model agrees with the supervised classification of dNBR values derived from the remote sensing portion of my study. Of the cells identified as possessing high burn severity per my model, 52.1% of these cells were also identified as high burn severity in the supervised dNBR image. The cells assigned moderate burn severity values by the model matched the dNBR result with 31.8% accuracy. Of the cells

identified as low burn severity, 36.8% of these cells were also identified as low burn severity in the supervised dNBR image. The model output matched the unburned severity class of the dNBR image 18.2% of the time. Overall accuracy assessment of burn severity between the von Neumann model output and the supervised classification of the dNBR image resulted in an accuracy of 41%.

Moore Neighborhood: Light Burn Probability Weightings

Due to computation time, I conducted five model runs and produced a grid identifying cells more than 50% likely to burn. It was evident that a pattern emerged within these five runs, thus additional runs would likely have little impact on the model results. I used a variant of the light wind weightings applied to the initial run of the von Neumann version of the CA model for the initial simulation using the Moore neighborhood version of the model. The following weights were applied to the burn probability grid of the model:

```

IF 1 burning upwind neighbor THEN P * 1.20
IF 2 burning upwind neighbors THEN P * 1.35
IF 3 burning upwind neighbors THEN P * 1.5
IF 1 burning downwind neighbor THEN P * 0.9
IF 2 burning downwind neighbors THEN P * 1.0
IF 3 burning downwind neighbors THEN P * 1.05
IF 4 burning neighbors THEN P * 1.15
IF 5 burning neighbors THEN P * 1.35
IF 6 burning neighbors THEN P * 1.5
IF 7 burning neighbors THEN P * 1.65
IF 8 burning neighbors THEN P * 1.75

```

While the lightly weighted von Neumann neighborhood model was unable to simulate the propagation of fire across the entire Hayman fire boundary, the Moore neighborhood model did allow for fire spread across the bulk of the study area using the light wind weights. Figure 38 displays the output from the first run of this variation of the model.

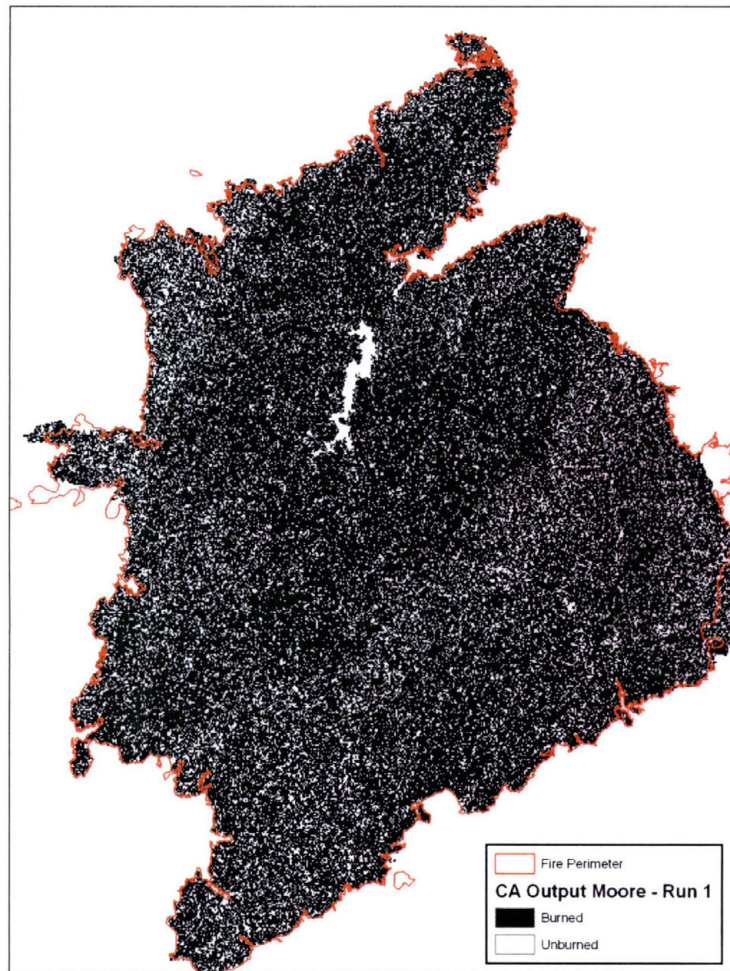


Figure 38: Output image of grid cells identified as burned by Moore neighborhood model with lower wind weightings

Although the Moore model did closely match the general shape of the Hayman fire perimeter, the lower weights applied to the burn probability grid resulted in misclassification of large numbers of pixels as unburned. Analysis of the output cells that were predicted as over 50% likely to burn resulted in an estimated burned area of 48,157 acres compared to an actual burned area of approximately 117,000 acres. It should be noted that looking at any one of the five runs using the lower wind weights produced an average burned area of approximately 109,000 acres. The process of averaging the five runs identifies only pixels more than 50% likely to burn, which

explains the lower estimated burned area using the average output. A review of the accuracy assessment points shows that of the cells identified as burned by the model, 92.3% of these cells were also classified as burned in the supervised classification of the dNBR image. A more revealing statistic shows that of the cells identified as burned by the classified dNBR image, the model output correctly predicted only 41.5% of these cells to be burned.

A review of table 5 and figure 39 show that the model output in this instance dramatically overestimated percent of total area classified as unburned and underestimated all other classes of burn severity. The model most closely estimated total percentage of the landscape classified as high burn severity. It is apparent that the weightings applied to the burn probability grid were too low to accurately identify burned versus unburned cells.

	Unburned	Low	Moderate	High
Model Results	65.6%	9.3%	3.5%	21.6%
BAER	15.2%	34.1%	15.9%	34.8%

Table 5: Percentage of total acreage assigned to each burn severity class

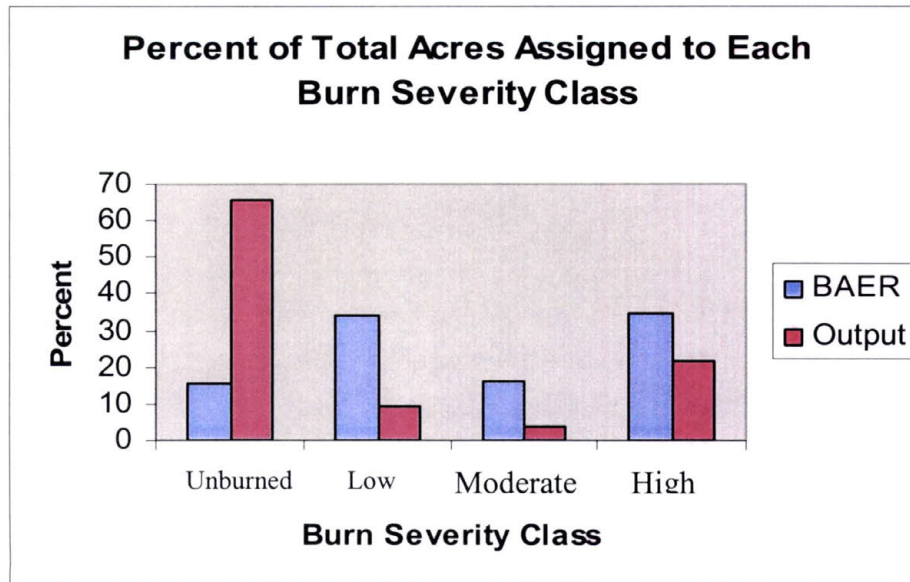


Figure 39: Percentage of total acreage assigned to each burn severity class

Although this variation of the CA model employing the Moore neighborhood failed to identify a large number of grid cells as burned, of the cells identified as burned, accuracy assessment was more encouraging. Of the cells identified as possessing high burn severity per my model, 53.8% of these cells were also identified as high burn severity in the supervised dNBR image. The cells assigned moderate burn severity values by the model matched the dNBR result with 50% accuracy. Of the cells identified as low burn severity, 27.3% of these cells were also identified as low burn severity in the supervised dNBR image. The model output matched the unburned severity class of the dNBR image only 4.9% of the time. Overall accuracy assessment of burn severity between the model output and the supervised classification of the dNBR image resulted in an accuracy of 21%. Figure 40 shows the classified burn severity output based on cells with greater than 50% likelihood of burning.

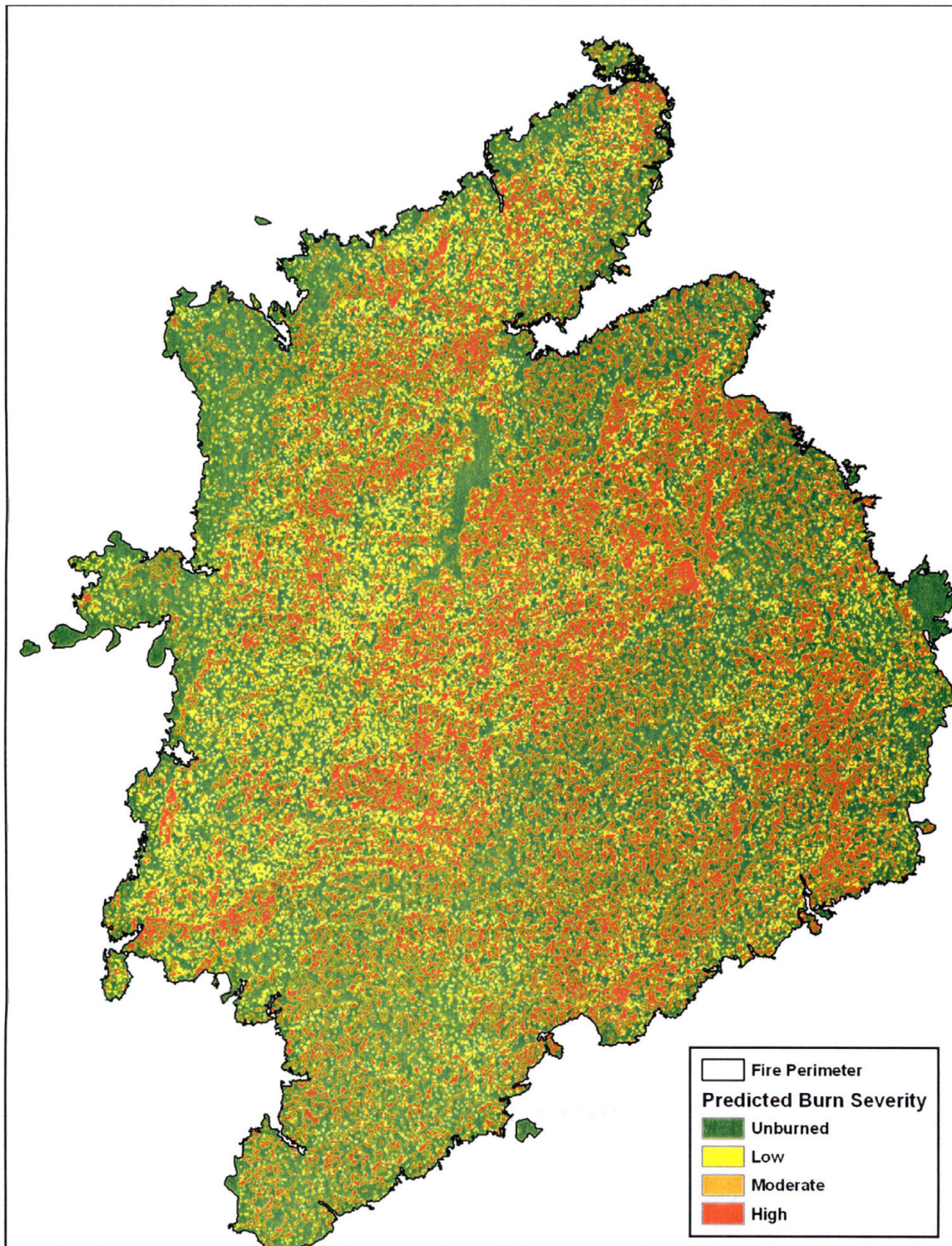


Figure 40: Predicted burn severity output from Moore neighborhood version of fire behavior model with lower wind weightings

Moore Neighborhood Higher Burn Probability Weightings

As the weights assigned to the burn probability grid in the previous variation of the model were too low to identify burned versus unburned cells across the study area, I modified the weights to increase the impact of wind direction on the burn probability grid. The following weights modified the burn probability values in this variation of the model:

IF 1 burning upwind neighbor THEN $P * 1.35$
 IF 2 burning upwind neighbors THEN $P * 1.55$
 IF 3 burning upwind neighbors THEN $P * 1.75$
 IF 1 burning downwind neighbor THEN $P * 0.95$
 IF 2 burning downwind neighbors THEN $P * 1.20$
 IF 3 burning downwind neighbors THEN $P * 1.35$
 IF 4 burning neighbors THEN $P * 1.50$
 IF 5 burning neighbors THEN $P * 1.65$
 IF 6 burning neighbors THEN $P * 1.75$
 IF 7 burning neighbors THEN $P * 1.85$
 IF 8 burning neighbors THEN $P * 1.95$

It appeared that the revised burn probability grid weighting rules improved the propagation of fire across the landscape as compared to the other Moore neighborhood version of the model. An average of five model runs produced a grid identifying the cells that are more than 50% likely to burn by the cellular automaton. The final output grid predicted a total burned area of 104,902 acres, which is 89.7% of the total area burned within the fire perimeter (Graham et al. 2003). A review of the accuracy assessment points shows that of the cells identified as burned by the model, 94.3% of these cells were also classified as burned in the supervised classification of the dNBR image. Overall, of the cells identified as burned by the classified dNBR image, the model correctly predicted 74.5% of these cells to be burned. Figure 41 shows the cells predicted to be more than 50% likely to burn by the cellular automata fire model.

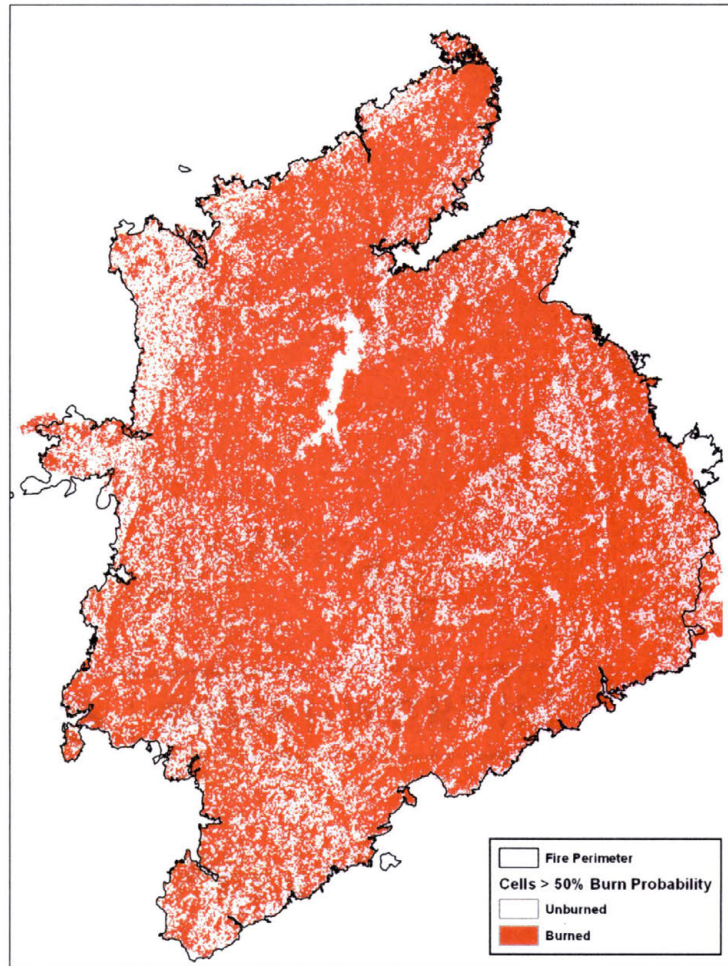


Figure 41: Cells identified as burned by Moore neighborhood model with higher burn probability weightings

A review of table 6 and figure 42 shows that the model overestimated total percentage of land classified as unburned or high burn severity and underestimated areas of low and moderate burn severity. Comparison of figure 40 and figure 43 shows that the higher wind direction weightings improved the accuracy of the model output.

	Unburned	Low	Moderate	High
Model Results	26.1%	21.1%	9.3%	43.5%
BAER	15.2%	34.1%	15.9%	34.8%

Table 6: Percentage of total acreage assigned to each burn severity class

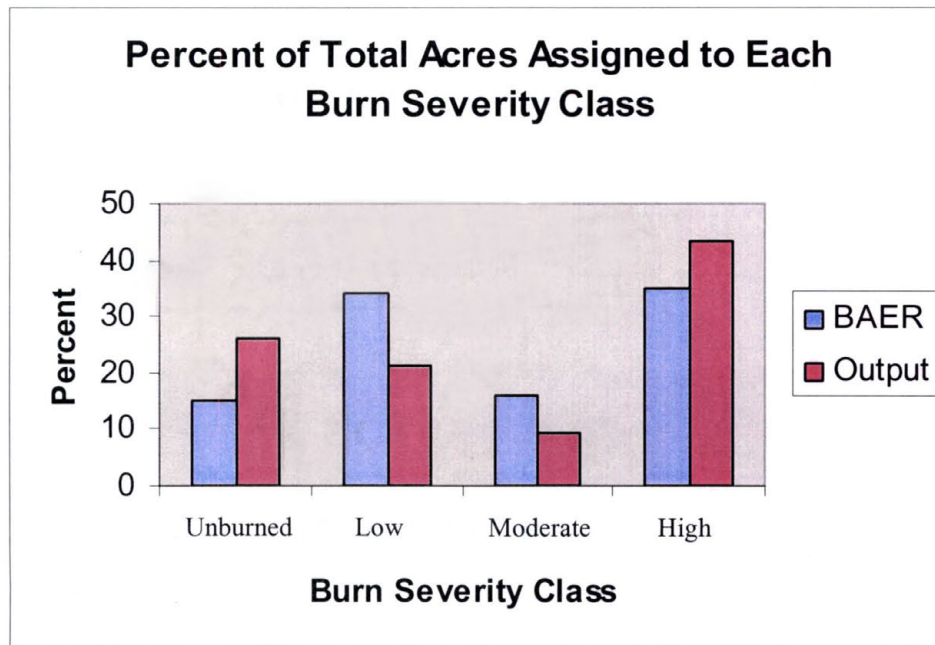


Figure 42: Percentage of total acreage assigned to each burn severity class

Analysis of the burn severity assessment points provides insight into the effectiveness of this variant of the model. Of the cells identified as possessing high burn severity per my model, 55.6% of these cells were also identified as high burn severity in the supervised dNBR image. The cells assigned moderate burn severity values by the model matched the dNBR result with 28.6% accuracy. Of the cells identified as low burn severity, 27.8% of these cells were also identified as low burn severity in the supervised dNBR image. The model output matched the unburned severity class of the dNBR image only 6.7% of the time. Overall accuracy assessment of burn severity between the model output and the supervised classification of the dNBR image resulted in an accuracy of 34%. Figure 43 shows the classified burn severity output based on energy release per cell for this version of the wildfire behavior model.

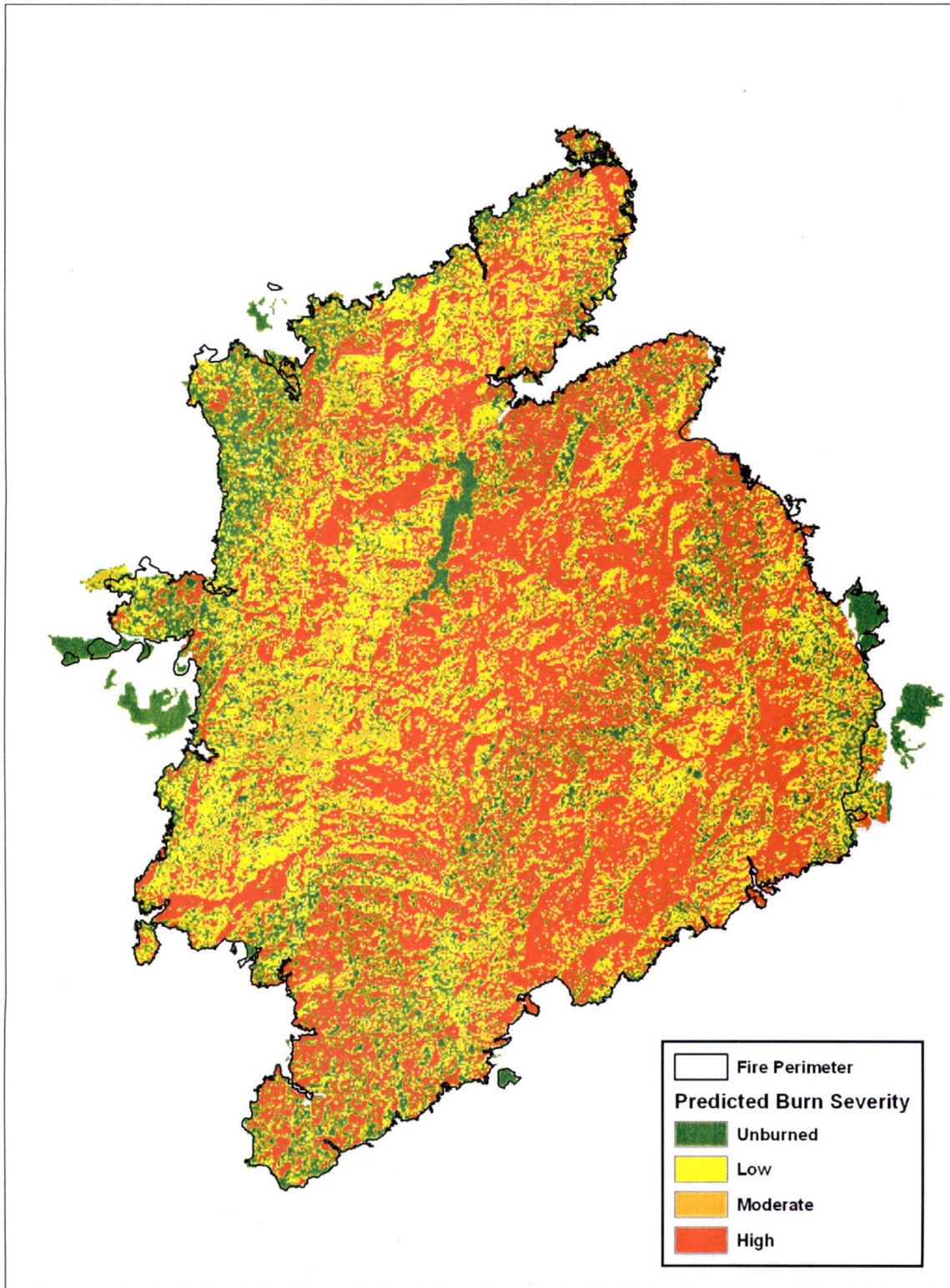


Figure 43: Predicted burn severity output from Moore neighborhood version of fire behavior model with higher wind weightings

CHAPTER XIII

DISCUSSION

Remote Sensing Portion of Study

A review of the results of unsupervised and supervised classifications of the differenced Normalized Burn Ratio (dNBR) output reveals that this algorithm does provide useful information at each of the three study sites. The dNBR algorithm, in conjunction with false color post-fire Landsat TM imagery, accurately delineated the fire boundary for each study site. The predicted fire perimeter agreed with the official BAER fire boundaries for the Missionary Ridge, Hayman, and Rodeo-Chediski fires with at least 89% accuracy on the low end for the Missionary Ridge fire. The ability of the dNBR output to produce highly accurate fire perimeter estimates in a timely manner will likely be valuable to BAER teams, forest managers, and fire ecologists among others.

In addition to providing accurate estimates of fire boundaries, classification of dNBR values using unsupervised and supervised methods yielded useful information regarding burn severity patterns at each of the three study sites included in my analysis. In each circumstance, supervised classification proved more effective than unsupervised classification. Figure 44 displays the improvements in accuracy using supervised versus unsupervised classification techniques.

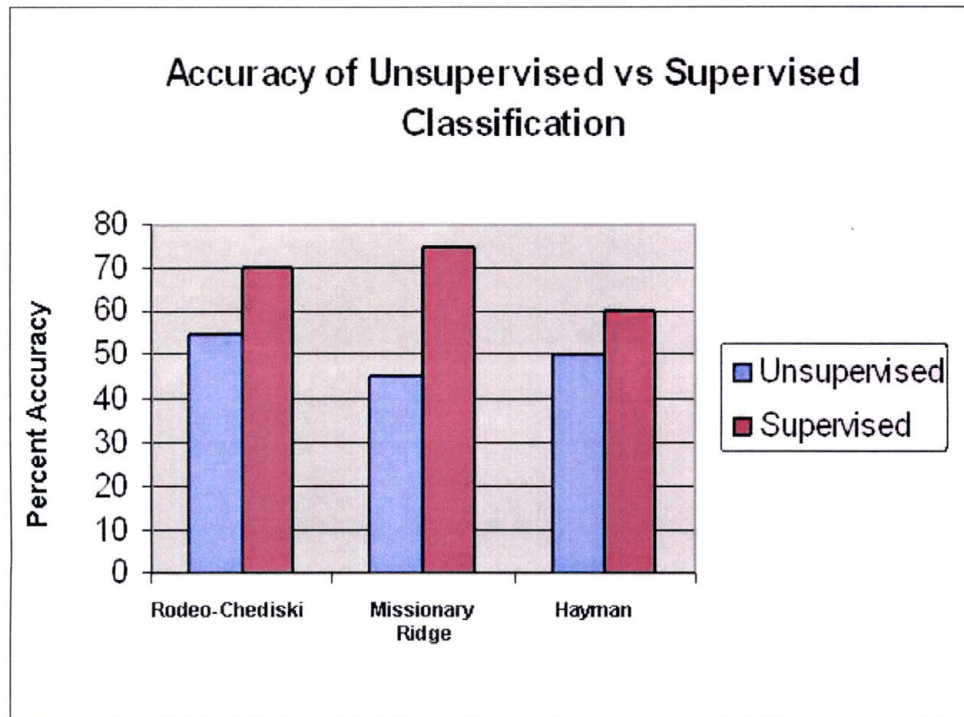


Figure 44: Comparison of accuracy of supervised versus unsupervised classification of dNBR image

It appears that unsupervised classification underestimated the percentage of total acreage assigned to unburned and low burn severity classes and overestimated percent of total burned area assigned to moderate and high burn severity classes. Supervised classification, on the other hand, varied in its ability to accurately assign pixels to the appropriate burn severity class. As a whole, supervised classification methods performed measurably better than unsupervised classification in assigning pixels to the correct burn severity class, as per the BAER team maps.

Limitations of the Remote Sensing Analysis of Burn Severity

Unsupervised classification appear to yield burn severity classification accuracy ranging from 45 to 55 percent, and supervised classification accuracy ranged from 60

percent for the Hayman fire to 75 percent for the Missionary Ridge fire. One drawback of the study is that the BAER burn severity maps available for the accuracy assessment portion of the study were lower resolution JPEG images with the exception of the Rodeo-Chediski severity map that was a much higher resolution TIFF image. The JPEG image of the Hayman study site was by far the lowest resolution image used for the accuracy assessment procedure. Unfortunately, no higher resolution burn severity map was available for accuracy assessment. Although the JPEG image of the Hayman burn severity map could be resampled to match the 30 meter spatial resolution of the dNBR output, no improvement in the quality of the BAER map data would result from this procedure. Note that the lowest supervised classification accuracy for any of the three fire events studied was associated with the Hayman fire. It must be noted that the lower supervised classification accuracy for this study site may be partially due to the poor resolution of the data from the BAER burn severity map used as a reference in the accuracy assessment procedure. The result of the supervised classification procedure does agree well visually with the BAER burn severity map.

A second limitation of the dNBR assessment of wildfire burn severity is the potential for cloud pollution in either the pre-fire or post-fire image affecting the results of the dNBR analysis. Figure 45 shows the impact of clouds and their shadows on the supervised classification output from the Missionary Ridge study site. The two large green areas in the inset image, identified as unburned per the supervised classification result, are due to the shadows cast by the two small clouds in the larger post fire image of figure 45. Multi-temporal analyses such as the dNBR algorithm are easily affected by changes in reflectance due to phenomena other than wildfire (Fraser, Fernandes, and

Latifovic 2003; Fraser, Li, and Cihlar 2000; Zhang, Wooster, et al. 2003). Substantial amounts of smoke are also visible in the post-fire image below, but infrared wavelengths penetrate smoke better than visible bands (Miller and Yool 2002). It does not appear that the smoke in the post-fire image had a substantial effect on the dNBR values.

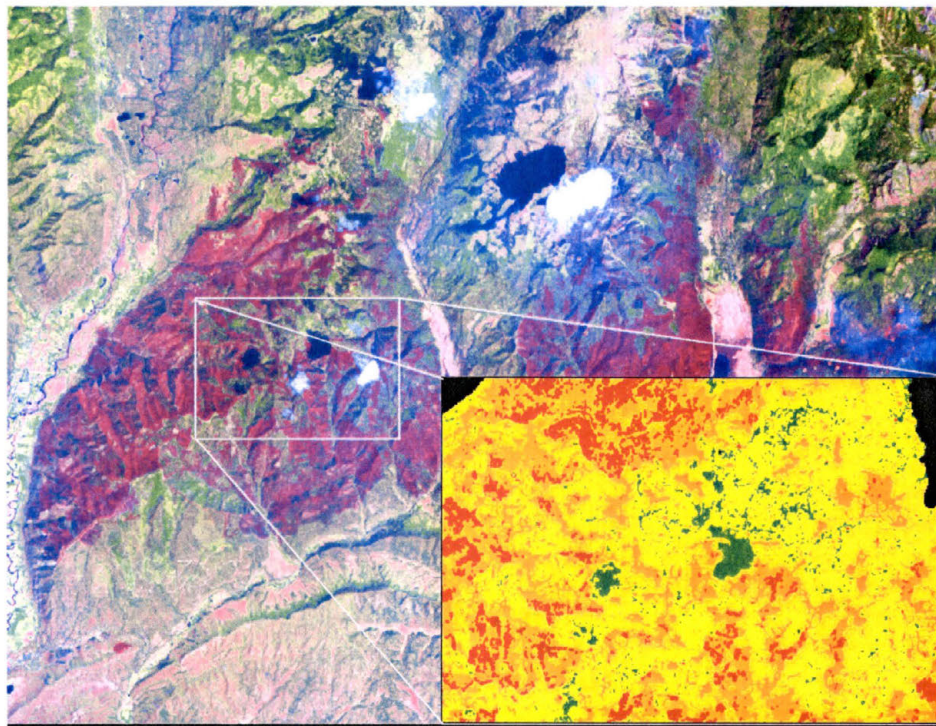


Figure 45: Inset image shows effects of clouds and cloud shadows on burn severity output from dNBR algorithm

Availability of quality pre-fire and post-fire Landsat TM or ETM + imagery is another limitation of the study. As BAER teams must assess burn severity and submit their forest rehabilitation recommendations to forest managers within eight days of fire containment, they are often hard-pressed to locate a post-fire image within this short time window. Additionally, locating a pre-fire image during the same season as the fire event is crucial to prevent misclassification of pixels due to seasonal variation in vegetation

reflectance (Fraser, Fernandes, and Latifovic 2003; Fraser, Li, and Cihlar 2000; Key and Benson 1999; Miller and Yool 2002; Zhang, Wooster, et al. 2003). These issues may occasionally be a hindrance to BEAR teams in employing this technique to assess wildfire burn severity within their tight timeframes.

A final limitation of the dNBR algorithm in this study relates to classification error due to “gray areas” or fuzziness in the classification thresholds for unburned, low, moderate, and high burn severity classes. While supervised classification may assign a cell to the high burn severity class, applying various classification thresholds could result in the cell being assigned to the moderate burn severity class. This is clearly a consideration for future studies employing the dNBR algorithm.

Wildfire Behavior Modeling Portion of Study

The results of both the von Neumann and Moore neighborhood versions of the wildfire behavior model constructed for this study show that a stochastic cellular automata model can produce useful information to decision makers such as forest managers and BEAR teams. Simulations using four different versions of the fire behavior were run. Two of these four model variants used the von Neumann neighborhood with either lower or higher burn probability weightings, and the other two employed the Moore neighborhood with both lower or higher wind weightings.

Results from each of these models showed that the lighter burn probability weightings were too low to produce output that accurately reflected the actual propagation of fire across the Hayman study area. It was apparent that the initial model based on the von Neumann neighborhood with the lower wind weightings was unable to

simulate a backing fire, which is the portion of a fire that slowly spreads in the opposite direction of the wind. Figure 34 reflects this problem as all fire spread follows the wind direction, which was primarily from southwest to northeast. Little or no fire spread occurred in the southern portion of the fire perimeter as the burn probability weights were too low to model a backing fire. The model that used the lower wind weightings with the Moore neighborhood did permit the spread of a backing fire, but the wind weightings were still insufficient to model the propagation of fire across the landscape with a high degree of accuracy.

The impact of the burn probability weights is apparent when comparing the output of the models based on low wind weights versus higher wind weights. The von Neumann and Moore neighborhood models that use the higher wind weightings identify many more cells as burned than the models incorporating the lighter wind weights. The averaged output identifying cells more than 50% likely to burn for both the von Neumann and Moore neighborhoods predicted a total burned area that came within 11% of the official area identified as burned (Graham et al. 2003).

Time management is an important consideration when assessing the accuracy of dynamic models such as the wildfire behavior model presented in this study. Although time was not strictly managed, it was taken into consideration to attempt to represent the varying rates of spread exhibited by each unique fuel type. As discussed previously, the spread probability layer of my model attempted to manage time by assigning high probability of spread at time $t + 1$ values to fuels that burn quickly and assigning lower probability of spread values to slower burning fuels. The spread probability layer was linked to the fire residence time layer to increase the likelihood of fire spread the more

time steps a burning cell continues to burn. As each time step in my model was intended to represent 10 minutes of real-time fire activity, I estimated that the model would need to run for approximately 2000 time steps to propagate from the point of ignition to the time when the fire had spread across the entire study area. A review of figure 46 shows the output of the wildfire behavior model in 200 time step intervals. The model burned across the Hayman study site in just over 1600 time steps. This is apparent by looking at the progress made between time step 1600 and step 1800. Only a very small portion of the northernmost tip of the fire continued to burn after time step 1600. Analysis of these results shows that my fire behavior model predicted the fire to burn for approximately 265 to 270 hours, or a total of about 11 days of fire activity. Graham et al. (2003) show that the majority of the total area burned over the course of the Hayman fire event occurred between June 8 and June 20, or a total of 13 days. Temporal accuracy of my model appears to be adequate considering the long duration of the fire event. Most existing studies that employed cellular automata to model wildfire used fire events that burned over a duration of less than one day (Clarke 1993, Berjak and Hearne 2002).

Although the model output produced a fair approximation of the total time required to propagate across the entire study area, the model performed somewhat poorly in representing the spatial accuracy of fire spread over time. For example, the actual Hayman fire burned over 60,000 acres by the end of June 9. The model output at time step 200, which equates to the second day of real-time fire activity, only predicted a total burned area of 2511 acres. It should be noted that the fire spread that occurred during the day of June 9th was unprecedented, resulting from a combination of extreme low humidity, low fuel moisture, extremely high winds exceeding 40 mph at times, and ideal

alignment of the winds with the topography of the South Platte River drainage (Graham et al. 2003).

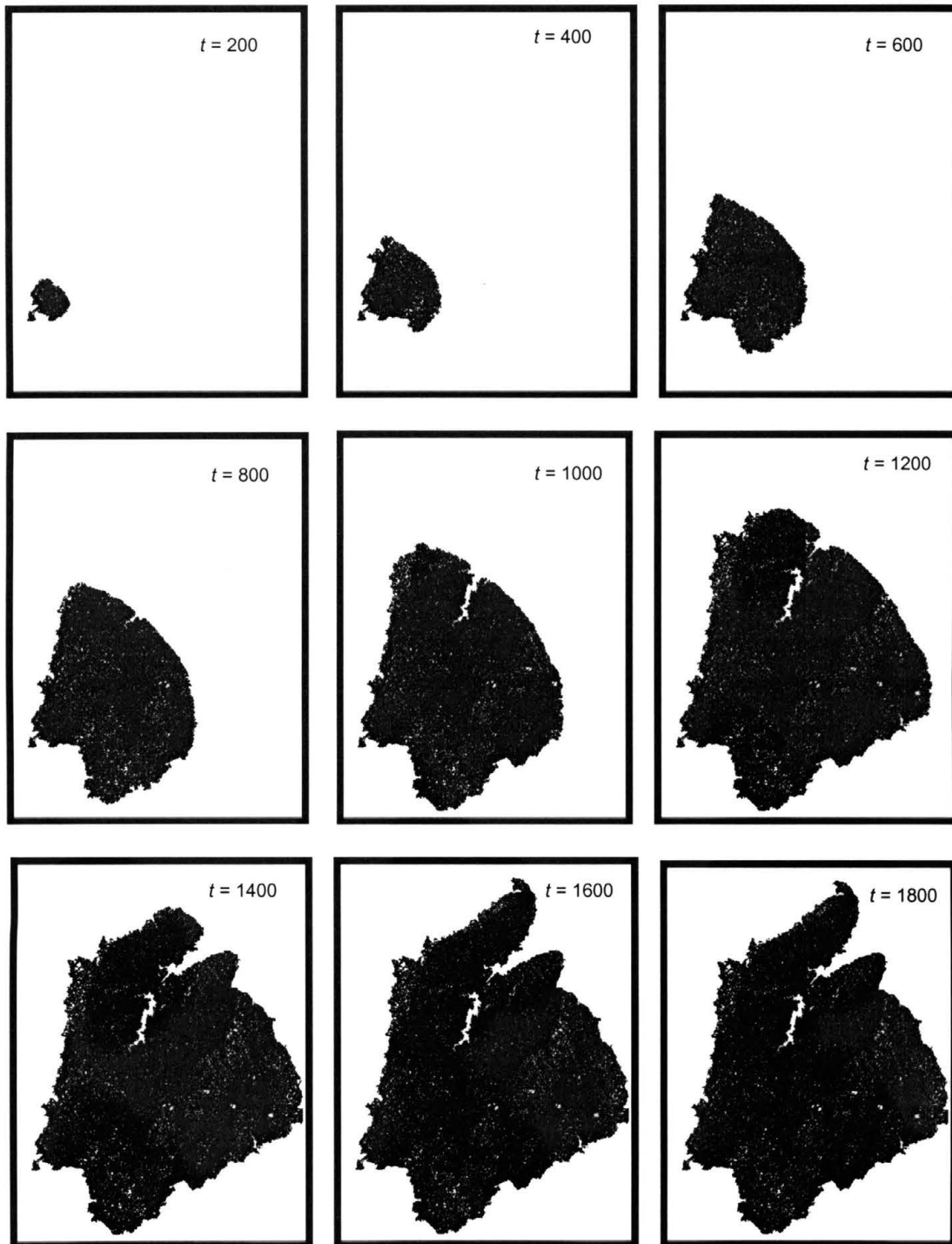


Figure 46: Images show progression of fire at 200 time step intervals as predicted by von Neumann version of fire behavior model with higher wind weights

One of the primary purposes of this model was to attempt to identify areas that have experienced severe wildfire that are of interest to BAER teams. BAER teams, in assessing areas negatively affected by severe wildfire, often focus on areas assigned either moderate or high burn severity (Graham, McCaffrey, and Jain 2004; Graham et al. 2003). Accuracy assessment of cells identified by my model to possess either moderate or high burn severity matched the supervised classification of the dNBR image with 80% or greater accuracy for each model variant. This fact shows that my cellular automata wildfire behavior model is able to provide valuable information to BAER teams and other decision makers either before, during, or after fire events. Figure 47 shows the improvement of the fire model to predict areas of either high or moderate burn severity, which are areas of primary interest to BAER teams.

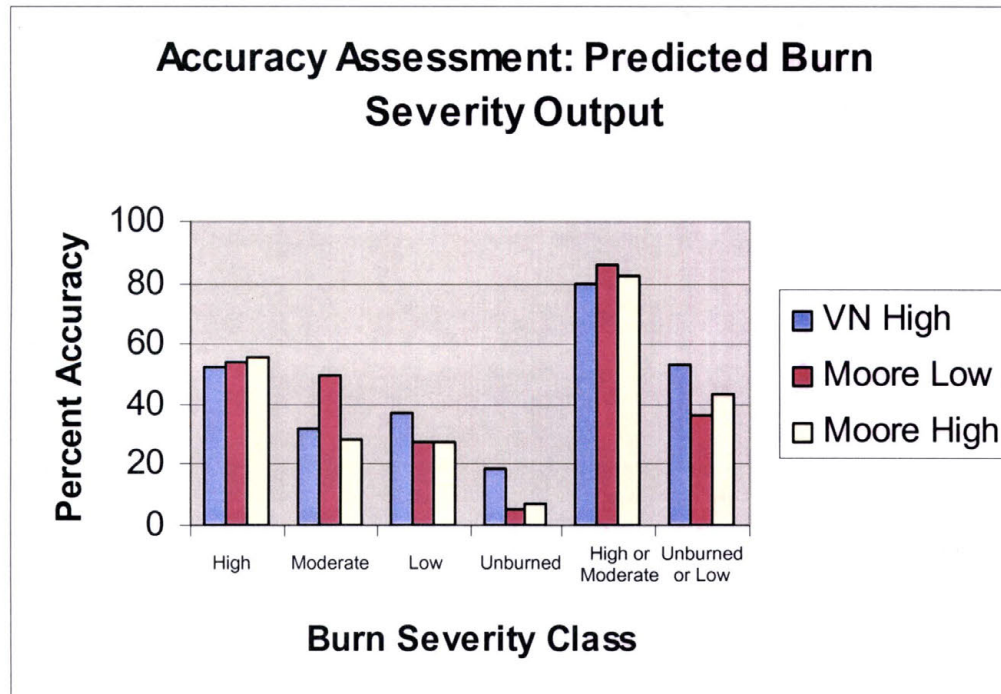


Figure 47: Predicted burn severity output from the fire behavior models. Note that all three versions of the fire behavior model identified areas classified as either high or moderate burn severity with at least 80 percent accuracy

Although wildfire behavior researchers know that there is a relationship between fuel, weather, and topographic variables that were discussed in this study with fire behavior, no statistically significant relationship has been established between any of these fire behavior variables and fire burn severity to date. I used SPSS statistical analysis software to conduct a stepwise multiple linear regression to determine if slope, aspect, fuel characteristics, or wind speed are able to predict burn severity using data gathered from the 100 random accuracy assessment points discussed in Chapter 10. Slope and aspect actually showed an extremely weak negative relationship with burn severity and were dropped from the stepwise model. Fuel type and wind speed show a weak positive relationship and remained in the model. The total adjusted r^2 for the model was 0.129. As fuel and wind variable values were assigned to each point to reflect increasing fuel loadings/fuel particle sizes and increasing wind magnitudes, I can determine that higher fuel loadings and higher wind speeds do correlate with higher burn severity values. Based on the F value of 8.350 that is significant at least to the 0.001 level, I am able to accept my proposed alternate hypothesis that fuel characteristics such as fuel loading and fuel particle size have a positive relationship with burn severity. On the other hand, I must reject my alternate hypothesis that terrain characteristics, such as slope and aspect, show a statistically significant relationship with wildfire burn severity.

Based on the output of the different variants of the wildfire behavior model constructed for this study, it is apparent that there is a relationship between fire residence time, which was linked to total energy output per cell in my wildfire behavior model. Previous studies have determined that there is no definitive link between fire intensity, which describes the amount of heat per square foot along the flaming fire front, and fire

burn severity, but fire residence time is generally not incorporated into a formula to produce an estimate of total energy output in these other studies (Graham, McCaffrey, and Jain 2004). Although no quantitative link between fire residence time/total energy output per grid cell can be made at this time, it is apparent that fire residence time is linked with wildfire burn severity to a degree. Future research is needed to further investigate the connection between fire residence time and wildfire burn severity.

Limitations of Wildfire Modeling Portion of Study

The results obtained from the cellular automata based wildfire behavior model are promising, yet more work needs to be done to improve the predictive capabilities of the model. Calibration is a critical concern for any environmental model that attempts to represent the dynamic movement of a phenomena across space and through time. Although I performed a very rudimentary calibration procedure while experimenting with the burn probability weightings to improve the propagation of fire across the landscape, a methodological approach is necessary to determine less arbitrary burn probability values for fuel type, wind speed, wind direction, slope, and aspect variables. Calibration of complex models involving a number of interrelated variables such as wildfire is not a simple task. Existing studies employing cellular automata techniques to model the propagation of wildfire have also used arbitrary weights to determine the likelihood of fire spread based on fuel, terrain, and weather variables (Clarke 1994, Hargrove et al. 2000; Karafyllidis and Thanalaikis 1997). Future research is necessary to develop valid burn probability values and valid weights for wind direction that are necessary to calibrate the cellular automata model presented in my study.

Fuel moisture is an important variable in wildfire behavior modeling as fires burn more slowly and less readily as forest fuels increase (Berjak and Hearne 2002; Clarke 1994, Hargrove et al. 2000; Karafyllidis and Thanalaikis 1997; Graham et al. 2003). I did not include fuel moisture in my model as fuel moistures were almost uniformly low during the bulk of the Hayman fire event. Fuel moisture levels would likely have little impact on determining which grid cells were likely to burn due to the record low fuel moistures during the fire, but it probably did have an impact on the speed at which the fire propagated per my model output. The primary reason that the lack of a fuel moisture component in my model is a limitation is that my model, if not limited to the data available within the Hayman fire perimeter, would probably not have stopped “burning” at the fire boundary. If the fuel, weather, and topography grids were extended beyond the fire perimeter, the model could have predicted that the fire would consume infinite acres of vegetated land. Unfortunately, due to the current design of the model and lack of data outside of the official fire perimeter, fire behavior could only be represented within the known fire perimeter. Inclusion of the fuel moisture component would allow for fire extinction when burning grid cells did not release sufficient heat to ignite neighboring cells possessing fuels with higher moisture content.

Firebrands have a substantial effect on the speed of fire propagation across space (Anderson 1982; Clarke 1994, Graham et al. 2003; Hargrove et al. 2000). Firebrands are burning embers carried by the wind which can potentially ignite unburned fuels at quite a distance from the main fire front. Firebrands are currently not supported by my model, although the initial spread probabilities used for the spread probability layer were increased to increase probability of spread for fuel types that typically produce large

quantities of firebrands, such as fuel models 8, 9 and 10. Incorporating firebrands in my model could improve the ability of my model to represent fire propagation over time more accurately.

A final limitation of the wildfire behavior model presented here is the lack of a fire suppression component. Due to the record size of the Hayman fire, fire managers initiated extensive fire suppression activities to attempt to slow down and hopefully stop the progress of the fire. Fire retardant drops and man-made fire breaks were the primary fire suppression activities that had an impact on fire progression across portions of the study area that can not be represented currently by my model. If detailed maps existed showing the locations of these fire suppression activities, the fuel layer included in my model could be adjusted to lower burn probabilities in areas where fire suppression activities occurred.

CHAPTER XIV

CONCLUSIONS / FUTURE RESEARCH OPPORTUNITIES

It is apparent that the increasing trend of larger, more severe wildfires requires immediate attention to limit the negative consequences of wildfire on the landscape. BAER teams are mandated to assess wildfire burn severity and submit their recommendations regarding rehabilitation efforts needed to mitigate soil erosion, landslide risk, and runoff of excess debris and soil into watersheds. Due to the strict time pressure on these BAER teams to deliver their findings to decision makers, new assessment methods are necessary to assess wildfire burn severity in a time efficient manner. Both the differenced Normalized Burn Ratio (dNBR) and cellular automata wildfire behavior model presented in this study have the potential to provide valuable information to BAER teams quickly and with a reasonable degree of accuracy.

Additional research into recently developed technologies could improve the ability to gain information about wildfire burn severity from remote sensors. Hyperspectral remote sensing is rapidly developing and could potentially yield more detailed assessments of burn severity using the large number of spectral bands available in new satellite sensors. LIDAR (Light Detection and Ranging) shows promise in assessing characteristics of the forest understory (Riano et al. 2003). Assessment of partially burned forest stands could yield valuable information regarding burn severity characteristics across a study area.

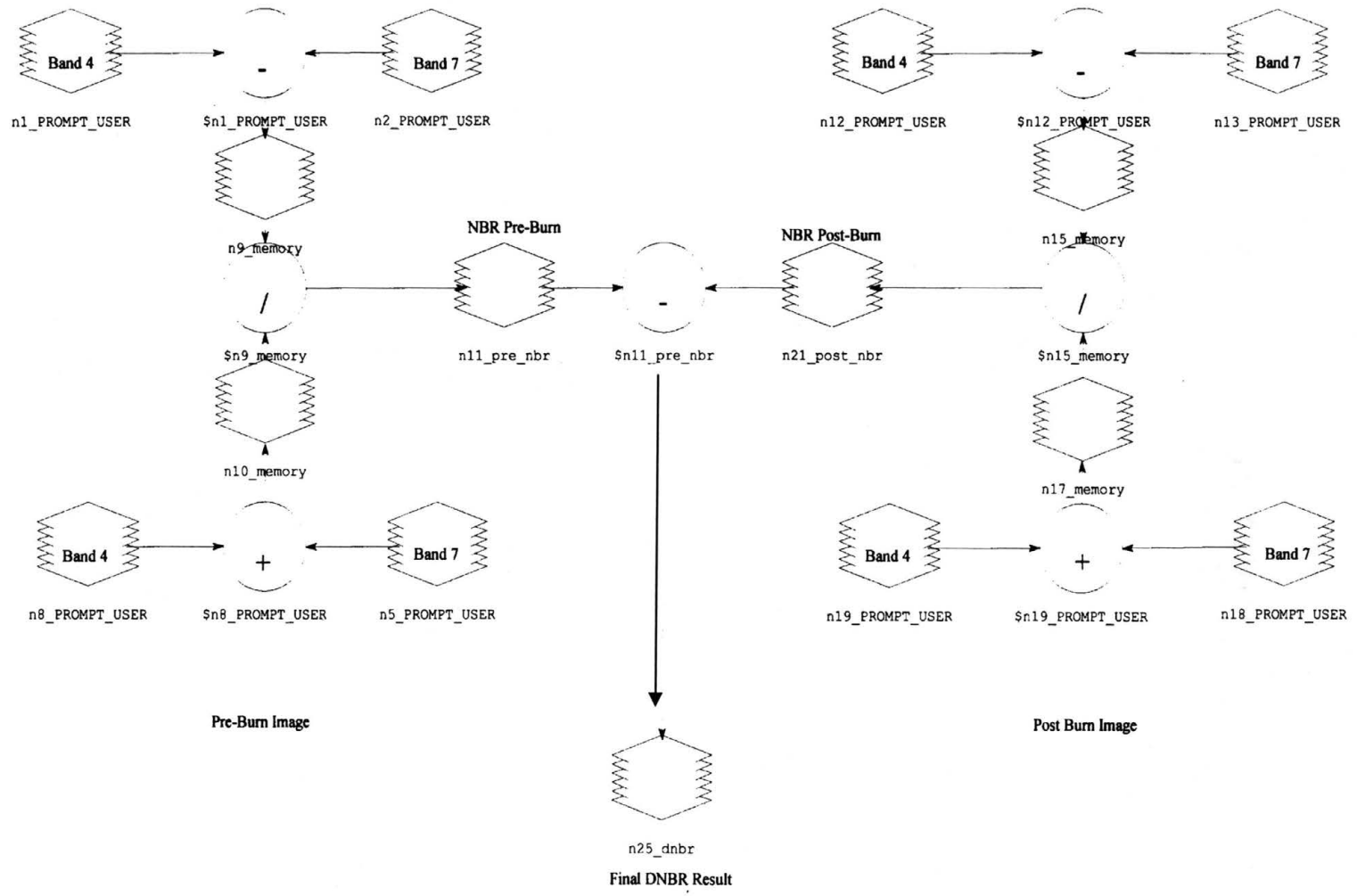
Many of the limitations of the fire behavior modeling portion of my study are issues that need to be addressed in the future to improve our ability to model the interaction of fuel, weather, and topographic variables across space and time. Burn probability values need to be derived for all variables included in future fire behavior models. Currently, the model presented in this study as well as others presented in the existing literature use somewhat arbitrary burn probability values (Clarke 1994; Hargrove et al. 2000; Karafyllidis and Thanalaikis 1997). Improved fuel mapping methods are needed to improve our ability to assess more specific fuel characteristics such as the distribution of large particle size fuels across space. The centimeter level accuracy of LIDAR could potentially produce a fuel map so accurate that the location of individual fallen logs could actually be represented in the fire behavior model, which would undoubtedly increase fire residence time at that point. As my study has suggested a link between fire residence time and burn severity, it is likely that burn severity would be higher where large particle size fuels are burning. Due to the difficulty of calibrating environmental process models, one of the most promising future research areas in the field of wildfire behavior modeling is in neural network modeling of wildfire. Current wildfire behavior models require a known set of rules to produce predictive output, but neural network algorithms have the ability to “learn” the rules as they go. Neural network algorithms are self-calibrating, in effect. McCormick, Brandner, and Allen (1999) discussed the application of neural network algorithms to fire modeling, but did not operationalize their proposed model. The potential of neural network algorithms toward fire modeling is encouraging.

Each of the two burn severity assessment methods presented have their strengths and weaknesses. Therefore, I propose that these two methods, used in conjunction with each other, may be more useful in providing information to the fire research community than either method alone. The dNBR algorithm can only be applied to a study area after the fire event has occurred, but little time is required to implement the algorithm and generate burn severity maps of a fire event. The wildfire behavior modeling technique requires calibration and a number of data sources to implement, but much of this data can be produced prior to or during a fire event, thus reducing the amount of time required to implement the model. An additional benefit of the cellular automata based fire model is that it can produce burn severity risk maps prior to the occurrence of fire events. These risk maps could provide valuable information to decision makers regarding potential areas where fuel treatment activities could reduce available fuel for future wildfires, thereby reducing the risk of severe wildfire in the future. Ongoing research into the application of remote sensing techniques toward wildfire as well as fire behavior modeling will continue to improve our ability to assess the impact of wildfire on the landscape. The future of wildfire behavior assessment is bright indeed.

APPENDICES

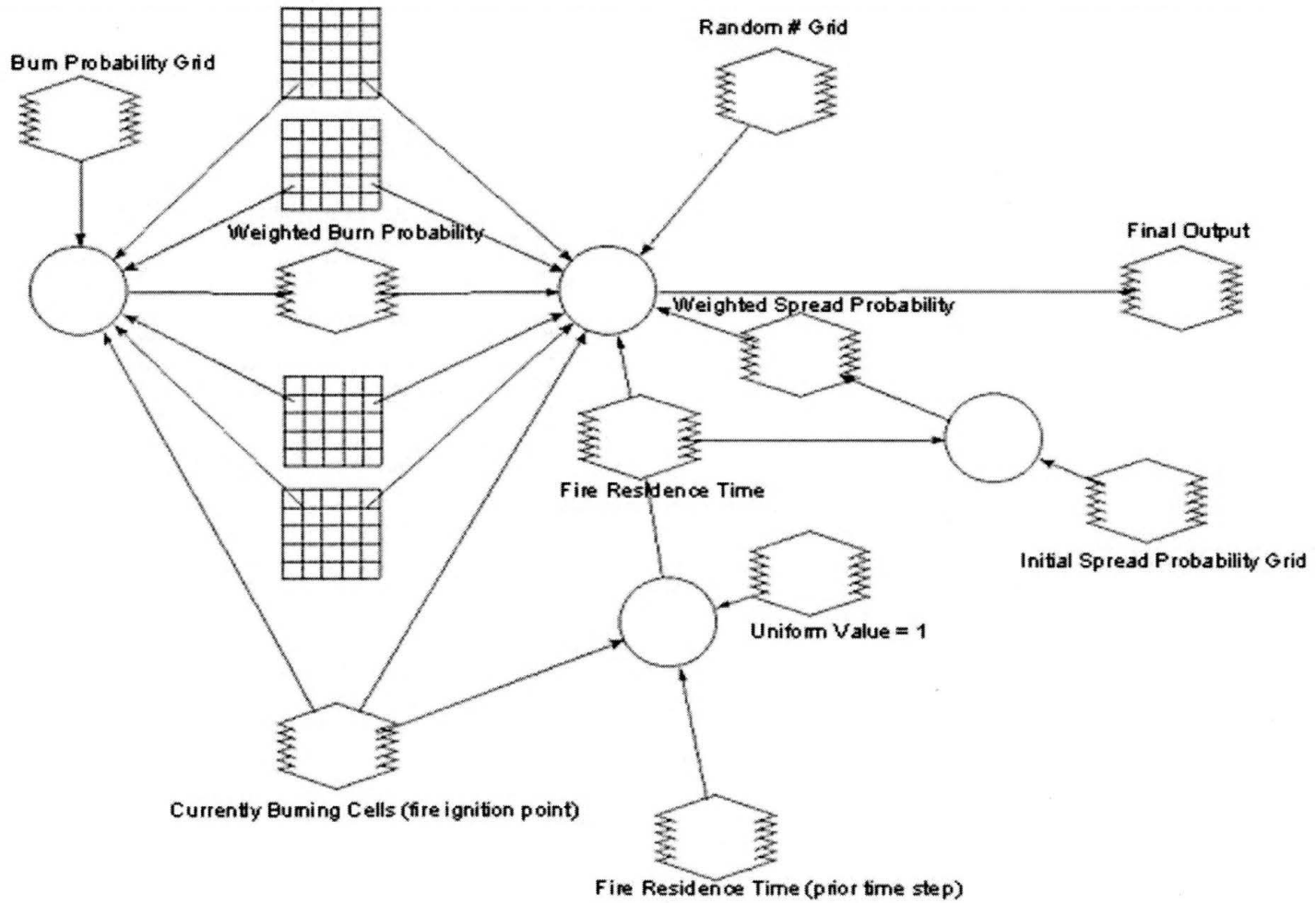
ERDAS GRAPHICAL MODEL OF DIFFERENCED NORMALIZED BURN RATIO
(dNBR) ALGORITHM

ERDAS SPATIAL MODELER LANGUAGE (SML) CODE / GRAPHICAL WILDFIRE
BEHAVIOR MODEL

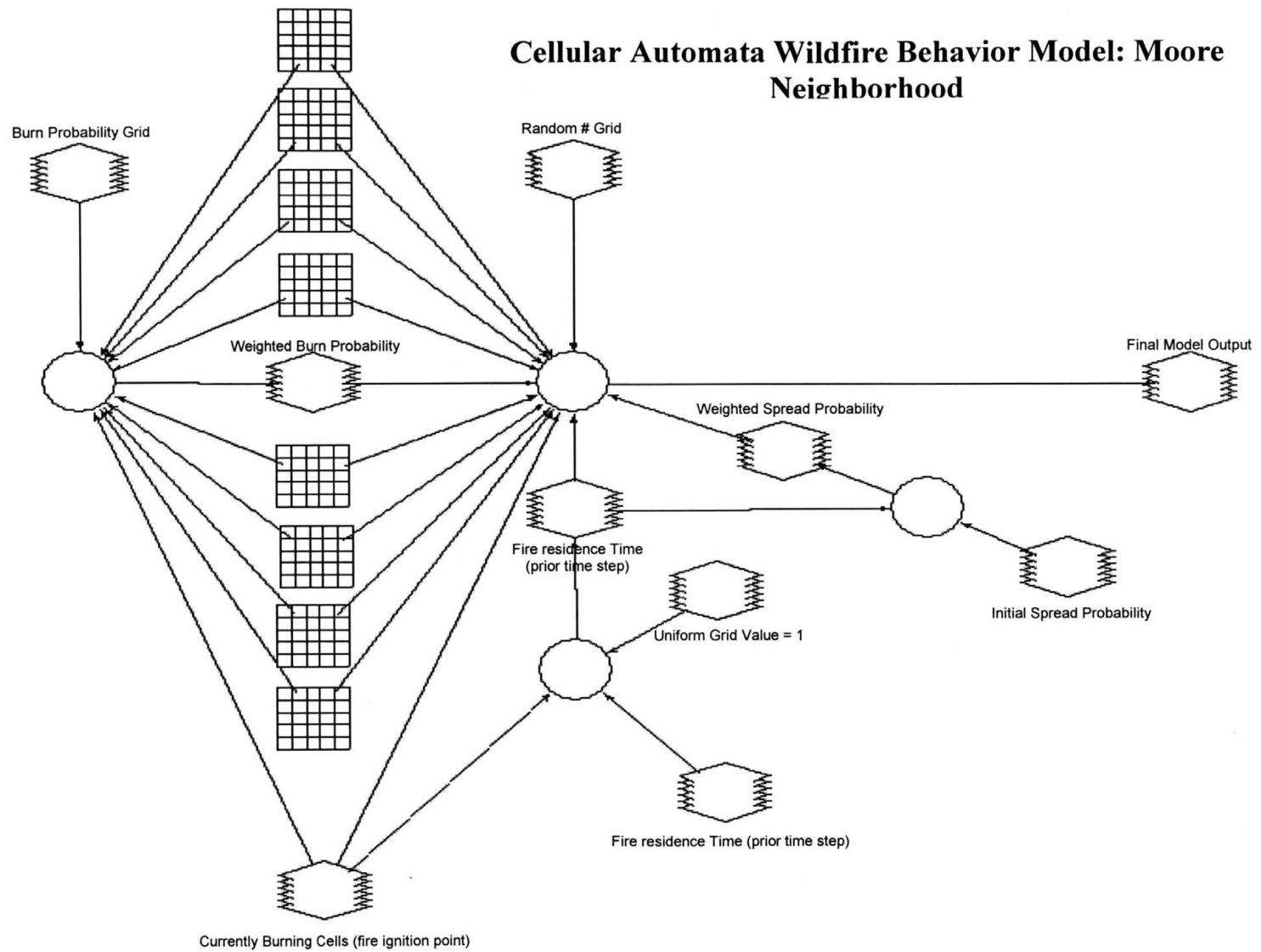


Differenced Normalized Burn Ratio

Cellular Automata Wildfire Behavior Model: von Neumann Neighborhood



Cellular Automata Wildfire Behavior Model: Moore Neighborhood



ERDAS Spatial Modeler Language (SML) Script: von Neumann Neighborhood Wildfire Behavior Model

```

COMMENT "Generated from graphical model:
/home/students/schmiedeskampc/Run_1/ca_wildfire_model.gmd";
#
# set cell size for the model
#
SET CELLSIZE MIN;
#
# set window for the model
#
SET WINDOW UNION;
#
# set area of interest for the model
#
SET AOI NONE;
#
# declarations
#
Float RASTER n1_calc7 FILE OLD NEAREST NEIGHBOR AOI NONE
"/home/students/schmiedeskampc/Run_1/calc7.img";
Float RASTER n3_burn_prob_mod FILE DELETE_IF_EXISTING USEALL ATHEMATIC
FLOAT SINGLE "/home/students/schmiedeskampc/Run_1/burn_prob_mod.img";
Integer RASTER n8_fire_start_1 FILE OLD NEAREST NEIGHBOR AOI NONE
"/home/students/schmiedeskampc/Run_1/fire_start_1.img";
Integer RASTER n11_residence_1 FILE OLD NEAREST NEIGHBOR AOI NONE
"/home/students/schmiedeskampc/Run_1/residence_1.img";
Integer RASTER n13_residence_time_minus_1 FILE DELETE_IF_EXISTING
USEALL ATHEMATIC 8 BIT UNSIGNED INTEGER
"/home/students/schmiedeskampc/Run_1/residence_time_minus_1.img";
Float RASTER n14_random_2 FILE OLD NEAREST NEIGHBOR AOI NONE
"/home/students/schmiedeskampc/Run_1/random_2.img";
Integer RASTER n15_ca_output_1 FILE DELETE_IF_EXISTING USEALL ATHEMATIC
8 BIT UNSIGNED INTEGER
"/home/students/schmiedeskampc/Run_1/ca_output_1.img";
Integer RASTER n16_all_value_1 FILE OLD NEAREST NEIGHBOR AOI NONE
"/home/students/schmiedeskampc/Run_1/all_value_1.img";
Float RASTER n17_spread_prob_3 FILE OLD NEAREST NEIGHBOR AOI NONE
"/home/students/schmiedeskampc/Run_1/spread_prob_3.img";
Float RASTER n19_spread_prob_mod FILE DELETE_IF_EXISTING USEALL
ATHEMATIC FLOAT SINGLE
"/home/students/schmiedeskampc/Run_1/spread_prob_mod.img";
FLOAT MATRIX n4_Custom_Float;
FLOAT MATRIX n5_Custom_Float;
FLOAT MATRIX n6_Custom_Float;
FLOAT MATRIX n7_Custom_Float;
#
# load matrix n4_Custom_Float
#
n4_Custom_Float = MATRIX(3, 3:
    0, 0, 0,
    1, 0, 0,
    0, 0, 0);

```

```

#
# load matrix n5_Custom_Float
#
n5_Custom_Float = MATRIX(3, 3:
    0, 0, 0,
    0, 0, 0,
    0, 1, 0);

#
# load matrix n6_Custom_Float
#
n6_Custom_Float = MATRIX(3, 3:
    0, 1, 0,
    0, 0, 0,
    0, 0, 0);

#
# load matrix n7_Custom_Float
#
n7_Custom_Float = MATRIX(3, 3:
    0, 0, 0,
    0, 0, 1,
    0, 0, 0);

#
# Set counter
#
integer i;
i=1;
#
# begin loop
#
WHILE (i LT 2000)
{
#
n13_residence_time_minus_1 = EITHER ($n11_residence_1 -
$n16_all_value_1) IF ( $n8_fire_start_1 EQ 0 ) OR $n11_residence_1
OTHERWISE ;
n19_spread_prob_mod = EITHER $n17_spread_prob_3 IF (
$n13_residence_time_minus_1 EQ 6 ) OR (EITHER $n17_spread_prob_3 IF (
$n13_residence_time_minus_1 EQ 5 ) OR (EITHER ($n17_spread_prob_3 *
1.15) IF ( $n13_residence_time_minus_1 EQ 4 ) OR (EITHER
($n17_spread_prob_3 * 1.35) IF ( $n13_residence_time_minus_1 EQ 3 ) OR
(EITHER ($n17_spread_prob_3 * 1.5) IF ( $n13_residence_time_minus_1 EQ
2 ) OR (EITHER ($n17_spread_prob_3 * 2) IF (
$n13_residence_time_minus_1 EQ 1 ) OR $n17_spread_prob_3 OTHERWISE)
OTHERWISE) OTHERWISE) OTHERWISE) OTHERWISE) OTHERWISE) ;
n3_burn_prob_mod = EITHER $n1_calc7 * 1.35 IF ( CONVOLVE (
$n8_fire_start_1 , $n4_Custom_Float ) + CONVOLVE ( $n8_fire_start_1 ,
$n5_Custom_Float ) EQ 1 ) OR (EITHER $n1_calc7 * 1.75 IF ( CONVOLVE (
$n8_fire_start_1 , $n4_Custom_Float ) + CONVOLVE ( $n8_fire_start_1 ,
$n5_Custom_Float ) EQ 0 ) OR (EITHER $n1_calc7 * .95 IF ( CONVOLVE (
$n8_fire_start_1 , $n6_Custom_Float ) + CONVOLVE ( $n8_fire_start_1 ,
$n7_Custom_Float ) EQ 1 ) OR (EITHER $n1_calc7 * 1.25 IF ( CONVOLVE (
$n8_fire_start_1 , $n6_Custom_Float ) + CONVOLVE ( $n8_fire_start_1 ,
$n7_Custom_Float ) EQ 0) OR (EITHER $n1_calc7 * 1.75 IF ( CONVOLVE (
$n8_fire_start_1 , $n4_Custom_Float ) + CONVOLVE ( $n8_fire_start_1 ,
$n5_Custom_Float ) + CONVOLVE ( $n8_fire_start_1 , $n6_Custom_Float ) +
CONVOLVE ( $n8_fire_start_1 , $n7_Custom_Float ) EQ 1) OR (EITHER
$n1_calc7 * 1.85 IF ( CONVOLVE ( $n8_fire_start_1 , $n4_Custom_Float )

```

```

+ CONVOLVE ( $n8_fire_start_1 , $n5_Custom_Float ) + CONVOLVE (
$n8_fire_start_1 , $n6_Custom_Float ) + CONVOLVE ( $n8_fire_start_1 ,
$n7_Custom_Float ) EQ 0 ) OR $n1_calc7 OTHERWISE) OTHERWISE)
OTHERWISE) OTHERWISE) OTHERWISE) OTHERWISE);
n15_ca_output_1 = EITHER 0 IF ( $n8_fire_start_1 EQ 0 ) OR (EITHER 1 IF
( $n8_fire_start_1 EQ 2 ) OR (EITHER ((CONVOLVE ( $n8_fire_start_1 ,
$n4_Custom_Float )) / 4) + ((CONVOLVE ( $n8_fire_start_1 ,
$n5_Custom_Float )) / 4) + ((CONVOLVE ( $n8_fire_start_1 ,
$n6_Custom_Float )) / 4) + ((CONVOLVE ( $n8_fire_start_1 ,
$n7_Custom_Float )) / 4) IF (( $n3_burn_prob_mod >= $n14_random_2 )
AND ($n19_spread_prob_mod >= RANDOM ( $n14_random_2 )) AND
($n13_residence_time_minus_1 > 0)) OR 1 OTHERWISE) OTHERWISE)
OTHERWISE);
n8_fire_start_1 = n15_ca_output_1;
n11_residence_1 = n13_residence_time_minus_1;
i = i + 1;
#
}
#
QUIT;

```

ERDAS Spatial Modeler Language (SML) Script: Moore Neighborhood Wildfire Behavior Model

```

COMMENT "Generated from graphical model:
/home/students/schmiedeskampc/Run_5_moore/ca_wildfire_model_moore.gmd";
#
# set cell size for the model
#
SET CELLSIZE MIN;
#
# set window for the model
#
SET WINDOW UNION;
#
# set area of interest for the model
#
SET AOI NONE;
#
# declarations
#
Float RASTER n1_calc7 FILE OLD NEAREST NEIGHBOR AOI NONE
"/home/students/schmiedeskampc/Run_1_moore/calc7.img";
Float RASTER n3_burn_prob_mod FILE DELETE_IF_EXISTING USEALL ATHEMATIC
FLOAT SINGLE
"/home/students/schmiedeskampc/Run_1_moore/burn_prob_mod.img";
Integer RASTER n8_fire_start_1 FILE OLD NEAREST NEIGHBOR AOI NONE
"/home/students/schmiedeskampc/Run_1_moore/fire_start_1.img";
Integer RASTER n11_residence_1 FILE OLD NEAREST NEIGHBOR AOI NONE
"/home/students/schmiedeskampc/Run_1_moore/residence_1.img";
Integer RASTER n13_residence_time_minus_1 FILE DELETE_IF_EXISTING
USEALL ATHEMATIC 8 BIT UNSIGNED INTEGER
"/home/students/schmiedeskampc/Run_1_moore/residence_time_minus_1.img";
Float RASTER n14_random_numbers FILE OLD NEAREST NEIGHBOR AOI NONE
"/home/students/schmiedeskampc/Run_1_moore/random_numbers.img";
Integer RASTER n15_ca_output_moore_1 FILE DELETE_IF_EXISTING USEALL
ATHEMATIC 8 BIT UNSIGNED INTEGER
"/home/students/schmiedeskampc/Run_1_moore/ca_output_moore_1.img";
Integer RASTER n16_all_value_1 FILE OLD NEAREST NEIGHBOR AOI NONE
"/home/students/schmiedeskampc/Run_1_moore/all_value_1.img";
Float RASTER n17_spread_prob_3 FILE OLD NEAREST NEIGHBOR AOI NONE
"/home/students/schmiedeskampc/Run_1_moore/spread_prob_3.img";
Float RASTER n19_spread_prob_mod FILE DELETE_IF_EXISTING USEALL
ATHEMATIC FLOAT SINGLE
"/home/students/schmiedeskampc/Run_1_moore/spread_prob_mod.img";
FLOAT MATRIX n20_Custom_Float;
FLOAT MATRIX n21_Custom_Float;
FLOAT MATRIX n22_Custom_Float;
FLOAT MATRIX n23_Custom_Float;
FLOAT MATRIX n24_Custom_Float;
FLOAT MATRIX n25_Custom_Float;
FLOAT MATRIX n26_Custom_Float;
FLOAT MATRIX n27_Custom_Float;
#
# load matrix n20_Custom_Float

```

```
#
n20_Custom_Float = MATRIX(3, 3:
    0, 0, 0,
    1, 0, 0,
    0, 0, 0);

#
# load matrix n21_Custom_Float
#
n21_Custom_Float = MATRIX(3, 3:
    0, 0, 0,
    0, 0, 0,
    1, 0, 0);

#
# load matrix n22_Custom_Float
#
n22_Custom_Float = MATRIX(3, 3:
    0, 0, 0,
    0, 0, 0,
    0, 1, 0);

#
# load matrix n23_Custom_Float
#
n23_Custom_Float = MATRIX(3, 3:
    0, 0, 0,
    0, 0, 0,
    0, 0, 1);

#
# load matrix n24_Custom_Float
#
n24_Custom_Float = MATRIX(3, 3:
    0, 0, 0,
    0, 0, 1,
    0, 0, 0);

#
# load matrix n25_Custom_Float
#
n25_Custom_Float = MATRIX(3, 3:
    0, 0, 1,
    0, 0, 0,
    0, 0, 0);

#
# load matrix n26_Custom_Float
#
n26_Custom_Float = MATRIX(3, 3:
    0, 1, 0,
    0, 0, 0,
    0, 0, 0);

#
# load matrix n27_Custom_Float
#
n27_Custom_Float = MATRIX(3, 3:
    1, 0, 0,
    0, 0, 0,
    0, 0, 0);

#
# Set counter
#
```

```

integer i;
i=1;
#
# begin loop
#
WHILE (i LT 2000)
{
#
n13_residence_time_minus_1 = EITHER ($n11_residence_1 -
$n16_all_value_1) IF ( $n8_fire_start_1 EQ 0 ) OR $n11_residence_1
OTHERWISE ;
n19_spread_prob_mod = EITHER $n17_spread_prob_3 IF (
$n13_residence_time_minus_1 EQ 6 ) OR (EITHER $n17_spread_prob_3 IF (
$n13_residence_time_minus_1 EQ 5 ) OR (EITHER ($n17_spread_prob_3 *
1.15) IF ( $n13_residence_time_minus_1 EQ 4 ) OR (EITHER
($n17_spread_prob_3 * 1.35) IF ( $n13_residence_time_minus_1 EQ 3 ) OR
(EITHER ($n17_spread_prob_3 * 1.5) IF ( $n13_residence_time_minus_1 EQ
2 ) OR (EITHER ($n17_spread_prob_3 * 2) IF (
$n13_residence_time_minus_1 EQ 1 ) OR $n17_spread_prob_3 OTHERWISE)
OTHERWISE) OTHERWISE) OTHERWISE) OTHERWISE ;
n3_burn_prob_mod = EITHER ($n1_calc7 * 1.35) IF ( CONVOLVE (
$n8_fire_start_1 , $n20_Custom_Float ) + CONVOLVE ( $n8_fire_start_1 ,
$n21_Custom_Float ) + CONVOLVE ( $n8_fire_start_1 ,
$n22_Custom_Float ) EQ 2 ) OR (EITHER ($n1_calc7 * 1.55) IF ( CONVOLVE
( $n8_fire_start_1 , $n20_Custom_Float ) + CONVOLVE ( $n8_fire_start_1
, $n21_Custom_Float ) + CONVOLVE ( $n8_fire_start_1 ,
$n22_Custom_Float ) EQ 1 ) OR (EITHER ($n1_calc7 * 1.75) IF ( CONVOLVE
( $n8_fire_start_1 , $n20_Custom_Float ) + CONVOLVE ( $n8_fire_start_1
, $n21_Custom_Float ) + CONVOLVE ( $n8_fire_start_1 ,
$n22_Custom_Float ) EQ 0) OR (EITHER ($n1_calc7 * .95) IF ( CONVOLVE (
$n8_fire_start_1 , $n24_Custom_Float ) + CONVOLVE ( $n8_fire_start_1 ,
$n25_Custom_Float ) + CONVOLVE ( $n8_fire_start_1 , $n26_Custom_Float
) EQ 2 ) OR (EITHER ($n1_calc7 * 1.20) IF ( CONVOLVE (
$n8_fire_start_1 , $n24_Custom_Float ) + CONVOLVE ( $n8_fire_start_1 ,
$n25_Custom_Float ) + CONVOLVE ( $n8_fire_start_1 , $n26_Custom_Float
) EQ 1) OR (EITHER ($n1_calc7 * 1.35) IF ( CONVOLVE ( $n8_fire_start_1
, $n24_Custom_Float ) + CONVOLVE ( $n8_fire_start_1 , $n25_Custom_Float
) + CONVOLVE ( $n8_fire_start_1 , $n26_Custom_Float ) EQ 0 ) OR
(EITHER ($n1_calc7 * 1.50) IF ( CONVOLVE ( $n8_fire_start_1 ,
$n20_Custom_Float ) + CONVOLVE ( $n8_fire_start_1 , $n21_Custom_Float )
+ CONVOLVE ( $n8_fire_start_1 , $n22_Custom_Float ) + CONVOLVE (
$n8_fire_start_1 , $n23_Custom_Float ) + CONVOLVE ( $n8_fire_start_1
, $n24_Custom_Float ) + CONVOLVE ( $n8_fire_start_1 ,
$n25_Custom_Float ) + CONVOLVE ( $n8_fire_start_1 , $n26_Custom_Float
) + CONVOLVE ( $n8_fire_start_1 , $n27_Custom_Float ) EQ 4) OR (EITHER
($n1_calc7 * 1.65) IF ( CONVOLVE ( $n8_fire_start_1 , $n20_Custom_Float
) + CONVOLVE ( $n8_fire_start_1 , $n21_Custom_Float ) + CONVOLVE (
$n8_fire_start_1 , $n22_Custom_Float ) + CONVOLVE ( $n8_fire_start_1 ,
$n23_Custom_Float ) + CONVOLVE ( $n8_fire_start_1 , $n24_Custom_Float
) + CONVOLVE ( $n8_fire_start_1 , $n25_Custom_Float ) + CONVOLVE (
$n8_fire_start_1 , $n26_Custom_Float ) + CONVOLVE ( $n8_fire_start_1 ,
$n27_Custom_Float ) EQ 3 ) OR (EITHER ($n1_calc7 * 1.75) IF ( CONVOLVE
( $n8_fire_start_1 , $n20_Custom_Float ) + CONVOLVE ( $n8_fire_start_1
, $n21_Custom_Float ) + CONVOLVE ( $n8_fire_start_1 ,
$n22_Custom_Float ) + CONVOLVE ( $n8_fire_start_1 , $n23_Custom_Float
) + CONVOLVE ( $n8_fire_start_1 , $n24_Custom_Float ) + CONVOLVE (
$n8_fire_start_1 , $n25_Custom_Float ) + CONVOLVE ( $n8_fire_start_1 ,

```

```

$n26_Custom_Float ) + CONVOLVE ( $n8_fire_start_1 , $n27_Custom_Float
) EQ 2) OR (EITHER ($n1_calc7 * 1.85) IF ( CONVOLVE ( $n8_fire_start_1
, $n20_Custom_Float ) + CONVOLVE ( $n8_fire_start_1 ,
$n21_Custom_Float ) + CONVOLVE ( $n8_fire_start_1 , $n22_Custom_Float
) + CONVOLVE ( $n8_fire_start_1 , $n23_Custom_Float ) + CONVOLVE (
$n8_fire_start_1 , $n24_Custom_Float ) + CONVOLVE ( $n8_fire_start_1 ,
$n25_Custom_Float ) + CONVOLVE ( $n8_fire_start_1 , $n26_Custom_Float
) + CONVOLVE ( $n8_fire_start_1 , $n27_Custom_Float ) EQ 1) OR
(EITHER ($n1_calc7 * 1.95) IF ( CONVOLVE ( $n8_fire_start_1 ,
$n20_Custom_Float ) + CONVOLVE ( $n8_fire_start_1 , $n21_Custom_Float
) + CONVOLVE ( $n8_fire_start_1 , $n22_Custom_Float ) + CONVOLVE (
$n8_fire_start_1 , $n23_Custom_Float ) + CONVOLVE ( $n8_fire_start_1 ,
$n24_Custom_Float ) + CONVOLVE ( $n8_fire_start_1 , $n25_Custom_Float
) + CONVOLVE ( $n8_fire_start_1 , $n26_Custom_Float ) + CONVOLVE (
$n8_fire_start_1 , $n27_Custom_Float ) EQ 0 ) OR $n1_calc7 OTHERWISE)
OTHERWISE) OTHERWISE) OTHERWISE) OTHERWISE) OTHERWISE) OTHERWISE)
OTHERWISE) OTHERWISE) OTHERWISE) OTHERWISE);
n15_ca_output_moore_1 = EITHER 0 IF ( $n8_fire_start_1 EQ 0 ) OR
(EITHER 1 IF ( $n8_fire_start_1 EQ 2 ) OR (EITHER ((CONVOLVE (
$n8_fire_start_1 , $n20_Custom_Float )) / 8) + ((CONVOLVE (
$n8_fire_start_1 , $n21_Custom_Float )) / 8) + ((CONVOLVE (
$n8_fire_start_1 , $n22_Custom_Float )) / 8) + ((CONVOLVE (
$n8_fire_start_1 , $n23_Custom_Float )) / 8) + ((CONVOLVE (
$n8_fire_start_1 , $n24_Custom_Float )) / 8) + ((CONVOLVE (
$n8_fire_start_1 , $n25_Custom_Float )) / 8) + ((CONVOLVE (
$n8_fire_start_1 , $n26_Custom_Float )) / 8) + ((CONVOLVE (
$n8_fire_start_1 , $n27_Custom_Float )) / 8) IF (( $n3_burn_prob_mod
>= $n14_random_numbers ) AND ($n19_spread_prob_mod >= RANDOM (
$n14_random_numbers )) AND ($n13_residence_time_minus_1 > 0)) OR 1
OTHERWISE) OTHERWISE) OTHERWISE);
n8_fire_start_1 = n15_ca_output_moore_1;
n11_residence_1 = n13_residence_time_minus_1;
i = i + 1;
#
}
#
QUIT;

```

WORKS CITED

- Anderson, H.E. 1982. *Aids to Determining Fuel Models for Estimating Fire Behavior*. USDA Forest Service General Technical Report INT-122.
- Bandini, Stefania, and Giulio Pavesi. "A model based on cellular automata for the simulation of the dynamics of plant populations." Paper presented at the International Environmental Modelling and Software Society iEMSs International Conference, Osnabruck, Germany, June 2004.
- Berjak, Stephen, and John Hearne. 2002. An improved cellular automaton model for simulating fire in a spatially heterogeneous Savannah system. *Ecological Modelling* 148: 133-51.
- Bobbe, Thomas, et al. 2001. *Field measurements for the training and validation of burn severity maps from spaceborne, remotely sensed imagery*. Available online at http://www.fs.fed.us/eng/rsac/baer/final_report_01B-2-1-01.pdf; Internet; accessed 21 October 2004.
- Brivio, P.A., M. Maggi, E. Binaghi, and I. Gallo. 2003. Mapping burned surfaces in Sub-Saharan Africa based on multi-temporal neural classification. *International Journal of Remote Sensing* 24, no. 20: 4003- 018.
- Brown, Daniel, et al. 2004. Spatial process and data models: Toward integration of agent-based models and GIS. *Journal of Geographical Systems* 6, no. 4: 1-44.
- Bryan, Brett. "Modeling the propagation of land clearance using cellular automata and the implications for nature conservation." Paper presented at the 4th International Conference on Integrating GIS and Environmental Modeling (GIS/EM4): Problems, Prospects, and Research Needs, Banff, Alberta, Canada, September 2000.
- Carlton, Donald. 2003. *The impact of changing the surface fire spread model*. Available online at http://fire.org/Download/Carlton_Model_Impacts.pdf; Internet; accessed 16 February 2005.
- Clarke, Keith, James Brass, and Philip Riggan. 1994. A cellular automaton model of wildfire propagation and extinction. *Photogrammetric Engineering and Remote Sensing* 60, no. 11: 1355 – 367.

- Clarke, Keith. "The limits of simplicity: Toward geocomputational honesty in modeling." Paper presented at the 7th International Conference on Geocomputation, Southampton, United Kingdom, September 2003.
- DeMoura, M. L., and L. S. Galvano. 2003. Smoke effects on NDVI determination of savannah vegetation types. *International Journal of Remote Sensing* 24, no. 21: 4225-231.
- Dozier, J. 1981. A method for satellite identification of surface temperature fields of subpixel resolution. *Remote Sensing of Environment* 11: 221-29.
- Franklin, Janet, et al. 2001. Simulating the effects of different fire regimes on plant functional groups in Southern California. *Ecological Modelling* 142, no. 3: 261-83.
- Fraser, R.H., R. Fernandes, and R. Latifovic. 2003. Multi-temporal mapping of burned forest over Canada using satellite-based change metrics. *Geocarto International* 18, no. 2: 37-47.
- Fraser, R.H., Z. Li, and J. Cihlar. 2000. Hotspot and NDVI differencing synergy (HANDS): A new technique for burned area mapping over boreal forest. *Remote Sensing of Environment* 74: 362-376.
- Giglio, Louis, and C. O. Justice. 2003. Effect of wavelength selection on characterization of fire size and temperature. *International Journal of Remote Sensing* 24, no. 17: 3515-520.
- Giglio, Louis, and Jacqueline Kendall. 2001. Application of the Dozier retrieval to wildfire characterization: A sensitivity analysis. *Remote Sensing of Environment* 77: 34-49.
- Glen-Lewin, David, Robert Peet, and Thomas Veblen. 1992. *Plant succession: Theory and prediction*. New York: Chapman and Hall.
- Graham, Russell, et al. 2003. *Hayman Fire Case Study*. USDA Forest Service General Technical Report RMRS-GTR-114.
- Graham, Russell, Sarah McCaffrey, and Theresa Jain. 2004. *Science basis for changing forest structure to modify wildfire behavior and severity*. USDA Forest Service General Technical Report RMRS-GTR-120.
- Hargrove, W.W., et al. 2000. Simulating fire patterns in heterogeneous landscapes. *Ecological Modeling* 135, 2-3: 243-63.

- Justice, C.O., et al. 2002. The MODIS fire products. *Remote Sensing of Environment* 83: 244-62.
- Karafyllidis, Ioannis, and Adonios Thanailakis. 1997. A model for predicting forest fire spreading using cellular automata. *Ecological Modelling* 99: 87-97.
- Key, Carl, and Nate Benson. 1999a. *A general field method for rating burn severity with extended application to remote sensing*. Available online at <http://nrmsc.usgs.gov/research/cbi.htm>; Internet; accessed 6 March 2004.
- Key, Carl, and Nate Benson. 1999b. *The Normalized Burn Ratio, a Landsat TM radiometric index of burn severity incorporating multi-temporal differencing*. Available online at <http://nrmsc.usgs.gov/research/nbr.htm>; Internet; accessed 6 March 2004.
- Key, Carl, and Nate Benson. 2004. Landscape assessment: Sampling and analysis methods. Available online at http://burnseverity.cr.usgs.gov/pdfs/LAv4_CBI_plot.pdf; Internet; accessed 21 October 2004.
- Koutsias, N., and M. Karteris. 2003. Classification analyses of vegetation for delineating forest fire fuel complexes in a Mediterranean test site using satellite remote sensing and GIS. *International Journal of Remote Sensing* 24, no. 15: 3093-104.
- Kushla, John, and William Ripple. 1997. The role of terrain in a fire mosaic of a temperate coniferous forest. *Forest Ecology and Management* 95, no. 2: 97-107.
- Legleiter, Carl, et al. 2003. Fluvial response a decade after wildfire in the northern Yellowstone ecosystem: A spatially explicit analysis. *Geomorphology* 54: 119-36.
- Lenihan, James, et al. 1997. *Fire Disturbance in the MCI Dynamic Global Vegetation Model*. Available online at <http://www.ice.ucdavis.edu/cafe/agenda97/FireManagement/Modeling/2lenihan.html>; Internet; accessed 15 October 2004.
- Liang, Jun, Lin Liu, and John Eck. "Simulating crimes and crime patterns using cellular automata and GIS." Paper presented at the UCGIS Annual Assembly and Summer Retreat, Portland, Oregon, June 2001.
- Lounsbury, John, and Frank Aldrich. 1986. *Introduction to geographic field methods and techniques*. New York: Macmillian Publishing Co.
- Maselli, Fabio, Stefano Romanelli, Lorenzo Bottai, and Gaetano Zipoli. 2003. Use of NOAA-AVHRR NDVI images for the estimation of dynamic fire risk in Mediterranean areas. *Remote Sensing of Environment* 86: 187-97.

- McCormick, Ronald, Thomas Bradner, and Timothy Allen. "Toward a theory of Meso-Scale wildfire modeling – A complex systems approach using artificial neural networks." Paper presented at the Joint Fire Science Conference and Workshop, Boise, Idaho, June 1999.
- Medler, Michael. "Modeling fire hazards with remotely sensed data from recent fires." Paper presented at the Joint Fire Science Conference and Workshop, Boise, Idaho, June 1999.
- Messina, Joseph, Stephen Walsh, Gabriela Valdivia, and Gregory Taff. 1999. *The application of cellular automata modeling for enhanced landcover classification in the Ecuadorian Amazon*. Available online at http://www.geovista.psu.edu/sites/geocomp99/Gc99/081/gc_081.htm; Internet; accessed 15 January 2005.
- Miller, Jay, et al. 2003. Cluster analysis of structural stage classes to map wildland fuels in a Madrean ecosystem. *Journal of Environmental Management* 68: 239-52.
- Miller, Jay, and Stephen Yool. 2002. Mapping forest post-fire canopy consumption in several overstory types using multi-temporal Landsat TM and ETM data. *Remote Sensing of Environment* 82: 481-96.
- Moreno, N., M. Ablan, and G. Tonella. "SpaSim: A software to simulate cellular automata models." In Proceedings of the IEMSS 2002 Conference on Integrated Assessment and Decision Support, Lugano, Switzerland, 2002.
- Nahmias, Jean, Herve Tephany, Jose Duarte, and Sophie Letaconnoux. 2000. Fire spreading experiments on heterogeneous fuel beds: Application of percolation theory. *Canadian Journal of Forest Research* 30, no. 8: 1318-328.
- National Interagency Fire Center. 2004. *After the fires: Let the healing begin*. Available online at http://www.nifc.gov/pres_visit/rehab.html; Internet; accessed 15 September, 2004.
- National Park Service and USGS. 2004. *National Burn Severity Mapping Project*. Available online at http://burnseverity.cr.usgs.gov/show_list.asp; Internet; accessed 15 October 2004.
- Oertel, D., et al. 2003. Airborne forest fire mapping with an adaptive infrared sensor. *International Journal of Remote Sensing* 24, no. 18: 3663-682.
- Patterson, Mark, and Stephen Yool. 1998. Mapping fire-induced vegetation mortality using Landsat Thematic Mapper data: A comparison of linear transformation techniques. *Remote Sensing of Environment* 65: 132-42.

- Perry, Laura, Claudia Neuhauser, and Susan Galatowitsch. 2003. Founder control and coexistence in a simple model of asymmetric competition for light. *Journal of Theoretical Biology* 222: 425-36.
- Riano, David, et al. 2003. Modeling airborne laser scanning data for the spatial generation of critical forest parameters in fire behavior modeling. *Remote Sensing of Environment* 86: 177-86.
- Rieske, L. K. 2002. Wildfire alters oak growth, foliar chemistry, and herbivory. *Forest Ecology and Management* 168 (September): 91-9.
- Robichaud, Peter et al. 2003. *Postfire rehabilitation of the Hayman Fire*. USDA Forest Service General Technical Report RMRS-GTR-114.
- Rothermel, R. C. 1972. *A Mathematical Model for Predicting Fire Spread in Wildland Fuels*. USDA - Forest Service Report INT-115, Intermountain Forest and Range Experiment Station.
- Scott, Andrew, and Timothy Jones. 1994. The nature and influence of fire in Carboniferous ecosystems. *Palaeogeography, Palaeoclimatology, Palaeoecology* 106 (January): 91-112.
- Senkowsky, Sonya. 2001. A burning interest in boreal forests: Researchers in Alaska link fires with climate change. *BioScience* 51, no. 11: 916-21.
- Shugart, Herman. 1984. *A theory of forest dynamics: The ecological implications of forest succession models*. New York: Springer-Verlag.
- Strahler, Alan, and Arthur Strahler. 2003. *Introducing physical geography*. New York: John Wiley and Sons.
- Ungerer, Matthew. "Implementation of cellular automata models in a raster GIS dynamic modeling environment: An example using the Clarke Urban Growth Model." Paper presented at the 4th International Conference on Integrating GIS and Environmental Modeling (GIS/EM-4): Problems, Prospects, and Needs, Banff, Alberta, Canada, September 2000.
- USDA Forest Service. 2002. *Missionary Ridge fire: The aftermath*. Available online at <http://www.fs.fed.us/r2/sanjuan/fire/missridge/baerpaper2.pdf>; Internet; accessed 31 October 2004.
- USGS. 2004. *Burn severity assessment with satellite remote sensing*. Available online at http://edc2.usgs.gov/fsp/burn_severity_assess.asp; Internet; accessed 15 September 2004.

- Weinstein, David, Kass Green, Jeff Campbell, and Mark Finney. 2004. *Fire growth modeling in an integrated GIS environment*. Available online at <http://gis.esri.com/library/userconf/proc95/to100/p092.html>; Internet; accessed 18 September 2004.
- Wilmes, Lloyd, et al. 2002. Rodeo-Chediski fire effects summary report. Available online at http://www.fs.fed.us/r3/asnf/salvage/publications/fire_effects/rc_fire_effects.pdf; Internet; accessed 31 October 2004.
- Wooster, M. J., B. Zhukov, and D. Oertel. 2003. Fire radiative energy for quantitative study of biomass burning: Derivation from the BIRD experimental satellite and comparison to MODIS fire products. *Remote Sensing of Environment* 86: 83-107.
- Wright, T. 2004. A tale of two fires. *American Forests* 109, no. 4: 28-31.
- Wu, Fulong. 2000. A parameterised urban cellular model combining spontaneous and self-organising growth. In *Geocomputation: Innovation in GIS 7*, ed. Peter Atkinson and David Martin, 73-85. London: Taylor & Francis.
- Zhang, X., J. L. Van Genderen, H. Guan, and S. Kroonenberg. 2003. Spatial analysis of thermal anomalies from airborne multi-spectral data. *International Journal of Remote Sensing* 24, no. 19: 3727-742.
- Zhang, Y.H., M.J. Wooster, O. Tutubalina, and G.L.W. Perry. 2003. Monthly burned area and forest fire carbon emission estimates for the Russian Federation from SPOT VGT. *Remote Sensing of Environment* 87: 1-15.
- Zieroth, Elaine, and Karl Siderits. 2003. *Draft environmental impact statement for the Rodeo-Chediski fire salvage project*. Available online at http://www.fs.fed.us/r3/asnf/salvage/publications/RodeoChediski_DEIS.pdf; Internet; accessed 21 October 2004.

VITA

Carl Wilson Schmiedeskamp was born in Orlando, Florida, on October 23, 1976, the son of Marjorie Eileen Schmiedeskamp and Carl Wilson Schmiedeskamp, Sr. After completing his work at Jacksonville High School in Jacksonville, Texas, in 1994, he entered Tyler Junior College. He received the degree of Bachelor of Science in 1998 from Stephen F. Austin State University. During the following years, he was employed as a claims representative at Progressive Insurance Corporation. In January 2003, he entered the Graduate College of Texas State University-San Marcos.

Permanent Address: 1805 Aquarena Springs Dr. #615
San Marcos, Texas 78666

This thesis was typed by Carl Wilson Schmiedeskamp.